TITLE DYNAMIC PROPERTIES OF AN AMMONIA MASER INCORPORATING A DISC RESONATOR.

AUTHOR JOHN A. DAVIS.

INSTITUTION and DATE

UNIVERSITY OF KEELE
1987

ACKNOWLEDGEMENTS

The author would like to thank:

Dr. D.C. Lainé for his enthusiastic guidance and unfailing help through this work.

Professor W. Fuller for the provision of experimental facilities.

His colleagues in the group, Mr. M.I. Abu-Taha and Mr. D. Jones for their help and encouragement throughout the work.

The technical staff of the Physics Department for their continued assistance.

Mr. M. Wallace for his technical assistance during times of experimental difficulty.

Mr. J. Minshull, Mr. K. Bell and Mr. J.D.H. White for their assistance in the design and construction of electronics circuits.

Mr. M. Daniels for preparation of the photographs reproduced in this thesis.

ABSTRACT

The oscillation properties of an ammonia maser employing dual molecular beams and a Fabry-Perot type disc resonator are investigated. The molecular beam flux is pulsed by the use of small fuel injection valves. The resulting gas pulses entering the maser resonator allow for the rapid build-up of maser oscillation sufficient to induce oscillation amplitude settling transients. The amplitude and polarization of these transients are investigated, and their modification under applied magnetic and electric fields is interpreted. Previous results of settling transients are also re-examined.

With an applied magnetic field a novel damped low frequency beating effect is observed following the onset of the pulsed maser oscillation. This is interpreted in terms of the beating of two elliptically polarized oscillations.

The gas pulses entering the resonant cavity are sufficiently intense to allow for pulsed maser oscillation on the J=K=4 and J=K=6 transitions of $^{14}NH_3$ at 24.139 and 25.056 GHz respectively. These are the first reported maser oscillations on these transitions.

The polarization properties of the disc resonator are investigated by the observation of the oscillation polarization ellipse originating within the maser cavity. A method is developed to study the time evolution of the oscillation polarization ellipse, following the opening of the fuel injector valve. The build-up of ellipses under conditions of both single and biharmonic oscillation are studied. The experiments are performed both with and without an applied magnetic field and under conditions of modified cavity anisotropy. A particular feature is the random quality in the evolution of successive oscillation pulses which suggests that the build-up in maser oscillation may be chaotic in nature.

CONTENTS

Acknowledgements

Abstract

CHAPTER 1	**INTRODUCTION**	
1.1	General introduction	1
1.2	The ammonia molecule	3
1.3	Cavity theory and oscillation conditions	5
1.4	Experimental apparatus	7
1.4.1	Vacuum system	8
1.4.2	Nozzle sources	9
1.4.3	Skimmer slits	10
1.4.4	State selectors	11
1.4.5	Resonant cavity, tuning and alignment	12
1.4.6	Microwave detection system	13
CHAPTER 2	**PULSED BEAM MOLECULAR BEAM MASER**	
2.1	Introduction	16
2.2	Pulsed molecular beam	17
2.3	Experimental arrangement	19
2.4	Comparison of pulsed and continuous operation of the maser	21
2.5	Introduction to oscillation amplitude settling transients	23
2.6	Experimental observation of oscillation amplitude settling transients	25
2.7	Biharmonic oscillation in a disc resonator molecular beam maser	29

2.8	Experimental observation of damped low frequency biharmonic oscillation under an applied magnetic field	30
2.9	Interpretation of the damped low frequency biharmonic oscillation	32
CHAPTER 3	**THEORETICAL EXPLANATION OF SOME OF THE TRANSIENT EFFECTS OBSERVED IN MASER SYSTEMS**	
3.1	Introduction	37
3.2	The origins of the maser equations	37
3.3	Numerical solutions to the differential equations	40
3.4	Maser theory applied to a pulsed beam and a molecular Q switched maser	40
3.5	Stark transients and Zeeman transients	42
3.6	A model of the maser gas pulse	44
3.7	The possibility of reaching a chaotic regime of operation of the ammonia maser	47
3.8	Period doubling	53
CHAPTER 4	**PULSED MASER OSCILLATION ON THE J=4,K=4 AND J=6,K=6 INVERSION TRANSITION OF $^{14}NH_3$ AT 24.139 AND 25.056 GHZ RESPECTIVELY**	
4.1	Introduction	56
4.2	Population distribution of the rotational states of $^{14}NH_3$	57
4.3	State selection process and dipole moment	58

	interaction	
4.4	Nozzle sources and rotational cooling	61
4.5	Experimental method and set up	63
4.6	Characteristics of the maser oscillation on the J=K=4 and J=K=6 inversion transitions of $^{14}NH_3$	65
CHAPTER 5	TIME EVOLUTION OF THE OSCILLATION POLARIZATION ELLIPSE DURING THE FORMATION OF A GAS PULSE	
5.1	Introduction	67
5.2	The method of Lissajous spirals	67
5.3	Filter circuits	70
5.4	Setting up procedure	71
5.5	Sources of measurement error	73
5.6	Experimental results	74
5.7	Low frequency biharmonic oscillation with an applied magnetic field	75
5.7.1	General comments	75
5.7.2	Experimental observations	76
5.7.3	Computer simulation of antiphase beats	79
5.7.4	Theoretical beat patterns	81
5.7.5	Preliminary interpretation of results	82
5.8	Single frequency oscillation on the J=K=2 transition of $^{14}NH_3$	85
5.8.1	General comments	85
5.8.2	Experimental observations	86
5.8.3	Preliminary interpretation of results	89

5.9	Oscillation on the J=K=2 transition of $^{14}NH_3$ with modified cavity anisotropy	93
5.9.1	General comments	93
5.9.2	Effect of placing a thin horizontal wire deeply into the fringe field of the resonator	94
5.9.3	The effect of placing a thin horizontal wire moderately deeply into the fringe field of the maser cavity	96
5.9.4	The effect of placing a horizontal wire slightly into the fringe field of the resonator	97
5.9.5	The effect of placing a vertical wire into the fringe field of the maser cavity	99
5.9.6	Maser operation with a thin vertical wire slightly immersed in the resonator	99
5.9.7	Maser operation with a thin vertical wire immersed slightly deeper into the fringe field of the resonator	104
5.10	General comments on the results obtained	106
CHAPTER 6	**SUGGESTIONS FOR FUTURE WORK**	
6.1	Introduction	109
6.2	Possible continuations of the experimental work	109
6.2.1	Lissajous figure work with the existing system	109

6.2.2	Possible modifications to the present system	110
6.2.3	Possible experimental work with the modified system	111
6.2.4	Construction of possible new maser systems	114
6.3	Possible extensions to the theoretical work	116
Appendix 1	An example of a computer program used in chapter 3	
References		

CHAPTER ONE

INTRODUCTION

1.1 GENERAL INTRODUCTION

The ammonia maser was first operated successfully by Gordon, Zeiger, and Townes in 1954. The MASER (Molecular Amplification by Stimulated Emission of Radiation) was the first quantum electronics device constructed, and operates in the centimetre region of the electromagnetic spectrum.

The maser depends for its operation on the principle of population inversion, that is changing the relative population of two or more energy states within an ensemble of molecules (or atoms). This requires a mechanism whereby population inversion is achieved and a resonant cavity in which the magnitude of the emitted radiation (at the transition frequency between the two energy states) may be enhanced. The ammonia maser employs electrostatic state selection of a collimated molecular beam (Gordon Zeiger and Townes 1955), in order to obtain a population inversion. The emitted microwave radiation occurs in a resonant cavity which may be of a cylindrical (closed type), or a disc or semiconfocal (open) type (Lainé 1975).

Molecular beam masers consist of several parts of which only the essential components are discussed here. A two stage vacuum pumping system is required to maintain two or more vacuum chambers at a pressure below 10^{-5} torr so that a molecular beam may be produced and sustained over several tens of centimeters without excessive scattering. A method to produce a strong molecular beam is employed. This normally includes either a single hole nozzle or an effusive source, situated in the first of the vacuum chambers. The boundaries between the two chambers of the vacuum system are formed by either a diaphragm or a skimmer. The centre portion only of the molecular beam passes through this orifice to emerge in the main vacuum chamber to produce a well collimated molecular beam.

State selection of the molecular beam is now undertaken by the use of strong inhomogeneous electric fields. The trajectory of a molecule of ammonia passing through a region of an inhomogeneous electric field will depend upon the energy state of the molecule. An electric field distribution may be found which will direct the upper state molecules towards the the beam axis and deflect the lower state molecules away from the axis, thus providing a population inversion on the axis of the molecular beam. The use of a carefully positioned series of metal bars or rods, held at electric potentials of the order of 10-50 kV with respect to each other, will produce the required field. Each maser system may employ one or more molecular beam which is then directed into the resonant cavity. If the population inversion is large enough and the microwave power generated in the resonant cavity is sufficient to overcome the losses, the condition for maser oscillation is satisfied. Microwave emission is coupled out of the maser cavity and detected by a superheterodyne receiver.

The present system is a double beam maser that employs a disc resonator. The system was constructed and described in detail by Al-Jumaily (1979) and will be briefly described later in this chapter.

The objective of this thesis is to study the dynamic properties of the build-up of maser oscillation in a Fabry Perot type of disc resonator. Small pulsed valves are used to modulate the gas flow of the two molecular beams used. Pulsed molecular beams enhance the maximum output power obtainable from the maser system (Chapter 2). A sharp leading edge is obtained on the gas pulses, the resulting rapid rise in the intensity of the molecular beam results in the sharp onset of the maser oscillation following the pulse of gas entering the resonant cavity. In Chapter 2 this is shown to induce oscillation amplitude settling transients (Self-induced Rabi oscillations) (Bardo and Lainé 1969). In an applied magnetic field a damped low frequency biharmonic

oscillation is observed. This is discussed in Chapter 2. A theoretical study of oscillation amplitude settling transients observed in this and other maser systems used at Keele is undertaken in Chapter 3. The improved performance of the maser employing pulsed molecular beams was used to obtain pulsed maser oscillation on the J=K=4 and J=K=6 transitions of $^{14}NH_3$. This is described in Chapter 4. The maser oscillation originating from a disc resonator is in general elliptically polarized. The output power originating from a disc resonator may be displayed in the form of a Lissajous figure representing the oscillation ellipse (Lainé and Yassin 1981). In Chapter 5 a method is developed to study the time evolution of the oscillation ellipse. A detailed investigation of the evolution of the oscillation ellipse was undertaken under a variety of operating conditions. Suggestions for extending the work are given in Chapter 6.

1.2 THE AMMONIA MOLECULE

The ammonia molecule may be considered as a symmetric top. The three hydrogen atoms form a triangle, and the nitrogen atom occupies a position either above or below the plane defined by these three hydrogen atoms. A line passing through the nitrogen atom which perpendicularly bisects the plane of the hydrogen atoms forms the axis of symmetry of the molecule.

The rotational energy levels of ammonia may be described by the following equation.

(1.1) $E_J = hBJ(J+1) + h(A-B)K^2$

where $A=h/8\pi^2 I_A$ = 189 GHz $B = h/8\pi^2 I_B$ = 298 GHz

Here J is the rotational quantum number of the molecules, K is a second rotational quantum number which is equal to the projection of J along the axis of symmetry of the molecule. A and B are rotational constants, I_A is the moment of inertia of the molecules about the

symmetry axis, and I_B is the moment of inertia of the molecules about an axis that is perpendicular to the symmetry axis and passes through the centre of mass of the molecule.

The fine structure of the ammonia spectrum is due to inversion splitting. The nitrogen atom may occupy a stable position on either side of the plane of the hydrogen atoms. Consider now the potential energy of the nitrogen atom as a function of the distance from the plane of the hydrogen atoms. Here, there are two potential wells, one on either side of the plane of the hydrogen atoms, separated by a potential well of finite height (Fig. 1.1). Due to quantum mechanical tunnelling the nitrogen may penetrate through the potential hill and pass into the second potential well. The quantum mechanical solution to such a system leads to the energy levels of ammonia being split into two sub-levels. This effect is termed inversion splitting. The amount of splitting of the energy levels of ammonia is highly dependent on the shape and height of the potential barrier which is itself dependent on the rotational state.

Rotation of the ammonia molecule about its axis of symmetry will cause the hydrogen atoms to move outwards, and this will reduce the height of the potential barrier and this leads to an increase in the inversion transition frequency. Rotation about a perpendicular axis passing through the centre of mass of the molecule will increase the height of the potential barrier and this leads to a decrease in the inversion transition frequency. Sherg, Baker and Dennison (1941) derived an expression for the wave number of the inversion transitions as a function of the J and K quantum numbers. This is given by

$$1/\lambda(\mathrm{cm}^{-1}) = 0.79347 - 0.0011(J^2 + J) + 0.0016K^2 \qquad (1.2)$$

The average deviation of the measured value from equation (1.2) is about 0.01% (Good 1946). The relative intensities of each of these inversion transitions is discussed in Chapter 4.

FIGURE 1.1

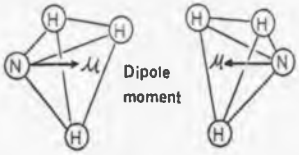

(a)

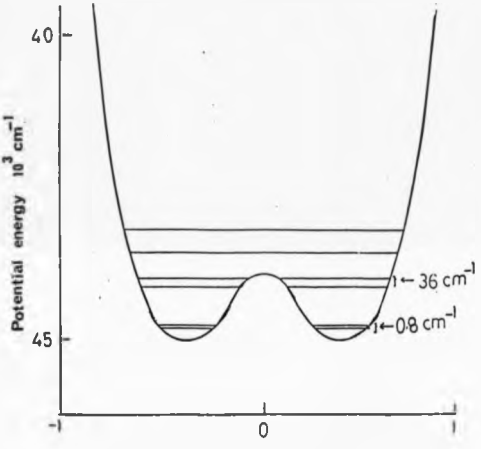

Potential curve for ammonia molecules showing energy level

Each inversion transition of $^{14}NH_3$ shows hyperfine sub-splitting, due to the spin of the hydrogen and nitrogen nuclei. The splitting of the hyperfine components is in many examples greater than the linewidth of the transition. This has led to maser oscillation on several hyperfine components of the J=K=1 inversion transition of $^{14}NH_3$ (Maroof and Lainé 1976). Since molecules contributing to the hyperfine satellite lines will not contribute to maser oscillation on the main line of a transition, the presence of hyperfine structure makes the oscillation condition harder to fulfil, and disturbs the relative oscillation strength of the inversion transition.

1.3 CAVITY THEORY AND OSCILLATION CONDITIONS

Cavity modes in the Fabry Perot resonator have been described by Schawlow and Townes (1958), who considered the cavity modes to be similar to those of a rectangular box. Consider first a closed rectangular cavity of dimensions 2l, 2a, and 2a, the resonant frequencies are given by

$$\nu_{rsq} = (c/4)[(q/l)^2 + (r/a)^2 + (s/a)^2]^{0.5} \quad (1.3)$$

where c is the speed of light and q, r, and s are integers. For a square open resonator of dimension 2a × 2a with a distance 2l between the cavity plates, the same resonant modes will be supported, but diffraction losses will be very large for modes with large values of the integers r and s.

For an open resonator with circular mirrors the frequency determining equation which is analogous to equation (1.3), is given by

$$\nu_{mnq} = (c/2)[(q/l)^2 + (2\chi_{mn}/\pi a)^2]^{0.5} \quad (1.4)$$

where χ_{mn} is the nth root of the mth order Bessel function of the first kind J_m, a is the radius of a disc and 2l the separation between discs. The electromagnetic field amplitude on a plane defined by one of the mirrors, with the origin of coordinates at the centre of the disc is

given in terms of r, as,

(1.5) $A = A_0 J_m(x_{mn} r/a)\cos(m\theta)$

The boundary condition A=0 when r=a is used for calculating the electromagnetic field amplitude.

The modes of the Fabry Perot cavity with circular mirrors are usually designated the $TEM_{m,n-1,q}$ modes. Calculating $J_m(x_{mn} r/a)$ as a function of r, it can be shown (Smart 1973) that the maximum of the electromagnetic field occurs at the centre of the mirror for the TEM_{001} mode and nearer the edge of the mirror for the TEM_{101} mode. The maser is operated on the TEM_{001} mode, although maser operation may be obtained on the next TEM_{101} mode (Al-Jumaily and Lainé 1979), (Chapter 2).

Open resonators lose energy through several mechanisms. Firstly there are diffraction losses due to the finite area of the cavity plates. Secondly there are conduction losses through the plates of the resonator itself. Finally there are the losses of power through the coupling holes taking power away from the resonator. The loaded cavity Q of a resonator may be given by the following expression

(1.6) $1/Q = 1/Q_t + 1/Q_c + 1/Q_d$

where Q_t, Q_c and Q_d are the quality factors due to losses through the coupling holes, the conduction losses and the diffraction losses respectively.

When the power emitted from the molecular beam equals the power loss from the resonator, the threshold for maser oscillation is obtained. The condition for oscillation in a disc resonator is discussed here. The microwave power P emitted from a cavity of length L with low power excitation and no saturation is given by (Shimoda et al 1956),

(1.7) $P = N\nu_0 E^2 \mu_{12}^2 L^2 \pi^2 / h v^2$

where ν_0 is the transition frequency, μ_{12} is the dipole moment matrix element, E is the microwave electric field, N is the flux density, h is Planck's constant and v is the velocity of molecules through the cavity. This equation holds for a disc resonator if the whole of the molecular beam passes along the symmetry axis of the resonator. This has to be modified if a uniform distribution of molecules through the cavity is assumed since L here corresponds to the diameter of the resonator discs to give (De Lucia 1969)

(1.8) $P = 2N\nu_0 E^2 \mu_{12}^2 \pi^2 L^2 / 3 h v^2$

The cavity Q factor may be expressed as

(1.9) $Q = 2\pi\nu_0 W/P$

where W is the energy stored in the cavity. The electric field within the cavity may be given in terms of the energy in the cavity W and the active volume V as

(1.10) $E^2 = 8\pi W/V$

By combining the above equations, the threshold flux for maser oscillation in a disc resonator molecular beam maser is given as N_{min} where

(1.11) $N_{min} = 3Vh\nu^2 / 8\pi^2 \mu_{12} Q L_2$

1.4 EXPERIMENTAL APPARATUS

The maser system employed here had been constructed by Al-Jumaily (1979). A detailed description of this apparatus is given earlier (Al-Jumaily 1979). Here a short account is given of the maser system and any modifications made to it relevent to the present work.

1.4.1 VACUUM SYSTEM

In general the objectives of the pumping system of any molecular beam device is to reduce the background gas pressure to level where the attenuation of the molecular beam is negligible. This requires reducing the background pressure of the vacuum chambers to a level where the mean free path of the molecules is greater than the molecular beam length. For ammonia at 1×10^{-6}torr , the mean free path of the ammonia molecules is of the order of 40cm. For the present system with its beam length of 40cm, background pressures of the order of 1.0×10^{-6}torr are required.

In order to produce intense molecular beams, differential pumping is required in a two or more chamber system. The present system consists of two side chambers which house the molecular beam sources, and the main chamber which houses the disc resonator and the state selector. The pumping system of the two side chambers consists of 6" diffusion pumps, and the main chamber a single 10" diffusion pump. All three diffusion pumps are backed by rotary pumps. To enhance the pumping speed of the maser system, large copper surfaces were placed within all three chambers. These were maintained at liquid nitrogen temperature with a circulating supply of liquid nitrogen. An attempt was made to enhance the pumping speed of the main chamber by constructing a very large area liquid nitrogen trap based on aluminium foil. With the use of this trap in addition to those already in use, no enhanced performance was observed with the maser system. However the operating time of the maser was substantially increased for normal continuous wave operation. Initially the maser could be operated for only two to three hours before the cold surfaces became heavily coated with ammonia and their pumping efficiency was reduced. With the larger area trap at least ten hours operation could be obtained.

A large proportion of the work undertaken in this thesis employs pulsed molecular beams. Here the period between each gas pulse allows

the background pressure in the maser chamber to be reduced to near the level obtained in the absence of the beam. A high intensity gas pulse then enters the chamber, passes through both vacuum chambers and is eventually attenuated by scattering from background gas molecules which accumulate within both the side and main chamber. In the present system the majority of the scattering of the molecular beam originating from the pulsed nozzle source takes place in the side chambers, due to rapid build up of the gas pressure here due to their relatively small volume. Direct scattering of the molecular beam off the bulkhead and skimmers, which divide the vacuum chambers, resulting in molecules being directly scattered into the beam path, is also a major limitation to the intensity of the pulsed molecular beam. The limiting factor for the maximum maser signal amplitude obtainable is caused by the molecular beam being attenuated significantly in the the time taken for the maser signal to establish itself within the resonant cavity. Increasing the size of the the maser side chambers may lead to an increase in the maximum pulsed maser oscillation signal obtainable.

1.4.2 NOZZLE SOURCES

The maser was initially operated with 100μm diameter single hole gas sources. On replacing these sources with 12.5μm wide 2mm long slit sources a significant improvement in operating performance was obtained on the J=K=2 transition, over operation with hole sources, for only single beam operation. For double beam operation the advantage obtained with a slit source was lost. The slit sources produced a fan-like sheet of molecules , which would be better suited to the geometry of the present system than the cone-like distribution of molecules obtained from a hole source (Sulkes et al 1982). The slit nozzle sources have a much larger surface area than the hole nozzle sources, and consequently a much higher gas flux. This was beneficial for single beam operation,

but for double beam operation heavy gas loading of the main maser chamber occurred, causing an attenuation of the molecular beams. The maser system was operated using effusive sources. However the maser signal produced was very weak. The effusive source has a width between 2-3mm, the width between the state selector bars at entrance being only 2.2mm. The extended geometry of the effusive sources therefore made them unsuitable for use in the present system. With pulsed beam operation the gas loading of the main maser chamber was not so critical. Here 2mm long 125μm wide slit sources produced the strongest pulsed oscillation on all the maser transitions yet observed with the present system. The combination of slit source sources and pulsed molecular beams is discussed at length in Chapter 4.

1.4.3 SKIMMER SLITS

The boundary between the side maser chamber and the main maser chamber is marked by the presence of skimmer slits. These are variable width slits with sharp edges, which prevent all but the central portion of the molecular beam from entering the main maser chamber. The ultimate limit of the performance of a molecular beam device is determined by the scattering of molecules off the skimmer slits. This was first observed by Decker et al (1963). In an attempt to overcome this multinozzle gas sources have been developed, such that each portion of the skimmer slit is close to a nozzle and so all the length of the skimmer may be utilized (Maroof 1975). With fast vacuum pumps and pulsed molecular beams, a solution to decrease the skimmer interference was to open the skimmer slits wider, and so increase the molecular beam flux entering the main maser chamber, without loading the gas pumps. The state selector bars were placed directly behind the state selector, and so opening the skimmer slits wide open, simply transfered molecular beam scatter from the skimmer slits onto the state selector bars. In

the design of molecular beam masers the skimmer slits and the state selectors must therefore be considered together.

1.4.4 STATE SELECTORS

In order to obtain a population inversion in the maser resonator, electrostatic state selection is employed in the present system. Electrostatic state selection utilizes the change of energy of a molecule as it is subjected to an electric field

The energy of the upper inversion state increases in an applied Stark field, whereas the energy of the lower inversion state decreases, with the exception of the M=0 states whose energies remain unaltered. In zero electric field the ammonia molecule has no average dipole moment as a result of its inversion properties. As the electric field is increased, the inversion transition is slowly quenched and an average dipole moment appears. The Stark energies of the inversion states of $^{14}NH_3$ are given by (Gordon 1955) as follows

(1.12) $$W = W_0 \mp [(h\nu_0/2)^2 + (\mu MKE/J(J+1))^2]^{0.5}$$

where W_0 is the average energy of the upper and lower inversion levels, ν_0 is the transition frequency in zero electric field and M is the projection of J in the direction of the electric field.

In a uniform applied Stark field there is no force acting on the molecules. However under an inhomogeneous electric field the molecules are subjected to a force of which the x component is given by,

(1.13) $$F_x = \partial W/\partial x = \mp[(\mu MK/J(J+1))^2 E(\partial E/\partial x)] + [(h\nu_0/2)^2 + (\mu MKE/J(J+1))^2]^{0.5}$$

The force on the lower state molecules is directed towards the region of high field density, and that for the upper state molecules is directed towards the region of low field density. The transverse ladder state selectors used in this work, consist of two parallel rows of vertical rods. The molecular beam passes through the two rows. Every

second rod in each row is held at a high potential, the remaining rods being earthed. The regions of high field density occur near the state selector rods, (ie off the axis of the molecular beam), whereas a region of relatively low field density is produced along the axis of the molecular beam. Hence state selection is obtained with upper and lower state molecules directed towards and away from the molecular beam axis respectively.

1.4.5 RESONANT CAVITY, TUNING AND ALIGNMENT

The maser cavity consists of two vertically positioned copper discs 22.5cm in diameter and seperated by approximately 6mm, corresponding to the half wavelength of the transition frequency under study. The cavity construction has been described at length by Al-Jumaily (1979). With operation of the maser on the lowest TEM_{001} mode, a cavity Q of approximately 6000 was reported by Al-Jumaily, whereas the Q value obtained by recent measurments was between 4000 and 4500. This suggests that the surface of the cavity plates has degenerated, either by the plates losing their flatness or by corrosion of the surface.

The relative orientation of the two cavity plates is maintained by pressure from three micrometer screws, on three glass rod spacers. The performance of the maser was critically dependent on the initial tuning of these micrometer screws. Fine tuning of the maser cavity was obtained by applying pressure to the frame holding one of the cavity plates. By this method a satisfactory cavity tuning mechanism was obtained. However the cavity was subject to thermal drift, and to a large frequency shift when the main vacuum chamber was evacuated. A proposal to supplement the present cavity tuning mechanism by cavity tuning via a series of piezo-electrics is discussed in Chapter 6.

The major difficulty in operating the maser is that of

alignment. For efficient use of the resonant cavity the central portion of the molecular beam must pass symmetrically midway through the entrance and exit gap of the state selectors, and then midway between the plates of the resonant cavity. In order to achieve this, a visible region He-Ne laser beam was directed along the molecular beam path and each component was aligned with respect to it. The use of a positioning mechanism (Chapter 2), ensured the correct alignment of the nozzle source. The maser performance was critically dependent upon this alignment.

1.4.6 MICROWAVE DETECTION SYSTEM

The double port coupling of the maser cavity to the associated waveguide allows for relatively simple detection of the maser signal. A detailed description of the microwave assembly has been given by Al-Jumaily (1979). Two possible methods of detection are used here. These are the crystal video and superheterodyne schemes.

Crystal video is the simplest detection scheme. It is used for the detection of cavity modes in the setting up procedure and the detection of absorption signals. It lacks sensitivity and is used for detecting the final stimulated emission maser signal only in exceptional circumstances. Microwave power is supplied by a klystron type Oki 24V10A. This power is attenuated and then fed to one port of the maser cavity. The reflected microwave power from the second cavity microwave port is then fed to a diode crystal (type IN26). The resulting electrical signal is displayed on a CRO. By sweeping the klystron frequency at 50Hz, the frequency dependence of the reflected microwave power leaving the maser cavity may be monitored, and hence the cavity modes may be displayed on the CRO.

Superheterodyne detection is used for detecting the maser stimulated emission and oscillation signals. Here the klystron power is

offset by 30MHz from the maser transition frequency. The klystron power is divided and attenuated, a portion being fed to each arm of the microwave loop. The klystron power in one arm is sent via an isolator and a circulator to a diode crystal. A 30MHz signal is fed to the diode crystal from a signal generator. Two 30MHz maser sidebands are then produced and these signals enter the maser cavity. One of these signals lies at the maser transition frequency. The reflected signal from the maser cavity in the second arm of the microwave loop is then mixed with the second portion of the microwave power. The mixing produced a 30MHz beat signal. This is converted via a crystal diode to an electrical signal. This signal is then amplified via a 30MHz intermediate frequency (I.F.) amplifier, detected and finally displayed on the CRO. Once the maser is adjusted to be above the threshold for oscillation the requirement to reflect microwave power through the maser cavity can be set aside and the second arm of the detection system may be used to set up a second channel of detection in order to detect the microwave power of the maser oscillation in a second linear polarization (Chapter 2).

The signal to noise ratio of the final maser signal is dependent on both the noise of the crystal diode and the I.F. amplifier. The noise of an I.F. amplifier increases as the operating frequency increases, and the noise of the crystal diode decreases as the operating frequency increases. At approximately 30MHz the combined noise of the crystal detector and I.F. amplifier is at a minimum (Ingram 1955). This frequency is therefore chosen as the offset frequency for the klystron power.

Originally the I.F. amplifiers consisted of a series of tuned circuits which when combined produced a gain of approximately 120db with a bandwidth of a few MHz. For the later work discussed in Chapter 5 these were replaced by amplifiers based on integrated circuit technology. This produced an increase in the signal to noise ratio of

the final signal of approximately three times using the replacement amplifiers. A second stage of superheterodyne frequency conversion was employed to reduce the IF signal from 30MHz to 45kHz in order to display Lissajous figures on an oscilloscope. This is described in detail in Chapter 5.

CHAPTER TWO

PULSED BEAM MOLECULAR BEAM MASER

2.1 INTRODUCTION

Pulsed molecular beams have recently been successfully employed in many applications. Recent developments, leading to small size pulsed nozzle sources, are readily incorporated into the present maser system. Conventional nozzle gas sources used for molecular beam maser work provide extremely intense molecular beams; this has led to strong maser oscillation, and the observation of several new non-linear oscillator phenomena. However to study such effects in more detail and to allow for the possibility of maser oscillation on new spectral lines (Chapter 4), an increase in beam intensity is required. To achieve these objectives the present system has been converted to accept pulsed molecular beams.

The disadvantages of a pulsed molecular beam maser is the intermittent nature of the oscillation power output, and the absence of a steady state level of oscillation. However, for studies of oscillation build-up effects and various amplitude modulation effects this is not a problem. Furthermore, it is still possible to observe the form of the oscillation polarization ellipse (Yassin and Lainé 1981), during the duration of the oscillation pulse (Chapter 5), and so obtain information on the form of the time evolution of the oscillation ellipse.

In this chapter a study of the build up of oscillation in a disc resonator is undertaken. Oscillation settling transients have been observed on several inversion transitions of ammonia and various novel low frequency beating effects have also been observed.

2.2 PULSED MOLECULAR BEAM

The basic idea of using a pulsed molecular beam is to reduce the gas loading on the diffusion pumps, and hence reduce the background pressure in the maser vacuum chambers. The molecular beam, on entering the maser chambers after the pulsed nozzle source is opened, is now travelling through background gas of lower pressure than would be possible with continuous wave operation, and so is scattered far less. Consider the side chambers of the maser. With no gas entering the system a pressure of 3×10^{-6} torr may be reached at optimum performance. In continuous gas flow operation, a pressure of 2×10^{-4} torr is usually obtained. The initial portion of the gas pulse will be entering the chamber when the pressure is near its lower limit and consequently the scattering of the molecular beam is considerably reduced.

There are many devices that have been constructed to produce pulsed molecular beams. It is important to establish the characteristics required of any valve or other pulsing mechanism. Firstly, there is a "time of silence" between the time that the molecules enter the resonance cavity and when oscillation first appears, which is of the order of 0.2ms. This is roughly the time of flight of molecules across the resonant cavity. There is little point in constructing a valve for the present system with a pulse duration less than 0.2ms. Secondly, any transient effect must be allowed time to develop before the valve is closed. These effects are typically of the order of a fraction of a millisecond, and so the ideal valve would give a gas pulse duration of a few milliseconds, and a time to open fully which is not greater than a sizeable fraction of a millisecond. Aligning a molecular beam maser is a slow and careful operation requiring constant reference to the emitted signal in the process. A valve which cannot produce a continuous gas supply by being open continously will prove extremely difficult to align.

The pulsed beam source used was based on an engine fuel injector valve Bosch type 0 280 150 025. This valve had an opening time of between 0.3ms and 0.5ms, and a pulse duration of approximately 5ms, which could be varied as required. This valve also had a repetition rate of up to 100Hz, and could be held in the open position indefinitely by the application of approximately 1 volt, (at 0.3 amps), across the coils of the valve. As is common practice with such a valve, the central pin on the gas outlet side was machined flat back to the valve body. The end of the valve was capped by a small chamber of volume $27mm^3$. The exit aperture of this cap could be changed to accommodate either hole or slit sources. In the majority of experiments, 0.1mm diameter hole sources were used for work on the J=K=1, J=K=2, and J=K=3 inversion transitions of ammonia. However, the strongest oscillation was obtained on the J=K=3 transition where two 125μm wide, 2mm long slit sources were used (Chapter 4). A modified cap of $3mm^3$ volume was used with these sources. A noticeable improvement was seen in various transient phenomena observed after this cap volume change due to the faster build-up of the gas pulse. Gas flow through a capped valve is treated theoretically (Chapter 3). A final advantage of using a fuel injector valve which is relevant to the maser system described in this thesis, is the relatively low cost.

It is interesting to note the effects that limit the effectiveness of a pulsed molecular beam maser system. The gas loading of the main chamber of the molecular beam maser has always been relatively light. However the need for large pumping speed in this chamber is noticeably reduced with pulsed gas operation. The duration of the maser oscillation signal is limited by the scattering of molecules by pressure build-up in the side chamber. A simple solution is to increase the size of the chamber by a large factor with only a moderate increase in pump size. This will increase the pulse duration

but will limit the repetition frequency of the valve. The ultimate limit of maser performance will be caused by the scattering of beam molecules by the skimmer slits and state selector bars. A combination of wide skimmer slits and a wide space between the rows of state selector bars may improve the situation. (A decrease in focusing force of the state selectors by increasing the spacing between the electrodes may be compensated by a higher working voltage). Ultimately for optimum performance with a disc resonator, a whole series of state selectors, skimmer slits and pulsed valves arranged around a horizontal maser cavity may be required (Chapter 6).

2.3 EXPERIMENTAL ARRANGEMENT

The first problem was that of housing the fuel injector valve within the existing side chamber of the maser. For the left hand chamber a mechanical positioning mechanism was constructed (Fig. 2.1). A slide rail enabled the nozzle-skimmer distance to be adjusted. The slide rail was then mounted on two threaded rods. The rotation of these rods gave transverse and azimuthal angle adjustment. Vertical adjustment was considered superfluous. The rubber fitting at the rear of the valve was fitted to an existing nozzle pipe and clamped. This rubber "joint" gave sufficient flexibility to allow for the sideways positioning of the valve. The right hand side chamber was fitted with a simpler system (Fig. 2.2). Here a brass sleeve was machined to fit over the valve which was then clamped to the existing nozzle pipe. In effect, the valve became an extension of the nozzle pipe. The positioning mechanism proved to be most successful.

A cooling system was introduced which consisted of a design of reinforced plastic pipe and copper tube. Chilled compressed air was passed through the pipe; however it was found that with only a low pulse frequency below approximately 10Hz, or with continuous operation, the

FIGURE 2.1 POSITIONING MECHANISM

FIGURE 2.2 SLEEVE

cooling system was not required.

The original method of pulsing the fuel injector valve solenoid current consisted of a relay, dc power supply, and a pulse generator. This was found to be unsatisfactory on account of the large back EMF produced when the circuit was broken. Instead, a thyristor current pulse unit was constructed (White 1984), which was triggered by a 3 volt square wave supplied by a pulse generator. To increase the initial opening rate of the valve, a series of high voltage capacitors discharged a 250 volt pulse across the valve in addition to the 12 volt supply pulse supplied by the main section of the current pulse unit. A circuit diagram of the current pulse unit is shown in Fig. 2.3. The current pulse unit was quite satisfactory, and two fuel injector valves could be operated simultaneously in parallel, from a single pulse generating unit. By this method, satisfactory syncronization of the gas pulse forming the two molecular beams could be achieved.

The final problem here was the detection of the oscillation pulses originating from the maser. An estimate is made of the time taken before a gas pulse becomes significantly attenuated which will give an indication of the lifetime of the resulting oscillation pulse. A gas flow into the maser of 10^{21} molecules s^{-1} may be obtained for pulsed molecular beams. Assume a lower flux of 10^{18} molecules s^{-1} entering the maser. This would correspond to a strong continuous beam. The volume of one of the side chambers is approximately 15000 cm^3 at 3×10^{-6}mb. If this chamber then reaches as high a pressure as 3×10^{-4}mb during a gas pulse, (which would significantly attenuate a molecular beam), and assuming negligible pumping rate, this will take approximately 0.1s. A simpler method to gain an estimate for the oscillation pulse duration would be as follows. Assuming scattered molecules reach a far wall of the side chamber and are then scattered directly back into the molecular beam. The path length is approximately

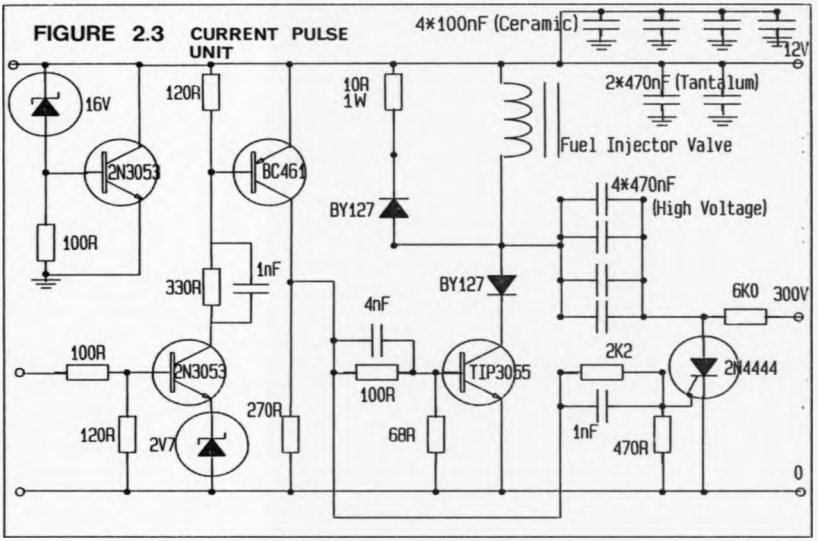
FIGURE 2.3 CURRENT PULSE UNIT
4*100nF (Ceramic)
12V
2*470nF (Tantalum)
16V
120R
10R 1W
Fuel Injector Valve
2N3053
BC461
BY127
4*470nF
(High Voltage)
100R
330R
1nF
BY127
6K0 300V
4nF
100R
2N3053
TIP3055
2K2
2N4444
270R
120R
2V7
100R
68R
1nF
470R
0

20cm before a scattered molecule may once again enter the molecular beam, it is assumed here that the molecular velocity approaches 1000m/s (Jones 1984), therefore considerable scattering of the molecular beam takes place within the first fraction of a millisecond of the start of the gas pulse. It was assumed that at optimum performance the oscillation pulses would have a duration of no more than a few milliseconds.

Detection of the maser oscillation pulse was achieved by displaying the oscillation power output against time on an oscilloscope triggered by the pulsing unit. This method proved quite satisfactory and so no complicated circuitry was required. By observation of the cavity mode of the maser in a frequency swept mode on the oscilloscope is was possible to detect pulses of stimulated emission, or oscillation, with the naked eye. However, the pulsed valves were operated initially to give a continuous beam while the maser parameters were optimised, after which pulsed operation was effected. The ability to use the pulsed valve in a continuous mode of operation proved extremely useful.

2.4 COMPARISON OF PULSED AND CONTINUOUS OPERATION OF THE MASER

The performance of the molecular beam maser under consideration here was dependent on many parameters, for example, alignment of the state selectors with nozzle pipe and resonator cavity; the Q factor of the cavity; background pressure of the nozzle chambers and main chamber; the type of nozzle source used; the mechanical coupling of waveguides to the cavity. Due to the large number of variables, comparisons of the performance of a maser system are only meaningful when experimental conditions are nearly identical. This can be achieved here since changing from continuous to pulsed use of the maser does not require an alteration of the physical parameters.

The trace (Fig. 2.4a) displays the time evolution of a typical

FIGURE 2.4
OSCILLATION PULSE

a

b

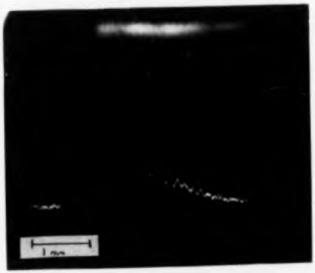

gas pulse. The trace may be considered in three parts. The initial flat region represents the time taken between the opening of the pulse valve and the onset of oscillation. This time period may be subdivided into three parts. Firstly the time taken for the molecular beam packet to reach the maser cavity, secondly, the time taken for the molecular flux entering the maser cavity to build up to the value required to reach the threshold of oscillation and, finally, the "time of silence" given as the time between reaching the condition for oscillation, and the onset of oscillation at the time of its first appearance above the receiver noise level.

The region of rapid oscillation build-up follows and finally the region of decay of the oscillation. This last phase is mainly caused by scattering of the pulsed beam by the rapid build-up of background gas in the nozzle chamber. The form of the oscillation build-up is treated theoretically in Chapter 3.

A pulse repetition frequency up to 100Hz could be obtained from the valves when operated by the thyristor pulse unit. However it was more usual to use a pulse repetition frequency of between one and ten Hz as this reduced wear on the valve, the cooling required, and more importantly gave a relatively large recovery time between each pulse for a given gas loading of the diffusion pumps.

Strong pulsed oscillation was obtained on the J=K=1, J=K=2, J=K=3, inversion transitions of $^{14}NH_3$. With single beam operation, pulsed and continuous wave oscillation could be obtained on the J=K=2 and J=K=3 transitions of $^{14}NH_3$. With double pulsed beam operation, oscillation could be obtained on the J=K=1 transition and the second order TEM_{101} modes of the J=K=2 and J=K=3 transitions of $^{14}NH_3$. All these modes have sustained continuous wave oscillation previously with this maser system although this could not be achieved at time of writing due to degradation of the cavity Q value. It was possible to estimate

the overfulfilment condition for each spectral line under consideration by examining oscillation amplitude settling transients. When R > 1, the oscillation condition is overfulfilled, and the value of R is known as the oscillation overfulfilment factor. The maximum values of R realised experimentally were as follows, J=K=1 transition 1.5, J=K=2 transition 3.0, J=K=3 transition 3.3. Using a pulsed molecular beam in the system under discussion the maximum oscillation overfulfilment factor is increased by approximately two. Although the threshold of oscillation is lower for pulsed beam oscillation the effect is not dramatic. This may be explained in part by the fact that at very low oscillation levels the time of oscillation build-up (which may be of the order of milliseconds), may become comparable with the pulse duration, and also that at a low state selector voltage the effectiveness of state selection is proportional to the square of the state selector voltage.

2.5 INTRODUCTION TO OSCILLATION AMPLITUDE SETTLING TRANSIENTS

Whenever the oscillation amplitude power output level in a maser system is varied abruptly by a large amount it is possible to induce oscillation amplitude settling transients (self-induced Rabi oscillations). These transients were predicted theoretically (Grasyuk and Oraevskii 1964), and are the subject of an extensive theoretical study (Chapter 3). There are several methods of changing the oscillation level in a molecular beam maser sufficiently rapidly to induce settling transients. These are summarized in the following paragraphs.

(a) Saturation broadening:- Here a high level signal is injected into the maser near the resonance frequency of the molecules which saturation broadens the spectral line thereby quenching the maser oscillation. On removing the injected signal, a rapid rise in the oscillation output power (or rise from thermaly generated noise if the

oscillation is completely quenched) follows (Shkakov 1969),(Lainé and Bardo 1969), (Lainé and Maroof 1975). The interpretation of the results of Maroof are discussed in Chapter 3.

(b) Stark or Zeeman broadening of the spectral line:- Here an electric or magnetic field is applied to the region within the cavity resonator with the effect of either stark or Zeeman broadening of the spectral line causing a drop in the maser output power level. This method was extensively studied by Lefrère (1974). The interpretation of some of the results obtained are discussed in Chapter 3.

(c) Abruptly altering the rate at which molecules in particular energy levels are supplied:- This method was first attempted by Grasyuk and Oraevskii (1964). Here the voltage applied to the state selectors was pulsed periodically. However amplitude settling transients occur on a time scale of 10^{-4} seconds and so the change in the number of active molecules entering the cavity in a time less than this value is required to induce self-induced Rabi oscillation transients. The state selectors used in this experiment had a length of the order of 10cm, and so the build-up of the the number of active molecules entering the cavity was smeared out between 10^{-3} and 10^{-4}s, due to the partial state selection of the portion of the molecular beam inside the state selectors when the EHT pulse was applied. Consequently, the self-induced Rabi oscillation phenomenon was not observed.

The use of a pulsed molecular beam to induce oscillation amplitude settling transients became a possibility if the opening time of the gas valve could be operated in a time of the order of 10^{-4} seconds and if the pulse of gas maintained its sharp profile during its time of flight between source and the maser cavity. Under conditions of high nozzle source pressure the velocity distribution of molecules within a molecular beam is much reduced, preserving the sharp leading edge of the gas pulse as it reaches the maser cavity. The use of pulsed

nozzle gas sources make the observation of oscillation amplitude settling transients possible.

The successful observation of oscillation amplitude settling transient by employing a pulsed molecular beam maser system is discussed here. Oscillation amplitude settling transients have been observed in the present system by the additional method of molecular Q-switching (Lainé and Al-Jumaily 1979) using an electric field of about $7kVm^{-1}$ by applying 40V to one of the cavity discs, which was electrically isolated from earth. In both cases oscillation settling transients could be observed under conditions of relatively low oscillation overfulfilment.

2.6 EXPERIMENTAL OBSERVATION OF OSCILLATION AMPLITUDE SETTLING TRANSIENTS

The experimental system employed was identical to that described earlier with the oscillation power output being displayed as a function of time on the oscilloscope. During the study, several different nozzle sources were used; for the J=K=1, J=K=2, J=K=3, transitions a 0.1mm diameter hole source, mounted on a cap of small volume was found suitable. The size of the cap was initially $27mm^3$; reducing it to $3mm^3$ greatly improved the amplitude of the transients observed, especially on the J=K=3 transition. The use of 125μm wide, 2mm long, slit sources on the J=K=3 transition with a $3mm^3$ cap volume gave a yet stronger oscillation overfulfilment factor. However a less well defined leading edge to the gas pulse weakened the oscillation amplitude settling transients observed. This was due to the lower nozzle pressure used.

Oscillation amplitude settling transients were observed on the J=K=1, J=K=2, and J=K=3 transitions. The transients observed on the J=K=3 and J=K=2 were damped oscillatory in nature having a period of approximately 6kHz (Fig. 2.5a;c). The transient observed on the J=K=1 transition consisted of a single oscillation spike (Fig 2.5b). Attempts

FIGURE 2.5
OSCILLATION TRANSIENTS

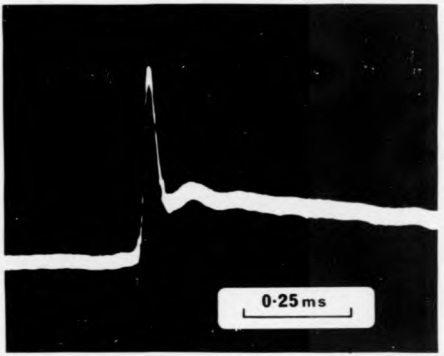

were made to observe settling transients with the second order TEM_{101} cavity modes of the J=K=2 and J=K=3 transitions. However at a high level of oscillation parameter R, biharmonic oscillation is observed with these modes, with a beat frequency of approximately 7kHz (Fig. 2.4b), due to oscillation on a Doppler split spectral line (Al-Jumaily and Lainé 1979). Here, the transient effect is partly obscured by the beat pattern.

An attempt was made to enhance the peak amplitude of the oscillation transients by combining the pulsed beam technique with that of molecular Q-switching in order to improve the sharpness of the oscillation build-up. No enhancement was observed which suggests the gas pulse must build up within a time comparable with the time of silence of the maser oscillation build-up, which is approximately 0.2ms.

The disc resonator under consideration here has two coupling ports. This enables two different linear polarizations to be observed simultaneously. Measuring the ratio of the maximum transient amplitude in the respective polarizations for several different gas pulses, it was found that this ratio differed considerably under near-identical conditions (Fig. 2.5Aa,b). In Fig. 2.5A the upper and lower traces display the components of oscillation with their electric field vectors orientated along the vertical and horizontal axes of the cavity respectively. The above effect was extremely noticeable, for in one linear polarization the transient build-up was damped oscillatory in nature, whereas in the second linear orthogonal polarization the oscillation build-up was only exponential with no observed transients. On successive gas pulses the linear polarization which displayed the strong settling transient would often reverse, and on a few occasions the oscillation transients in the two orthogonal polarizations would have approximately equal amplitude. This indicates that the oscillation build-up has a maximum amplitude in different directions of polarization

FIGURE 2.5A OSCILLATION TRANSIENTS

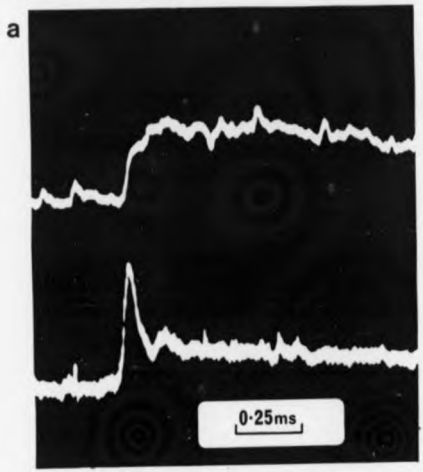

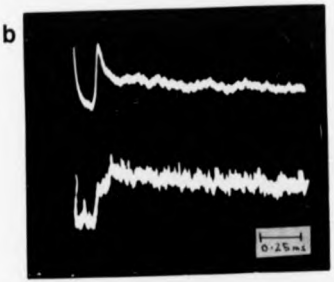

in successive pulses. This is consistent with the work of Al-Jumaily (1979) and will be further examined in detail in Chapter 5. This effect was observed at all values of EHT and also with the application of an electric field within the cavity volume. In general, the linear polarization with the microwave electric field aligned along the molecular beam axis produced the strongest transients.

On application of a static magnetic field applied in a direction perpendicular to the plane of the cavity plates, the build-up process became more stable; near-identical transients were observed in the two linear orthogonal polarizations and the variation in the build-up process between successive gas pulses was minimal (Fig. 2.6). This last effect can be explained simply from the static characteristics of the maser. Applying a magnetic field will drive the oscillation to circularity, hence all directions of oscillation build-up are identical, whereas an applied electric field will not change the polarization of the output power, which is in general elliptical. The oscillation settling transients in the two linear orthogonal polarizations were slightly out of phase during the oscillation build-up process (Fig. 2.6).

On applying a static potential difference between the cavity plates it was found that approximately 35V corresponding to an electric field of approximately $50Vcm^{-1}$ would completely quench the oscillation. With partial quenching, the oscillation settling transients were still observed with a noticeable increase in their period (Fig. 2.7a,b). This was similar to an effect observed by Lefrere (1974) where settling transients were observed in a closed cavity resonator in the presence of an inhomogeneous electric field. Here a large increase in self-induced Rabi oscillation period (by almost a factor of two) was observed from 10kHz (Fig. 2.5) to approximately 6kHz (Fig. 2.7a,b). For both the J=K=2 and the J=K=3 inversion transitions of $^{14}NH_3$ there were marked

FIGURE 2.6
OSCILLATION TRANSIENTS

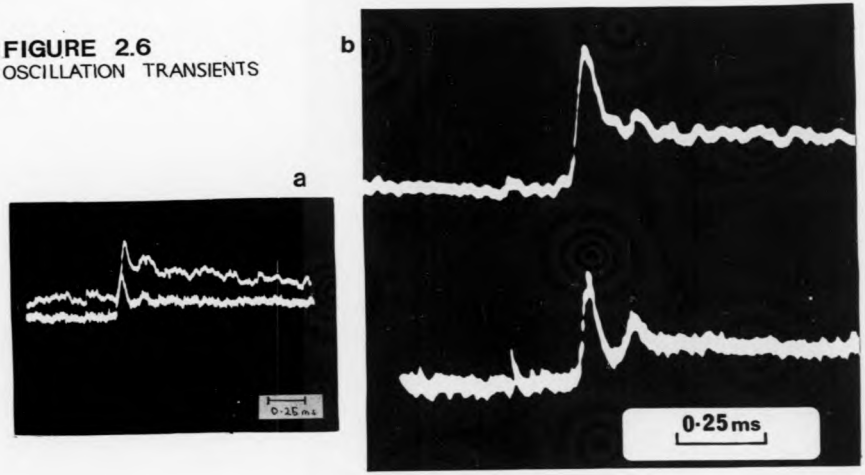

FIGURE 2.7 STARK AND ZEEMAN TRANSIENTS

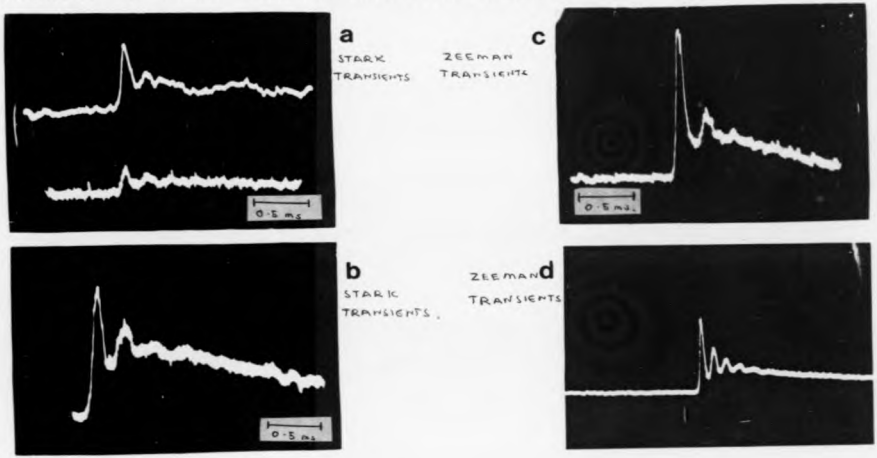

slowings in the decay constants. In zero applied electric field, two cycles of the oscillation transient (Fig 2.5) could be observed strongly and a third weakly; with 19 Volts applied across the cavity plates, four clear cycles of the oscillatory oscillation transients could be observed on the J=K=3 transition (Fig. 2.7a,b). The slowing of the decay constant was first observed in a closed resonator again by Lefrere (1974) in an inhomogeneous electric field, and will be discussed theoretically in Chapter 3.

It is predicted theoretically that the effect of applying a magnetic field to the maser cavity with its direction perpendicular to the cavity plates will also have the effect of slowing the decay constant and increasing the period of the transients, using a model of single frequency oscillation on a slightly Zeeman split spectral line. This is again studied theoretically in Chapter 3. and leads to the prediction of chaotic behaviour (Oraevskii 1981). For the J=K=2 transition, oscillation amplitude settling transient effects were obscured by the observation of a low frequency beat phenomenon which will be discussed later (Chapter 2). For the J=K=3 transition the beat effect was intermittent in nature and settling transients could be observed in an applied magnetic field. An increase in the period of the oscillatory settling transients was observed, and a slowing of the decay constant and enhancement of their third cycle was also observed in direct comparison with zero field transients (Fig. 2.7c), although the effect was neither as strong as predicted theoretically or observed experimentally with an applied electric field. A thin horizontal wire was placed in the fringe field of the maser cavity (Chapter 5) at a maximum depth of approximately 2cm. Here the oscillation became highly linearly polarized in the horizontal direction. Although strong pulsed oscillation was not obtained from the maser system at the time the experiment was performed, it was found that on applying a magnetic field

across the cavity plates as above, there was a dramatic slowing in the transient decay constant with a maximum of seven oscillation periods observed (Fig. 2.7d). The application of either an electric or magnetic field reduces the oscillation level of the pulse while enhancing the number of periods of the self-induced Rabi oscillation.

2.7 BIHARMONIC OSCILLATION IN A DISC RESONATOR MOLECULAR BEAM MASER

The first account of biharmonic oscillation and the associated beating effects in a disc resonator molecular beam maser was reported by Barchukov, Prokhorov and Savranskii (1963). A possible explanation for the beat effect was given (later) in terms of a Doppler split spectral line (Krupnov and Skvortsov 1965). The beat frequency was given as 3.8kHz, increasing to 5.4kHz under the application of an electric field. On placing a thin wire across the interior of the resonator cavity, (which presumably dramatically altered the anisotropy of the cavity), a low frequency beat was observed at 600Hz.

Low frequency biharmonic oscillations were observed in a disc resonator molecular beam maser (Lainé, Smart and Corb 1976). Here highly non-sinusoidal beats were observed between 250Hz and 750Hz, those at 750Hz under the application of an electric field. In these experiments a careful check was made to confirm that only a single maximum of the microwave electric field was present inside the cavity. On studying these beats in two linear polarizations an antiphase relationship was found between oscillations with orthogonal linear polarizations.

Using the maser system under study here, operated on the TEM_{001} cavity mode with a single maximum of microwave field across any diameter, no steady state continuous wave beating effects could be observed. Only after the application of a relatively strong magnetic field perpendicularly to the cavity plates did the two Zeeman components

break into biharmonic oscillation at 4.8kHz (Yassin 1981).

Upon operating the maser on the TEM_{101} mode with two maxima of microwave field, biharmonic oscillation could be obtained at a frequency of 7.5kHz presumably due to biharmonic oscillation on the split spectral line (Al-Jumaily 1979).

From this work it would appear that the beating effects could be grouped into two categories: (a) The high frequency beats that have a frequency greater than or equal to the natural width of the spectral line (approximately 4.8kHz), and which may be simply explained by biharmonic oscillation on Zeeman or Doppler split spectral lines. (b) Low frequency beats less than 4.8kHz whose origin is less obvious.

2.8 EXPERIMENTAL OBSERVATION OF DAMPED LOW FREQUENCY BIHARMONIC OSCILLATION UNDER AN APPLIED MAGNETIC FIELD

The pulsed beam maser system was operated as previously discussed. On the application of a magnetic field with the field direction again perpendicular to the plane of the cavity plates, a damped low frequency beating effect was observed on both the J=K=2 and the J=K=3 inversion transitions (Fig. 2.8). Fig. 2.8c,d show beat frequencies of 3.9kHz and 2.1kHz respectively. For the J=K=1 transition no beating effect could be obtained. The onset of the beating effect occurred at 1×10^{-4}T for the J=K=2 inversion transition of $^{14}NH_3$ corresponding to a beat frequency of 800Hz. As the magnetic field increased so did the associated beat frequency. At low fields the beat effect lasted only for few beat cycles, the amplitude modulation dying away to leave an unmodulated oscillation. At higher fields the modulation depth was nearly 100% and persisted for the whole of the length of the gas pulse. At still higher levels of magnetic field the oscillation amplitude was almost completely quenched. Here the beats become very dependent upon cavity tuning and it was possible to tune the

FIGURE 2.8 **BEAT EFFECT**

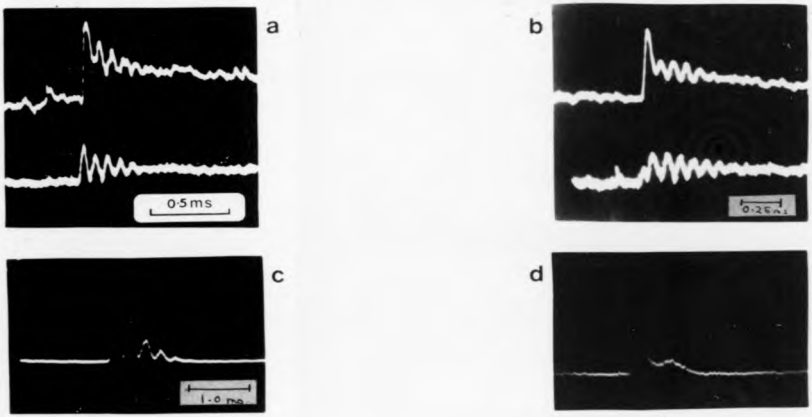

resonator cavity to a position where a completely unmodulated oscillation amplitude was observed. For the J=K=3 transition, the onset of low frequency occurred at a magnetic field of 1.6×10^{-4}T. The beats observed here were highly dependent upon cavity tuning for all values of magnetic field. It was possible to find a position of the cavity tuning to give unmodulated oscillation output at all levels of the magnetic field. The beat effects were highly dependent on the maser parameters and successive gas pulses produced markedly different effects. The beat effect was evident on one pulse and yet often absent on the following pulses (or vice-versa), where operating conditions must have been nearly identical.

The beating effect was observed in two linear orthogonal polarizations. The beats were in antiphase on the J=K=3 transition (Fig. 2.8a,b). All the beats discussed in this chapter, observed by the present detection system were sinusoidal. However, the same beating effect is studied in depth in Chapter 5. These beats, observed under relatively low applied magnetic field are highly non sinusoidal. They persist for only two or three complete periods at the most. The present beats discussed in this chapter are photographed at a frequency in excess of 2kHz, compared with 1-2kHz for the beats discussed in Chapter 5. The present beats are produced in the presence of a larger applied magnetic field. This has had the effect of driving the two oscillation components to near-circularity, resulting in a sinusoidal beat pattern. On rotating the waveguide to observe two linearly orthogonal polarizations, the beat effect condition became noticeably harder to satisfy. This suggests that rotating the waveguide significantly alters the anisotropy of the cavity, and that the condition for the observation of low frequency beats is cavity anisotropy dependent.

The system was returned to continuous wave operation, and the pulsed beam switching was replaced by the molecular Q-switching

technique. Here the low frequency beating effect was still obtained.

Using pulsed molecular beams, strong oscillation could be obtained on the second order cavity modes with both the J=K=2 and J=K=3 ammonia inversion transitions. Here two beats effects were observed. Firstly high frequency beats are observed at frequencies of 7.5kHz and 8kHz for the J=K=2 and J=K=3 transitions respectively. The beats observed on the J=K=2 transition were continuous and lasted for the whole duration of the oscillation pulse (Fig. 2.4b), whereas the high frequency beats observed on the J=K=3 transition were damped and lasted 4 to 5 beat cycles. On application of an electric field across the plates of the cavity a noticeable decrease in the frequency of the beats was observed. This beat effect is caused by the Doppler splitting of the spectral line into two components which then beat against each other and is well documented (Al-Jumaily 1979). Secondly a low frequency beating effect, presumably of the same origin as those described above, was observed when a weak magnetic field was applied. It is possible to observe these two different beating effects simultaneously.

2.9 INTERPRETATION OF THE DAMPED LOW FREQUENCY BIHARMONIC OSCILLATION

To understand the low frequency beat effect it is necessary to consider the static characteristics of the disc resonator molecular beam maser under the application of a weak magnetic field. Under many operating conditions there are two possible polarization orientations which are in general elliptical for the oscillation output power. These two oscillations occur at different frequencies (Yassin et al 1985). In the presence of applied magnetic field these two oscillation polarizations tend to circularity (Yassin 1981), and the frequency difference between them increases to the order of several kHz before Zeeman beats set in at a frequency of 4.8kHz. It is proposed here that the difference of frequency in jumping from one stable oscillation

polarization to another in the static case corresponds to the beat frequency observed here. The initial gas pulse shock-excites both of the possible elliptical oscillations. These oscillations then beat against each other to give the low frequency beating effect. The tuning of the maser cavity and anisotropies in the maser system itself will favour oscillation on one of these elliptical oscillations rather than both simultaneously. This oscillation will then become the stronger one. The weaker oscillation will give way to the strong oscillation and eventually die. Hence the beat effects die away to give a "steady state" power output. At relatively high fields, the damped beats give way to continuous beats as the condition for Zeeman biharmonic oscillation is reached. At yet higher fields the two Zeeman components become further split and since these can have slightly different oscillation thresholds, an almost quenched oscillation will give "continuous" oscillation on one component only.

Consider now the J=K=1 transition. Here a strong state selector anisotropy is present as a result of which the oscillation power output is linearly polarized along the axis of the molecular beam. With continuous wave studies on this transition neither elliptical oscillation nor frequency jumps have been observed, presumably due to the strong anisotropy present. With pulsed beam operation, even with a relatively large oscillation overfulfilment factor R no beating effect could be observed on the application of a magnetic field. Presumably if a larger overfulfilment factor could have been obtained, biharmonic oscillation would have been realized with a large applied magnetic field as the condition for Zeeman beats was eventually fulfilled.

It is proposed that the lowest frequency at which beats are obtained is dependent on the anisotropies (including both cavity and state selector) of the maser system. For a nearly perfectly isotropic system very low frequency beats may be obtained under the application of

a very small magnetic field. When one of the cavity waveguides was rotated in order to study the beat effect in two linear orthogonal polarizations the beat effect became far harder to observe, being intermittent in nature. Successive gas pulses often showed a change from beats to a unmodulated gas pulse and then returning to beats on the next pulse. The magnetic field required to produce beats was also somewhat increased, and the modulation depth of the beating effect was much reduced. This effect is related to build-up effects discussed in Chapter 5 where almost identical initial conditions produce largely different gas pulse shapes.

It is proposed here that the occurrence of beats in a gas pulse is dependent on the time during the pulse that the thresholds for the two components are satisfied, the rate of build-up of the stronger oscillation component and the Zeeman splitting of the spectral line. For example if there is a significant time between the occurrence of the thresholds for the stronger and weaker components, there may be a large build-up of the strong oscillation component before the threshold for the weak component is satisfied. Any oscillation on the weak component will now be phase locked to the strong component of oscillation before it has had time to develop. If the thresholds for the two components are met within a relatively short time interval, there is very little build-up of the strong component before the onset build-up of the weaker component, and therefore there is no strong oscillation for the weaker component to which it can be phase locked and so the weaker oscillation component builds up independently at its own oscillation frequency, giving biharmonic oscillation. Rotating the waveguide changed the cavity anisotropies significantly and changed the initial conditions within the maser cavity leading to a weakening of the beat effect.

It is also proposed that under a moderate applied magnetic field, the two components of the low frequency beats are nearly circular

in polarization, with the electric field vectors rotating in opposite directions. The sum of these two oscillations gives a linearly polarized resultant which rotates in time at the frequency of the observed beats. At relatively low applied magnetic fields the two beating oscillation components may be either elliptically or linearly polarized, which will lead to a non-sinusoidal beat pattern. This is observed and discussed in Chapter 5. The above is consistent with antiphase beats.

Finally it is interesting to compare the low frequency beats observed here with the beating effects observed by previous authors. On applying an electric field across the cavity plates of the maser while observing high frequency beats on the second order TEM_{101} mode due to a Doppler split spectral line (Al-Jumaily 1979), a decrease in beat frequency was observed, as stated earlier. This may be explained by the electric field broadening of both components which increases their coupling and allows the two oscillation components to be frequency pulled towards each other. For the beats of the type observed by Smart(1974) and Barchukov et al (1963) an increase in electric field increased the beat frequency. For both experiments zero magnetic field beats are observed. For the present system an applied electric field along with the applied magnetic field has the effect of decreasing the beat frequency. An explanation of a near perfect isotropic system in which the earth's magnetic field is sufficient to induce beats may be proposed; however this can be discounted because a near-isotropic system would produce near-circular oscillation components and give sinusoidal beats. However the beats obtained by Smart (1974) were highly non-sinusoidal which suggests that they were obtained by beating together of two highly elliptical oscillations. Highly non-sinusoidal low frequency beats in both zero and an applied magnetic field are observed and discussed in Chapter 5. The best explanation so far for

these beats appears to be that they are induced by the anisotropy of the system which somehow lifts the degeneracy of the $\Delta M = \pm 1$ transitions so that low frequency beats may occur. This is consistent with the work of Barchukov et al (1963) where a wire is placed inside the maser cavity, which must greatly increase the anisotropy. A low frequency beat at 50Hz was obtained. The effect of the anisotropy still appears to be a puzzle. For moderate anisotropy, the beat effect in a weak magnetic field is removed, yet for higher anisotropy values zero field beats are induced. Low frequency beats are discussed further in Chapter 5.

CHAPTER THREE

THEORETICAL EXPLANATION OF SOME OF THE TRANSIENT EFFECTS OBSERVED IN MASER SYSTEMS

3.1 INTRODUCTION

This chapter is concerned with the interpretation of the results of the settling transient experiments described in Chapter 2. An explanation of the observed stark transients is presented and a comparison is made with previous work undertaken by Lefrere (1974). The final sections of this chapter are a brief study of the possibility of obtaining chaotic behavior within a molecular beam maser system.

3.2 THE ORIGINS OF THE MASER EQUATIONS

A semiclassical approach is used to interpret the dynamic properties of a maser system, that is the radiation field is described classically and the radiating molecules are treated quantum mechanically. Starting from Maxwell's equations the equations below may be derived for an ideal two level system. These form a closed system of equations for the maser and are given below (Oraevskii 1964a)

$$(3.1)\quad \partial^2\varepsilon/\partial t^2 + (\omega/Q)(\partial\varepsilon/\partial t) + \omega_0^2\varepsilon = -4\pi[\partial^2/\partial t^2]\int_V NP(x,t)E\partial v$$

$$(3.2)\quad \partial^2 P/\partial t^2 + (2/\Gamma_2)(\partial P/\partial t) + \omega_{ab}^2(1 + 1/\omega_{ab}^2\,\Gamma_2^2)P = -2(|\mu_{ab}|^2/h)\omega_{ab}(D + D_0)$$

$$(3.3)\quad \partial D/\partial t + D/\Gamma_1 = (2/h\omega_{ab})\varepsilon(\partial P/\partial t + P/\Gamma_2)$$

Here t is real time, Q is the quality factor of the cavity, ε and P are respectively the electric field within the cavity and the molecular polarization, D and D_0 are the population differences between upper and lower levels and rate of pumping of the active medium. Γ_1 and Γ_2 are the relaxation times of level population and polarization governing spectral linewidth respectively, ω is the resonance frequency of the resonator, N is the density of active molecules, $|\mu_{ab}|$ is the matrix element of the electric dipole moment of the particles, and

$\omega^2(1 + 1/Q) = \omega_0^2$.

Following the procedure of Oraevskii (1964), the following equations are obtained.

(3.4) $-X_0\phi_0' = \delta X_0 + k_1 V_0$

(3.5) $-X_0' = h_0 X_0 + k_1 U_0$

(3.6) $-V_0\phi_0' + U_0' = -h_2 U_0 \cdot h_2 X_0 W_0 - k_2 X_0$

(3.7) $U_0\phi_0' + V_0' = -h_2 V_0$

(3.8) $W_0' = -h_1 W_0 + h_2 X_0 U_0$

X_0 is proportional to the electric field within the resonator,

U_0 and V_0 are proportional to the imaginary and real parts of the molecular polarization,

W_0 is proportional to the population difference between the upper and lower inversion states.

Here $h_1 = 1/\omega_{21}\Gamma_1$, $h_2 = 1/\omega_{21}\Gamma_2$, $2h_0 = (1/Q)(\omega_0/\omega)$ $2k_2 = 2h_2 D_0$, $2k_1 = 4\pi N|\mu_{12}|^2 h^{-1}\Gamma_2$, $\omega_p^2 = (\omega_{ab}^2 + 1/\Gamma_2^2)$, $\delta = 0.5(\omega_0^2 - \omega_p^2)/\omega_p^2$

The assumption is made that the Q factor of the spectral line is much greater than the Q factor of the cavity, which is itself much greater than unity. Under steady state conditions the left hand terms of the above equations which contain time derivatives become zero. The expression for the output power which is proportional to $(X_0)^2$ can be obtained,

(3.9) $X_0^2 = [k_1 k_2/h_0 h_2 - 1 - \delta^2/(h_2 + h_0)^2]h_1/h_2$

At resonance, X_0 and $(X_0)^2$ are at a maximum, therefore $\delta = 0$ and from (3.4) $\phi_0' = -k_1 V_0/X_0$. Substituting into eqn (3.7) gives $-U_0 k_1 V_0/X_0 + V_0' = -h_2 V_0$ therefore $V_0' = -V_0(h_2 - k_1 U_0/X_0)$. U_0 and X_0 are of opposite signs except for the chaotic regime of operation; thus $V_0' = -V_0$, and therefore at resonance $V_0 = 0$.

Consider the system at resonance, the simplified equations may be applied.

(3.10) $-X_0' = h_0X_0 + k_1U_0$

(3.11) $U_0' = -h_2U_0 - h_2X_0W_0 - k_2X_0$

(3.12) $W_0' = -h_1W_0 + h_2X_0U_0$

Here as before,

X_0 is proportional to the electric field inside the resonator

U_0 is proportional to the polarization of the active medium

W_0 is proportional to the population inversion

The series of equations (3.10 - 3.12) can be used to display oscillation amplitude settling transients quite successfully.

The steady state solutions here, which correspond to normal continuous wave maser action as again obtained for $X_0' = U_0' = W_0' = 0$

(3.13) $X_0 = (h_1/h_2)[(k_1k_2/h_0h_1)-1]^{1/2}$; $U_0 = -(k_1/h_0)X_0$; $W_0 = h_2h_0/h_1k_1$

For an ammonia maser $h_1=h_2$ and $h_0>>h_1$.

To produce oscillation amplitude settling transients it is required to switch one of the maser parameters rapidly, so it is important to consider how switching techniques affect the maser equations. The number of state selected molecules entering the maser cavity is proportional to k_2, therefore a variation in the beam intensity, for example switching on and off a pulsed nozzle source, will produce a change in the value of k_2. An approximate functional time dependence for the number of state selected molecules entering the maser should therefore allow the settling transients to be simulated numerically.

The effect of a spectral line Q switched maser is a little less obvious. Here the spectral line width is being artificially broadened hence the value of h_2 is being increased as Γ_2 is made smaller. However since $k_2 = h_2N_0$ and the rate of pumping of state selected molecules remains the same, k_2 is also increased. Now k_1 is proportional to Γ_2, therefore k_1 is also decreased. Hence k_2 is proportional to h_2.

The series of equations (3.10 3.12) are all first order coupled

differential equations which make them ideal for numerical solution.

The parameters h_0, k_1, k_2, h_2, are all known approximately and therefore numerical solutions could be found easily for the system.

3.3 NUMERICAL SOLUTIONS TO THE DIFFERENTIAL EQUATIONS

The standard Taylor series method was used to solve the differential equations. Taylor series expansion gives

(3.14) $f(x+h) = f(x) + hf'(x) + [h^2/2!]f''(x) + \text{-------} + [h^n/n!]f^n(x)$

The equation may be extended to solve a series of equations (Jain 1979). The system of differential equations (3.10 - 3.12) could be differentiated several times to give several terms in practice. Terms up to the third derivative were calculated and added to the series. However it was found simpler and more efficient in terms of computer time to use only the first derivative, hence the differential equations could be used in their original form. Initially the program was written in BASIC but later it was rewritten in FORTRAN as this was found to be more efficient. A step length of T = 2500 printing every 250 iterations, gave a suitable display. A computer graph plotting routine which plotted up to 200 points was then used to give graphical solutions relatively quickly. A check on the accuracy of the plots could be made by reducing the step length and increasing the number of iterations between each printed value. The programs were executed on the Keele GEC 4000 series mini computer. Examples of the programs are shown in Appendix 1. An example of the traces produced is shown in Fig. 3.1, which is similar to the exponential traces of Chapter 2.

3.4 MASER THEORY APPLIED TO A PULSED BEAM AND A MOLECULAR Q SWITCHED MASER

The simplest build-up situation which may be considered theoretically is one where a maser parameter is rapidly changed so that

FIGURE 3.1

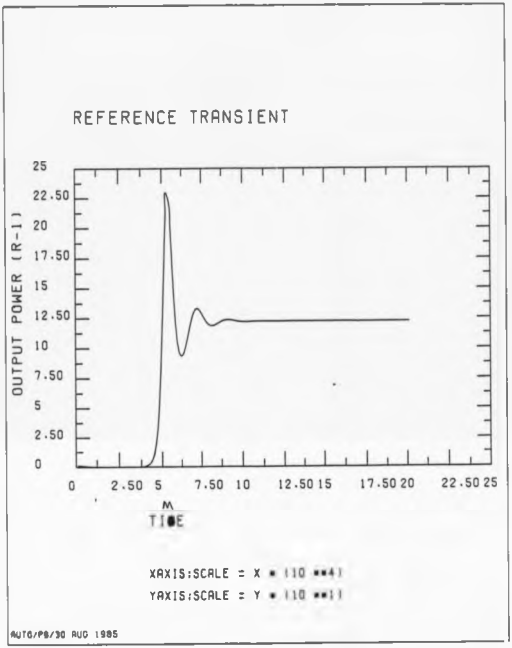
REFERENCE TRANSIENT
OUTPUT POWER (R-1)
25
22.50
20
17.50
15
12.50
10
7.50
5
2.50
0
0
2.50
5
7.50
10
12.50
15
17.50
20
22.50
25
TIME
XAXIS:SCALE = X * 110 **4)
YAXIS:SCALE = Y * 110 **1)
AUTO/PB/30 AUG 1985

the speed of switching is far more rapid than the period of any oscillation amplitude settling transients observed. This is easily obtained with a molecular Q-switched maser where an electric field placed across the maser cavity is repeatedly applied to produce fast nonmechanical switching. The maser system considered in the previous chapter, operated under conditions of high pressure molecular beams with a small sized nozzle cap produced an extremely rapid build-up, and so was a very good approximation to the above system. Extensive experimental results with a molecular Q-switched maser were obtained by Lefrere (1974) who used a closed cavity resonator.

Consider now the build-up of oscillation in either a pulsed beam or molecular Q-switched maser. For the pulsed beam maser, the cavity Q value is approximately 4500, the spectral linewidth is approximately 5kHz, and so parameters h_0, h_1 and h_2 in the maser equations are determined. On applying the equations to the systems discussed here, values of parameters k_1 and k_2 were chosen to give the best fit with experimental results. However at low levels of the oscillation overfulfilment parameter the traces obtained were independent of the ratio k_1/k_2. For a constant overfulfilment condition R where $R=(k_1k_2/h_0h_1)$ the ratios h_0/h_1, h_0/k_1, h_1/k_1, h_1/k_2 and k_1/k_2 were varied in turn and the results are displayed graphically (Fig. 3.2 - 3.4). It was found that the ratio of the height of the first transient to that of the steady state oscillation level and the ratio of the height of the first transient to that of the second were both independent of the parameters k_1, k_2, h_0, h_1 and were dependent only upon the overfulfilment parameter R. Hence an observation of the shape of an oscillation amplitude settling transient enables an estimate of the overfulfilment condition of the maser oscillation to be obtained. Increasing the overfulfilment factor by increasing the number of state selected molecules entering the cavity (parameter k_2) also slightly

FIGURE 3.2

EFFECT OF BOTH HO AND K1 BEING INCREASED

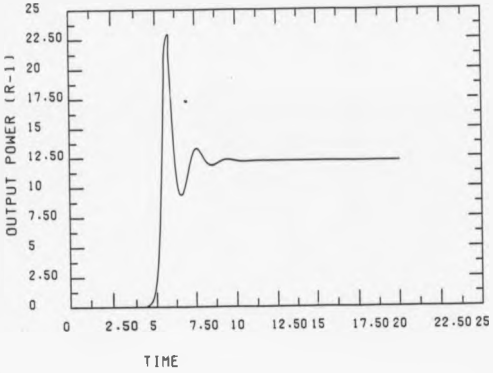

EFFECT OF BOTH HO AND K2 BEING DECREASED

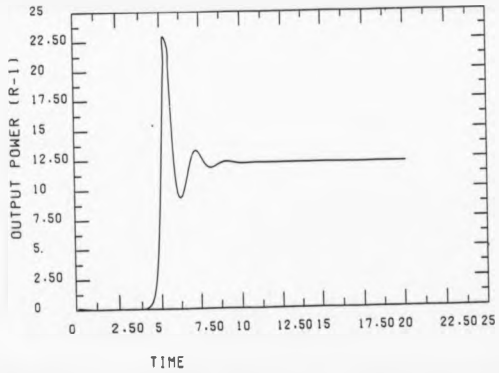

FIGURE 3.3

EFFECT OF INCREASING RATIO HO/H1

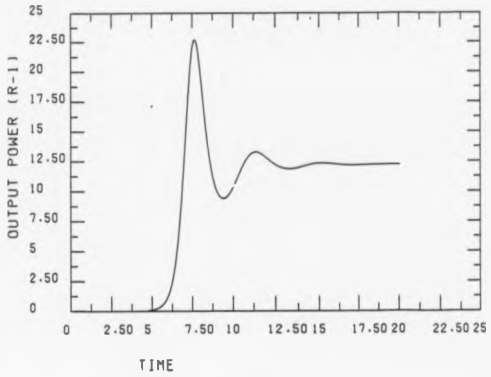

EFFECT OF INCREASING RATIO K1/K2

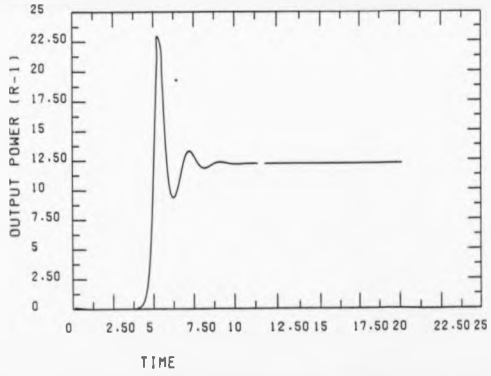

FIGURE 3.4

EFFECT OF BOTH H1 AND K2 BEING DECREASED

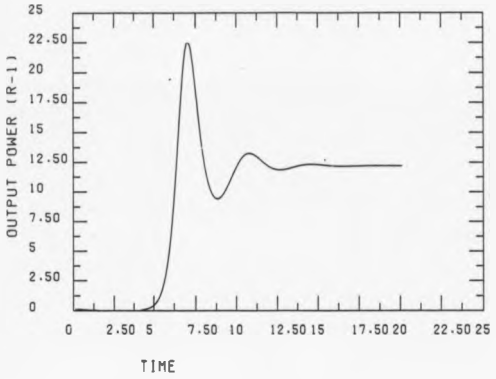

EFFECT OF BOTH H1 AND K1 BEING DECREASED

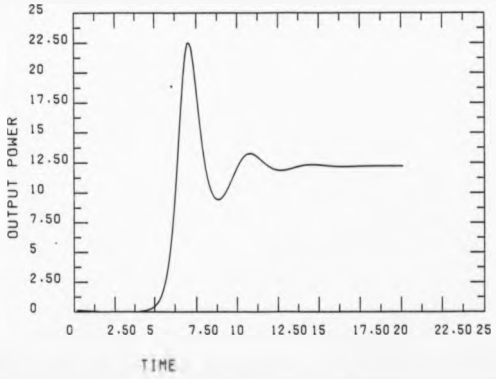

decreases the period of the transients. For the transients observed using the molecular Q switched maser, values of cavity Q of 9000 and spectral linewidth of 5kHz were substituted into the maser equations in agreement with those reported by Lefrere and Lainé (1974). For both systems the initial values of X_0 and U_0 were set at small finite values to simulate thermal noise. The exact initial values are not important as build-up of both X_0 and U_0 is exponential in nature during the very early stages.

3.5 STARK TRANSIENTS AND ZEEMAN TRANSIENTS

On application of a weak stark electric field across the plates of the open resonator pulsed molecular beam maser, the form of the oscillatory oscillation settling transients are changed. The period of the transients increases and the decay constant becomes longer until at least four clear oscillatory transients may be observed (compared with three in zero field), and the total output power level has been somewhat reduced (Chapter 2)(Fig. 2.7). Similar results have been obtained by Lefrere (1974) where an electric field is used to partly quench a maser oscillation and the change in maser output power level induces transients (molecular Q switching). Here the transients produced in the presence of an electric field are step down transients rather than the step up transients studied in the pulsed beam system (Fig. 3.5b). However it can be shown from the maser equations that both the period and the decay constant of the transients depend on the final steady state conditions, and not on whether step up or step down transients are being studied. Other differences between the two experiments are as follows. The pulsed beam maser employed a uniform Stark field in an open disc resonator, whereas the molecular Q switched maser employed an inhomogeneous electric field inside a cylindrical resonator. On application of a static magnetic field perpendicular to the plates of

FIGURE 3.5 STARK TRANSIENTS

STARK SWITCH

a

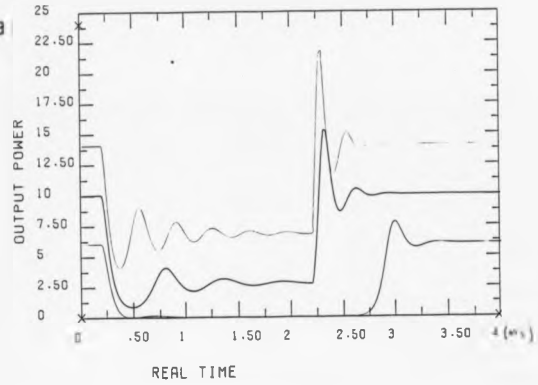

b After Lefrere 1974

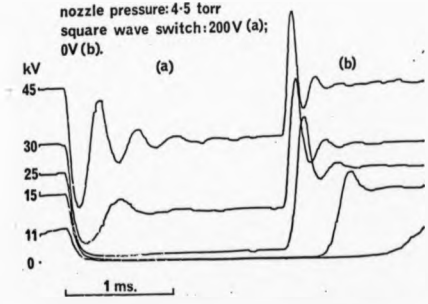

the open resonator of the pulsed beam system, similar results were obtained, with a lengthening of the decay constant and an increase in the period of the transients, although the effect was not as marked. An explanation of the electric field induced effect in terms of "Forced Regenerative Nutation" has been proposed (Lefrere and Laine 1974). However it would appear that either the applied electric or magnetic field modifies the spectral line shape by either Stark or Zeeman splitting.

It was assumed that the application of an electric field across the maser cavity inhomogeneously broadened the spectral line. The maser equations may now be modified to account for this inhomogeneous broadening. Consider to a first approximation, that the Stark broadened transition resembles a Zeeman split line, i.e. the spectral line is split into two main components whose spectral profiles overlap. This system may then be considered as two coupled non-linear oscillators whose resultant oscillation frequency lies midway between the transition frequency of the two components. This system has been studied by Oraevskii (1981) and will be discussed later (Chapter 3) in relation to chaos theory. The system may be described by the following equations.

(3.17) $X_0' = -h_0 X_0 - k_1 U_0$

(3.18) $U_0' = h_1(-U_0 + (B\xi W_0/\alpha) + X_0 Z_0)$

(3.19) $Z_0' = h_1(-Z_0 + CR + X_0 U_0)$

(3.20) $W_0' = h_1(-W_0 - (\alpha\xi U_0/B))$

Here $h_2 = h_1$. ξ represents the frequency shift of each component of the spectral line. It is assumed that the two components are of equal intensity and are situated symmetrically about the centre frequency of the resonator mode. This is therefore a very rough approximation.

Solving these equations numerically with $\xi = 0.85$ theoretical curves were obtained (Fig. 3.5a). These curves agreed well with the

experimental step-up transients observed in the presence of a Stark field and also the step-down transients obtained by Lefrere (1974) (Fig. 3.5b). The decay constant of the Stark transients predicted by this split spectral line model are much smaller than the decay constants of the zero field transients. This agrees well with experimental results (Fig. 3.5). The period of the theoretically predicted Stark transients is also greater than the period of the zero field transients although the difference is not as great as observed experimentally. The main discrepancy appears in the amplitude of the Stark step-down transients which is somewhat smaller than the amplitude of those obtained experimentally. Despite its simplicity, the split spectral line model explains the major features of the experimentally observed Stark and Zeeman transients.

Consider finally the lowest trace of the step-down Stark transients (Fig. 3.5a) during the application of the electric field. Here the oscillation threshold condition was not fulfilled. The residual output power level was sufficient, however, to allow for a build-up of oscillation power from the residual signal with a "time of silence" of approximately 0.45 milliseconds without taking into account the effect of thermal noise.

3.6 A MODEL OF THE MASER GAS PULSE

During work considered earlier in this chapter it was assumed that the variation of the maser parameters occurred much faster than the duration of the dynamic effects which follow such changes. However the process of switching the pulsed beam which is necessary to study the ensuing maser power build-up may be a relatively slow process. Therefore the time dependence of the number of active molecules entering the maser cavity must be considered by making the parameter k_2 in the dynamic maser equations change in a finite rather than instantaneous

time.

Consider first the passage of gas through the gas valve. The gas is initially held in the supply pipe behind the valve at a pressure P_1. The gas then passes through a variable sized orifice of size $A_1(t)$ into a small cap of volume V_1 at a pressure P_2. A slit or circular hole source is attached to this cap, of area A_2. The assumption here is that the flux of molecules leaving the valve is proportional to the pressure inside the cap at P_2. The time variation of the pressure P_2 inside the cap may be written as follows.

(3.21) $dP_2/dt = \alpha(P_1 - P_2)A_1(t) - \alpha P_2 A_2$

Now the variable size of the valve orifice $A_1(t)$ is due to a mechanical plunger being moved from rest due to a force being applied through the magnetic effects of the solenoid. The movement of this plunger and hence the orifice size will take the form (Bassi et al 1981)

(3.22) $A_1(t)=(\beta t^2)$

where the opening time is between 0.3ms and 0.5ms. This expression will not remain accurate as the plunger approaches its fully open position. Initially the cap is empty of gas and $P_2 = 0$. In the later stages of gas build-up the term $P_1 - P_2$ is small and the pressure builds up slowly to reach an asymptotic limit. A time dependence for P_2 can now be obtained by solving the above differential equation for P_2 numerically, since the parameter α can simply be determined from the volume of the cap and kinetic theory. However it is neater if an analytical function can be used to approximate the curves as this can be carried forward in a modified form to feed into the dynamic equations. A time dependence of the form

(3.23) $P_2 = P_0[1-\exp(-Bt^2)]$

is chosen as an analytic approximation. This function is proportional to t^2 at small t and reaches an asymptotic limit P_0 at large t. As the molecular beam leaves the cap and passes through the maser a

large fraction of the molecules in the beam are scattered by background gas. The time dependence of the intensity of a molecular beam downstream passing through background gas is given by Beers Law (Bassi et al 1981) as

(3.24) $I(t) = I_0(t)\exp[-\sigma dn(t)]$

$I_0(t)$ is the flux of molecules leaving the valve nozzle, σ is the cross section of scattering of the beam by background molecules, and $n(t)$ is the average density of molecules in the background gas. Consider now a fixed point downstream. The total number density of molecules in the background gas at time t is given by N_d

(3.25) $N_d = C\int_0^t K(1 - \exp(-Bt^2))$

Here C is a parameter which is partially dependent on the size of the vacuum chamber. It is assumed here that the initial scattering is negligible and that the number of molecules contributing to the scattering process in the background gas is proportional to the number of molecules entering the chamber. The final form of the gas pulse downstream of the nozzle valve is given by F(t) where:

(3.26) $F(t) = D[1 - \exp(-Bt^2)]\exp[-C\int_0^t K(1 - \exp(-Bt^2))]$

Here C and D are constants. It has been assumed during this derivation that the molecular beam has a negligible velocity spread, which will only be valid when the maser is operated under a relatively high source pressure, and so the above equation may have to be modified. The vast majority of the scattering of the molecular beam takes place in the side chamber, the background gas in the main chamber and hence the scattering effects are limited by the gas dynamic shutter effect (Bassi et al 1981). Thus, the molecular beam is heavily attenuated in the maser side chamber, and therefore relatively few molecules reach the main chamber during the gas pulse and so scattering in this chamber remains small. It is also assumed that scattering by the state selector bars remains proportional to the number of molecules in the beam, as is

FIGURE 3.6

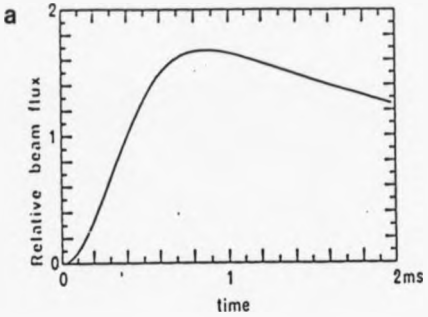

CALCULATED TIME EVOLUTION OF GAS PULSE

RESULTING OSCILLATION BUILDUP

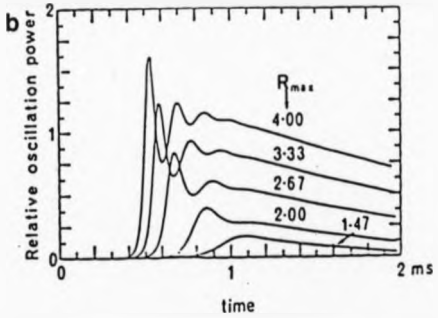

the fraction of molecules state selected. The above equations can thus be used as an approximation to the number of active molecules entering the resonator as a function of time.

The calculated shape of the gas pulse is shown in Fig. 3.6a. The oscillation output power level computed as a function of time, computed for various levels of the oscillation overfulfilment condition R, displaying the theoretical transients, is shown in Fig. 3.6b. There is a reasonable similarity between the transients observed experimentally and those calculated theoretically using the dynamic equations of Oraevskii. It would be interesting to measure directly the intensity of the molecular beam entering the maser cavity as a function of time, which could then be compared with the curve obtained from the equation above, and also give a more reliable result to enter into the dynamic maser equations.

3.7 THE POSSIBILITY OF REACHING A CHAOTIC REGIME OF OPERATION OF THE AMMONIA MASER

The oscillation amplitude settling transients considered so far in this chapter have all been exponentially damped, so that the transients finally give way to a steady state level of maser oscillation power output. Continuous pulsations of maser oscillation have however been obtained by the modulation of a parameter of the system (Bardo and Laine 1969). Solutions may be found to the equations governing the dynamic properties of the maser system where the output power varies continuously as a function of time, and a steady state solution is never reached. A set of initial conditions may be obtained where both a time varying solution and a steady state solution may exist for the same set of equations (Oraevskii 1981).

The equations which govern the dynamic properties of the maser system may be written in the following form (Oraevskii 1981).

(3.27) $\dot{x} = -\sigma(x - y)$

(3.28) $\dot{y} = -y + xz$

(3.29) $\dot{z} = -b(z-r) + (1-r)xy$

These equations have been normalised so that under steady state condition $|x| = |y| = z = 1$. For the present maser system under consideration $b=1$ $\sigma \simeq 1000$ The above equations are identical in form to those considered earlier.

(3.10) $-X_0' = h_0X_0 + k_1U_0$

(3.11) $U_0' = -h_2X_0 - h_2X_0W_0 - k_2X_0$

(3.12) $W_0' = -h_1W_0 + h_2X_0U_0$

The first problem was therefore to equate parameters. Let $X_0 = Ax$; $U_0 = By$; $W_0 = (Cz+D)$; therefore $X_0' = Ax'$ $U_0' = By'$; $W_0' = Cz'$. The time derivatives X_0' and $\dot{x}$ are differentiated with respect to different slow times ($x_0' = h_2\dot{x}_0$), and these equations are only totally valid when the resonance frequency of the cavity resonator is equal to the centre frequency of the spectral line, which then becomes the oscillation frequency. Substitution gives

(3.30) $-Ah_2\dot{x} = -h_0Ax + k_1By$

(3.31) $Bh_2\dot{y} = -h_2By - h_2Ax(Cz+D) - k_2Ax$

(3.32) $Ch_2\dot{z} = -h_1(Cz+D) + h_2Ax8y$

Equating coefficients:

$\sigma = -Bk_1/Ah_2$; $AC/B = 1$; $-h_2D - k_2 = 0$; $-D/C = Br$; $(1-r) = AB/C$ this gives $A = [(k_2k_1/h_2h_0) - 1]^{1/2}$; $B = -(h_0/k_1)[(k_2k_1/h_2h_0) - 1]^{1/2}$; $C = h_0/k_1$ $D = -k_2/h_2$; $r = k_2k_1/h_2h_0$

For the maser system under consideration the following parameters were chosen, $h_0 = 1.2\times10^{-4}$, $h_1 = 1.3\times10^{-7}$, $k_1 = 1.0\times10^{-4}$ $k_2 \geq 2\times10^{-7}$, this gives $\sigma = 923$ and $b = 1$.

Consider the phase space diagrams formed by plotting values of x,y,z on three mutually orthogonal axes. The chaotic regime is characterized by the property that two trajectories in the phase space

which follow very close paths, separated by a small finite element, diverge so that at a later time the two trajectories have a large separation in the phase space. The effect of this is that any small perturbation in the system will completely change the pattern of the maser output power. The maser output power is then predicted to appear as a series of irregular spikes.

The important study here is to determine how the onset of the strange attractor (chaotic) regime is dependent on the overfulfilment condition R. Ruelle (1980) gives a definition of a strange attractor. For very large overfulfilment parameter values, the whole phase space becomes a strange attractor. The value of R required for this to happen (R_0) is given by Oraevskii (1981), as the condition for every point in the phase space to become unstable. This however does not always lead to chaotic behaviour, as uniform modulation of the maser output power may follow. For the maser system under consideration the value of R_0 is approximately 1000, that is using the measured cavity Q and molecular Q-values in the dynamic equations, sufficient molecules must enter the cavity resonator per second so that the oscillation threshold is overfulfilled 1000 times before the whole of the phase space becomes unstable.

Following the method of Oraevskii a simple study of the maser equations was undertaken. The theoretical result of increasing the maser overfulfilment factor R is shown (Fig. 3.7 - 3.8). At R > 1000 continuous modulation of the maser output power is predicted, although without chaos. Successive oscillation spikes increase in amplitude (Fig. 3.8b) and decrease in width. The oscillation power level predicted between each spike decreases successively to a very low level. Eventually the oscillation level reached between each oscillation spike will drop below the level of thermal noise. This will lead to a series of irregular oscillation spikes determined by thermal noise in the maser

FIGURE 3.7

a

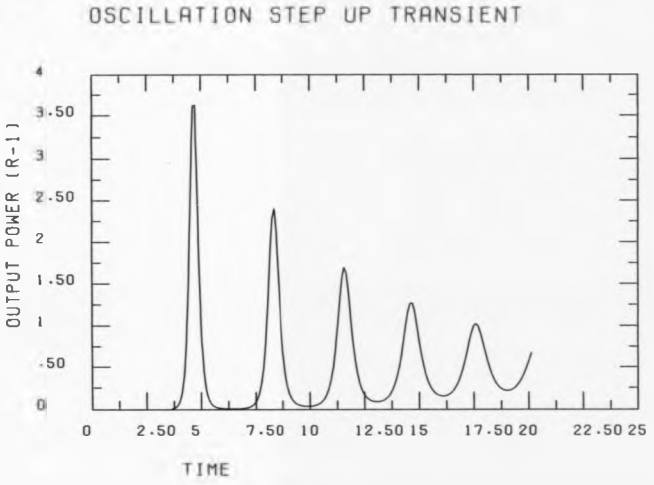
OSCILLATION STEP UP TRANSIENT
OUTPUT POWER (R-1)
4
3.50
3
2.50
2
1.50
1
.50
0
0
2.50
5
7.50
10
12.50
15
17.50
20
22.50
25
TIME

FIGURE 3.8

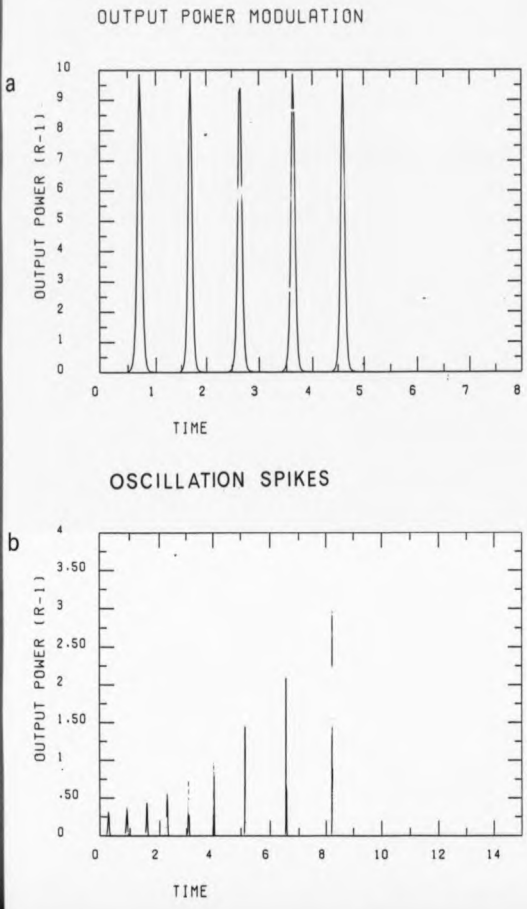
OUTPUT POWER MODULATION
a
OUTPUT POWER (R-1)
10
9
8
7
6
5
4
3
2
1
0
0
1
2
3
4
5
6
7
8
TIME
OSCILLATION SPIKES
b
OUTPUT POWER (R-1)
4
3.50
3
2.50
2
1.50
1
.50
0
0
2
4
6
8
10
12
14
TIME

cavity.

The maximum overfulfilment parameter R obtained in the present maser even with pulsed beam operation is approximately 3.5 and so any attempt to reach the chaotic regime with the present system is hopeless.

Consider now a maser oscillation on a spectral line split slightly into two components, by, for example a magnetic field to give two Zeeman components. Let the spectral line components be placed symmetrically about the centre of the resonance, and the intensities of the components be equal. The system may be described by the following set of equations (Oraevskii 1981) which are an extension of those given earlier.

(3.33) $\dot{x} = -\sigma(x-y)$

(3.34) $\dot{y} = -y + \xi w + (1+\xi^2)xz$

(3.35) $\dot{z} = -(z-r) + (1-r)xy$

(3.36) $\dot{w} = -w - \xi y$

The system has been normalized as before. When the two component oscillations are resolved, $\xi = 1$ and the system breaks into biharmonic oscillation. Here x, z are as defined earlier, y is the half sum of the imaginary part of the polarization of the two components, and w is the half difference of the real parts of the polarization. From earlier, $x = X_0/A$; $y = U_0/B$; $z = (W_0-D)/C$. Changing variables, $Z_0 = (W_0-D)$; $z = Z_0/C$ and substituting into the above equations:

(3.37) $X_0'/(A\,h_2) = (h_0/h_2)[X_0/A - U_0/B]$

(3.38) $U_0'/(B\,h_2) = -U_0/B + \xi w + (1+\xi^2)(X_0/A)(Z_0/C)$

(3.39) $Z_0'/(C\,h_2) = -(Z_0/C - R) + (1-R)(X_0/A)(U_0/B)$

(3.40) $w_0'/h_2 = w_0 - U_0\xi/B$

Now $(1-R) = AB/C$, also adding $W_0 = \alpha w$

(3.41) $X_0' = -h_0 X_0 - k_1 U_0$

(3.42) $U_0' = -h_2(-U_0 + (B\xi W_0/\alpha) + X_0 Z_0(1+\xi))$

(3.43) $Z_0' = h_2(-Z_0 + CR + X_0 U_0)$

(3.44) $W_0' = h_2(-W_0 - (\alpha\xi U_0/B))$

Two problems remain, firstly the normalization has not been completely lost, as the steady state value of the output power is independent of ξ. Increasing ξ splits the spectral line into two components, and therefore a corresponding decrease in output power occurs in reality. Replacing the $1 + \xi^2$ term by unity gives an acceptable dependence of the output power on ξ, so it would appear that the ξ part of this term has been added as part of the normalization. Output power dependence is now given by:

(3.45) $X_0^2 = (R - \xi^2 - 1)$

and so when $\xi = 1$, which corresponds to the complete resolution of the two components and the onset of Zeeman beats, the threshold for oscillation has been increased to 2R. Therefore the above equation in U_0' is rewritten as

(3.46) $U'_0 = h_1(-W_0 + (B\xi W_0/\alpha) + X_0 Z_0)$

Secondly the value of the parameter α has not been determined. The time derivatives of X_0, U_0, and Z_0, were found to be independent of α. The value of B/α was initially set at unity, and this was varied on successive computer calculations to check that the form of the curves were independent of α. The equations are now in a form where all the parameters are known for the maser system under consideration.

The critical value for the whole of the phase space to support strange attractor solutions to the dynamic equations is given by Oraevskii as

(3.49) $R_* = \sigma\,[\sigma(1 - \xi^2) + 4]/(\sigma - 2)(1 + \xi^2)$

The $(1 + \xi^2)$ term follows from the normalization and so may be dropped, which gives

(3.50) $R_* = \sigma\,[\sigma(1 - \xi^2) + 4]/(\sigma - 2)$

For $\xi = 1$ $R_* = 4$ and so at the onset of biharmonic oscillation the overfulfilment factor required for the whole of the phase space to give strange attractor solutions to the dynamic maser equations has been reduced from approximately 1000 times to 4 times.

The results of a theoretical study of the onset of chaos performed by the solution of equations (3.41 - 3.44) is shown in Fig. 3.9. In each successive trace the value of ξ is increased, the slowing of the transient decay constant and the onset of chaos is predicted. Fig. 3.10 show the variation of the parameters X_*, Z_* and W_* during chaotic operation in terms of phase space diagrams. The condition for the onset of chaotic operation was predicted to be $R \geq 5$ for $\xi = 0.999$. Consider the open resonator maser which is being studied at present. The onset of Zeeman beats occurs well below the condition for complete splitting of the spectral line. In general, two possible oscillation frequencies occur in this system even at very low applied magnetic fields, and so the frequency-locking effect which causes the single frequency oscillation on a partly split spectral line and the transition to chaotic operation is lost or substantially weakened. Despite this an enhancement in the oscillation settling transients is observed and a slowing of the decay constant, which is the first stage in the transition to chaotic regime of operation. With the maser cavity anisotropy modified by the placing of a thin wire in the fringe field of the cavity (Chapter 2), the slowing of the decay constant was dramatic.

The application of an electric field across the plates of the resonator will split the spectral line into many Stark components. This splitting is very inhomogeneous, with the main line initially split into

FIGURE 3.9 SEQUENCE TO CHAOS

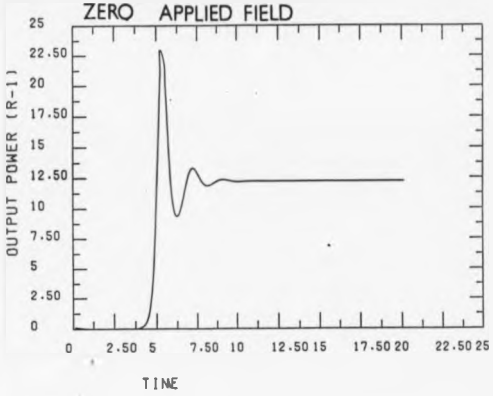

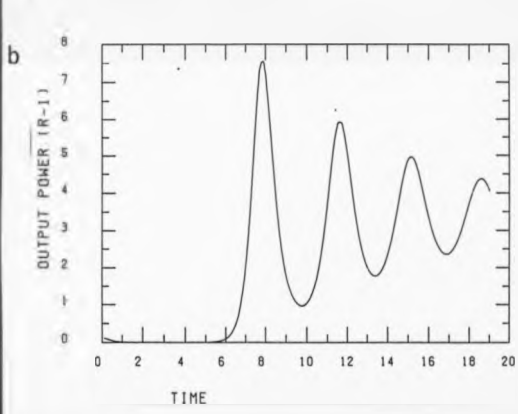

FIGURE 3.9

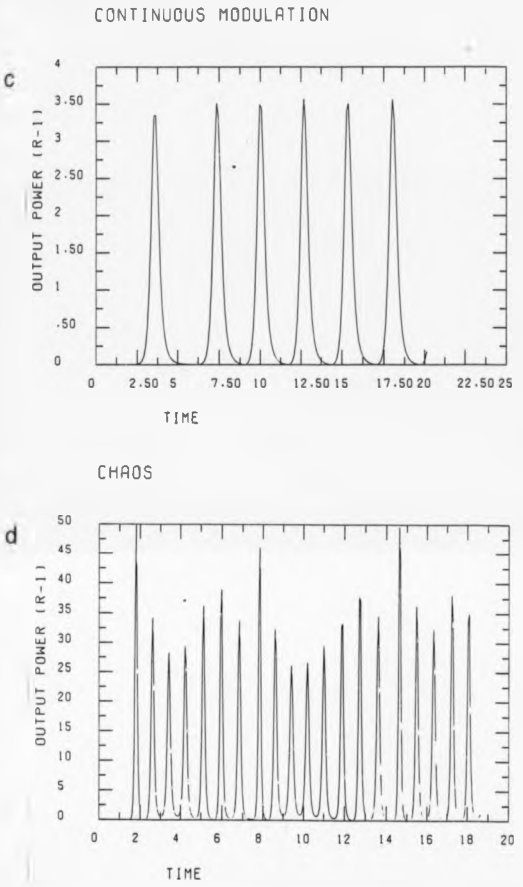
CONTINUOUS MODULATION
c
OUTPUT POWER (R-1)
4
3.50
3
2.50
2
1.50
1
.50
0
0
2.50 5
7.50 10
12.50 15
17.50 20
22.50 25
TIME
CHAOS
d
OUTPUT POWER (R-1)
50
45
40
35
30
25
20
15
10
5
0
0
2
4
6
8
10
12
14
16
18
20
TIME

FIGURE 3.10

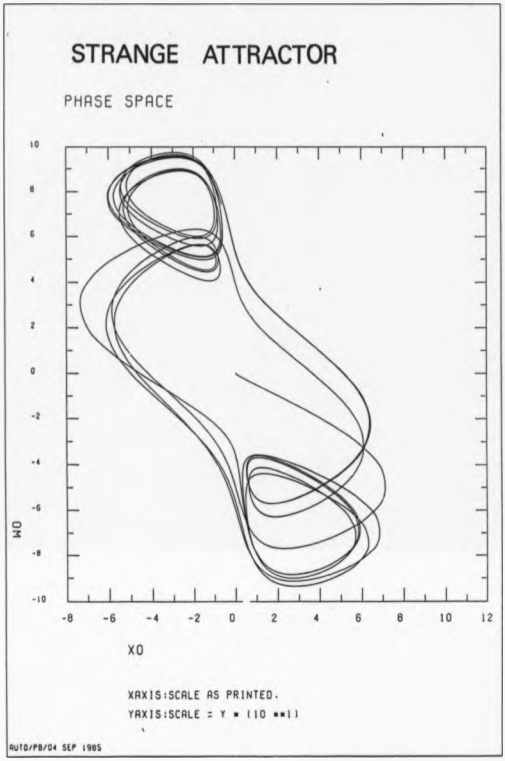

PHASE SPACE

FIGURE 3.10

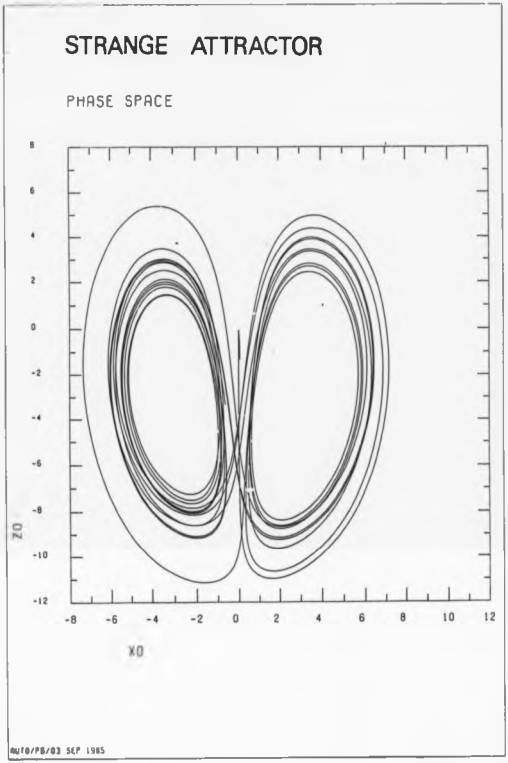

XO.ZO

FIGURE 3.10

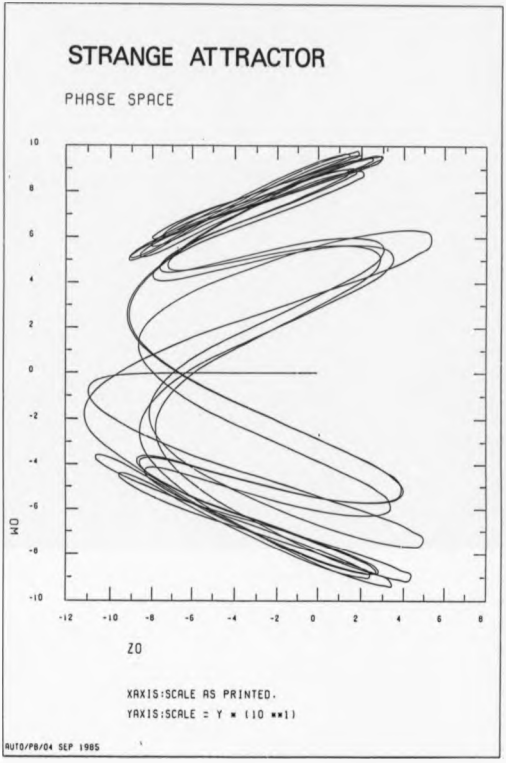

ZO WO

only two or three clusters of lines. For the J=K=3 transition three clear clusters of lines were observed when 18 volts was applied across the cavity plates and the maser was operated in the spectroscopic mode. These clusters will act like the Zeeman components discussed above. On studying the present maser with an applied electric field across the cavity plates (Chapter 2), a large increase in the number of observed transients was obtained, with an extremely marked slowing of the decay constant. The number of transients observed was determined mainly by the length of the oscillation pulse. A condition was reached where a marked slowing of the decay constant could be observed for a relatively small increase of both applied electric field and overfulfilment factor.

3.8 PERIOD DOUBLING

The transition between a non-chaotic system and a chaotic system may show the phenomenon of period doubling (Cvitanovic 1984, Fairbairn 1986, Kadanoff 1983). This has been studied in detail in many physical systems (Libchabera et al 1982, Giglio et al 1981).

Consider a non-chaotic system which is periodic in nature. By plotting two of the systems variables against each other a phase space diagram is produced. This is represented by Fig. 3.11a. As this system is excited and the non-linearities become significant, the phase space diagram may become modified and a fine splitting appears on the trajectory; this is represented by Fig. 3.11b. Here the trajectory in phase space has closed upon itself after two cycles and the period of the system has been doubled. On exciting the system further a second fine splitting may occur, and the process repeats itself. At this stage however a very slight increase in the excitation, will induce further period doubling and a region of chaos is reached. This description of the transition from a non-chaotic to a chaotic system is extremely common.

FIGURE 3.11 PHASE SPACE DIAGRAMS

a

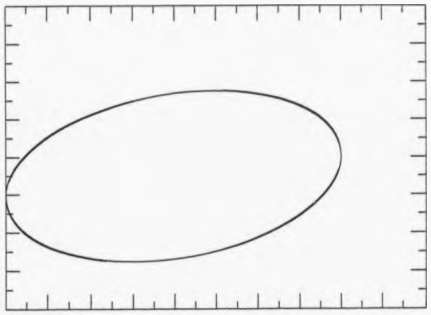

CLOSED PHASE SPACE TRAJECTORY

PHASE SPACE TRAJECTORY SHOWING PERIOD DOUBLING

b

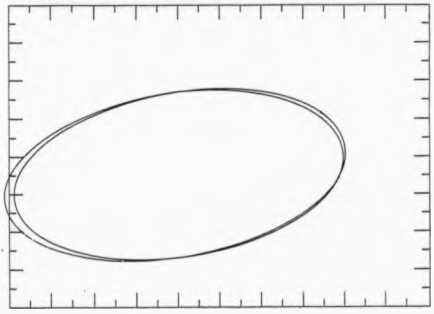

Consider a maser system. The series of equations (3.41) to (3.44) may be solved in the case where $\xi > 1$. At low levels of the maser overfulfilment parameter R the solution represents biharmonic oscillation (Oraevskii 1981). The solution is a periodic variation of the oscillation output power. This is shown as a plot of output power versus time, as shown in Fig. 3.12a. Upon increasing the value of the overfulfilment parameter R a region of period doubling is predicted in Fig. 3.12b. The period doubling effect decays very slightly in time (the variation between successive maxima amplitudes becomes less), and therefore the phase space trajectories for the system are not quite closed. Further increase of R (Fig. 3.12c), predicts a period doubling effect where the variation in amplitude of successive maxima increases. After several cycles of period doubling, chaos is reached (Fig. 3.12d). The chaotic regime is reached earlier (Fig. 3.12e) on increasing R further. An expanded trace showing the structure of the oscillation pulses is shown in Fig. 3.12f. The model used is biharmonic oscillation on a spectral line split into two equal components. The value of ξ is 1.5 and R takes values between 10 and 30.

The maser system operated by Maroof obtained these high levels of oscillation overfulfilment (Maroof and Lainé 1974). With an injected microwave signal in the maser cavity a series of oscillation pulsations were obtained (Lainé and Maroof 1977). The proposal here is that the injected microwave signal inhomogeneously broadens the spectral line by the dynamic stark effect (Lainé and Truman 1977). The split spectral line model is a first approximation to this inhomogeneous broadening. In reality the spectral line is split into three or more components each of different intensity. Many of the pulsation effects observed by Maroof are obtained with the maser cavity tuned off resonance. This is not accounted for in the model.

An example of the pulsation obtained by Maroof is shown in

FIGURE 3.12

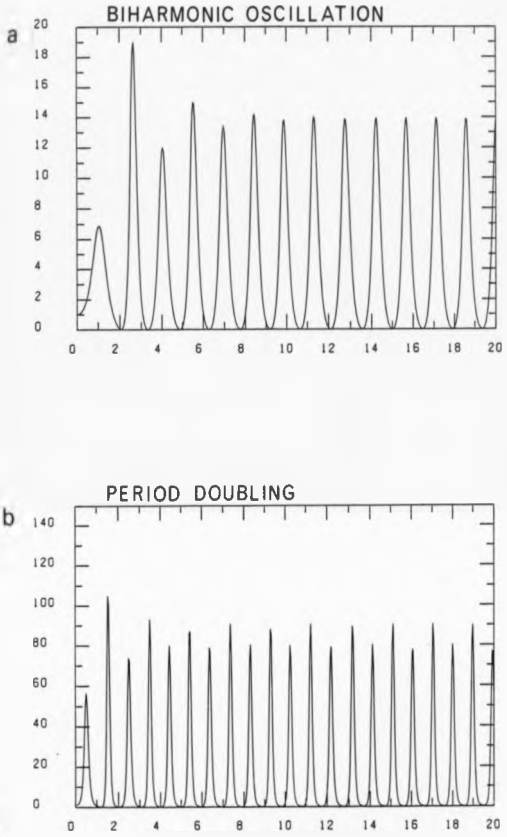
a
BIHARMONIC OSCILLATION
20
18
16
14
12
10
8
6
4
2
0
0 2 4 6 8 10 12 14 16 18 20
b
PERIOD DOUBLING
140
120
100
80
60
40
20
0
0 2 4 6 8 10 12 14 16 18 20

FIGURE 3.12

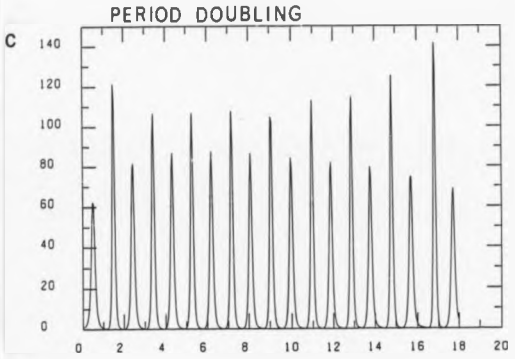
c
PERIOD DOUBLING
140
120
100
80
60
40
20
0
0
2
4
6
8
10
12
14
16
18
20

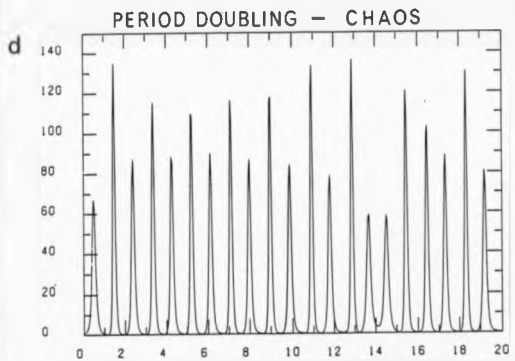
d
PERIOD DOUBLING – CHAOS
140
120
100
80
60
40
20
0
0
2
4
6
8
10
12
14
16
18
20

FIGURE 3.12

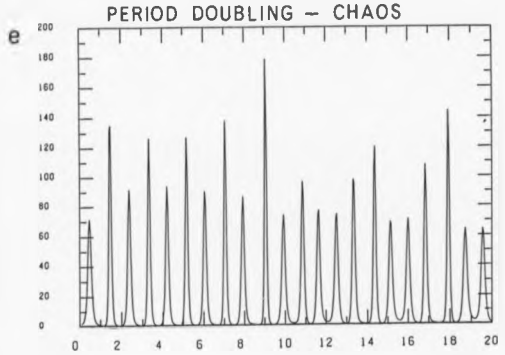
e
PERIOD DOUBLING – CHAOS
200
180
160
140
120
100
80
60
40
20
0
0
2
4
6
8
10
12
14
16
18
20

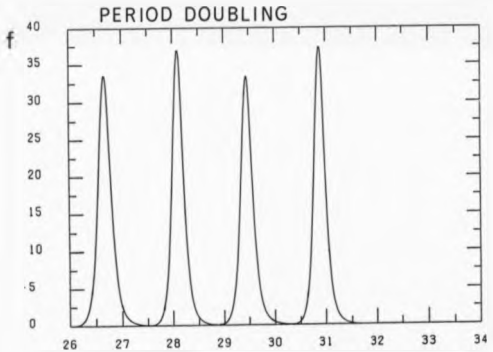
f
PERIOD DOUBLING
40
35
30
25
20
15
10
5
0
26
27
28
29
30
31
32
33
34

Fig. 3.13a. showing clearly a period doubling effect. The shape of the pulses are similar to those predicted theoretically. This may be due to the universal nature of period doubling effects rather than because of the accuracy of the model.

Pulsation effects were observed by Maroof with a two cavity maser system, observing oscillation pulsations in the second cavity (Lainé and Maroof 1974). This system is difficult to interpret, there also being an injected microwave signal in the second cavity. A trace is shown where the second stage of period doubling is present (Fig. 3.13b). This is the clearest evidence of the onset of chaos in an ammonia maser to date.

FIGURE 3.13

OSCILLATION AMPLITUDE PULSATIONS

AFTER MAROOF 1974

INTERPRETED AS A PERIOD DOUBLING

EFFECT

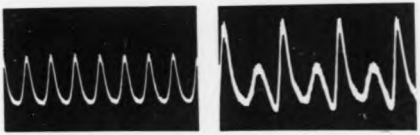

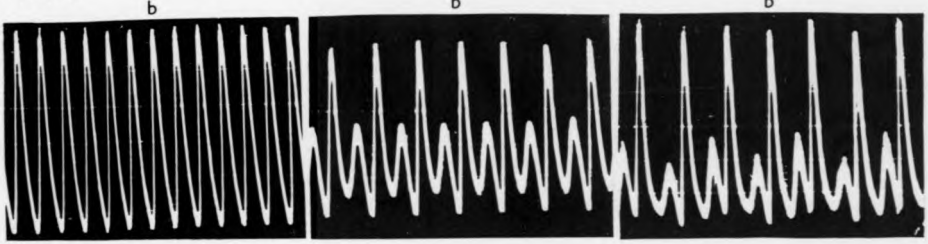

CHAPTER FOUR

PULSED MASER OSCILLATION ON THE J=4,K=4 AND J=6,K=6 INVERSION TRANSITION OF $^{14}NH_3$ AT 24.139 AND 25.056 GHZ RESPECTIVELY

4.1 INTRODUCTION

The number of microwave transitions on which molecular beam maser oscillation has been obtained is somewhat limited, there being eleven reported examples in the maser literature (Lainé 1975). For the common isotope of ammonia $^{14}NH_3$ maser oscillation has been reported on the J=K=1, J=K=2, J=K=3, and J=3 K=2 transitions. For the maser system under consideration in this thesis, with its open resonator of relatively low quality factor of 4500, continuous wave oscillation has been obtained on the J=K=1, J=K=2, and J=K=3 transitions. However the characteristics of the output power and polarization properties of each of these maser oscillations are somewhat different, in particular the J=K=I transition exhibits a linear output power polarization only. Oscillation polarization bistability (Lainé and Yassin 1981), has been observed on the J=K=2 and J=K=3 transitions. The polarization bistability (polarization flips), on each transition were shown to be significantly different (Yassin 1981). Low frequency beats have been observed (Chapter 2) on the J=K=2 and J=K=3 transitions in the presence of a weak applied magnetic field, but not on the J=K=1 transition. The possibility of obtaining maser oscillation on additional transitions of NH_3 would help establish how the oscillation characteristics change with the quantum numbers J and K.

The use of pulsed molecular beams has produced enhanced overfulfilment factors on the strong transitions of $^{14}NH_3$, which suggests that pulsed oscillation may be realizable on weaker transitions. Once pulsed oscillation is obtained on a given transition, careful adjustment of the maser parameters would possibly enhance the time duration of the oscillation pulse. It may then be possible under

favourable circumstances to obtain continuous wave oscillation on the same transition.

It is possible to observe the form of the time evolution of the oscillation polarization ellipse, during an oscillation pulse by the method of Lissajous spirals (Chapter 5), and so information on the form of the oscillation polarization ellipse may be obtained without the need for continuous wave oscillation.

The number of molecules per unit time required to enter the maser cavity in order to overfulfil the maser oscillation condition is dependent on the following;- the fractional population of the given J,K state; the focusing force of the state selectors for the given J,K state; and the transition probability, again for the given J,K state. Each of these will be considered in turn, in order to determine which maser transitions have a high probability of producing maser oscillation.

4.2 POPULATION DISTRIBUTION OF THE ROTATIONAL STATES OF $^{14}NH_3$

The variation of state population with rotational temperature for $^{14}NH_3$ is given by Townes and Schawlow (1955) as F_{JK} where,

(4.1) $F_{JK} = [S_{IK}(2J+1)/(4I^2+4I+1)](B^2Ch^3/(kT)^3)^{0.5}$
$\times\exp-([BJ(J+1)+(C-B)K^2]h/kT)$.

Here, F_{JK} = state population, I = 0.5, $B = B_0 = 298\times10^9$ Hz, $C = A_0 = 189\times10^9$ Hz, (Townes and Schawlow p640), $h = 6.6\times10^{-27}$ erg sec, $k = 1.38\times10^{-16}$ erg per dyne, S_{IK} = 6(if K = 3N±1), 6(if K = 0), 12(if K = 3N and K>0), (Townes + Schawlow Table(3-6) + equations 3.46)

Here the approximation h(B+C) << kT is made. The normalization factor used in the derivation is obtained by summing over a large number of states; here the sum is replaced by an integral. If the above inequality is not satisfied, which corresponds to rotational temperatures below 50K, the summation takes place over only a few states

and so the integral becomes inaccurate. Simplifying equation (4.1) gives,

$$(4.2)\quad F_{JK} = [S_{(I,K)}(2J+1)6.13/T^{1.5}] \times\exp-([(298\times10^{9}(J(J+1))-109\times10^{9}(K^{2})]4.78\times10^{-11}/T).$$

The rotational temperature at which the state population is at a maximum is given by simply differentiating the above expression as,

$$(4.3)\quad T_{PM} = 3.18[2.98(J(J+1))-1.09(K^{2})].$$

A series of curves of state population against rotational temperature are shown in Fig. 4.1. For rotational temperatures below 50K the fraction of molecules in the rotational state F_{JK} is given by (Townes and Schawlow 1955),

$$(4.4)\quad F_{JK} = [S_{(I,K)}(2J+1)\exp-([BJ(J+1)+(C-B)K^{2}]h/kT)] +[\sum_{J=0}^{J=\infty}\sum_{K=0}^{K=J} S_{(I,K)}(2J+1)\exp-([BJ(J+1)+(C-B)\,K^{2}]h/kT)].$$

The summation in the denominator converges quite rapidly as the value of J is increased. The summation can thus be performed numerically on a microcomputer. A series of curves are shown in Fig. 4.2 giving the fractional populations for T<100K of the major ammonia molecule inversion transitions. From the curves the transitions J=2 K=1, J=3 K=2, J=K=4, J=K=6, and J=4 K=3 are shown to have maximum state population above 4%, and are considered as potential transitions for maser oscillation.

4.3 STATE SELECTION PROCESS AND DIPOLE MOMENT INTERACTION

Consider now the focusing forces of state selection acting on molecules in the different J, K states. The focusing force within an electrostatic type of ladder state selector may be given by the following expression (Gordon 1955),

FIGURE 4.1

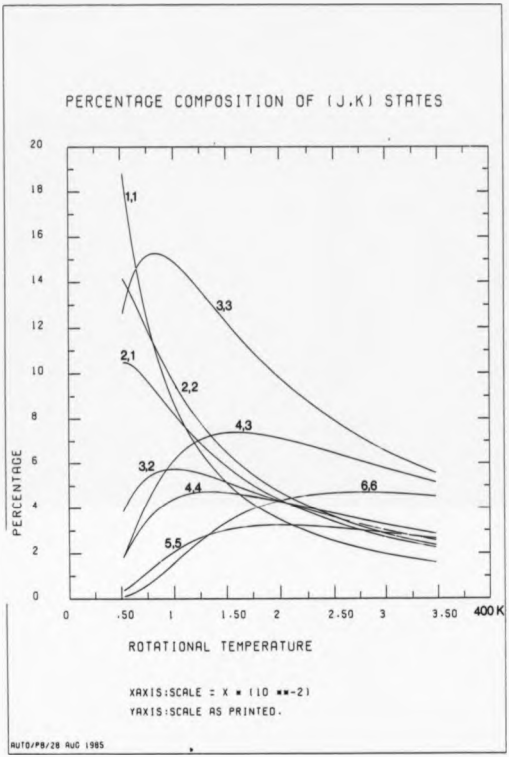
PERCENTAGE COMPOSITION OF (J,K) STATES
PERCENTAGE
20
18
16
14
12
10
8
6
4
2
0
1,1
3,3
2,1
2,2
4,3
3,2
4,4
6,6
5,5
0
.50
1
1.50
2
2.50
3
3.50
400 K
ROTATIONAL TEMPERATURE
XAXIS:SCALE = X * (10 **-2)
YAXIS:SCALE AS PRINTED.
AUTO/PB/28 AUG 1985

FIGURE 4.2

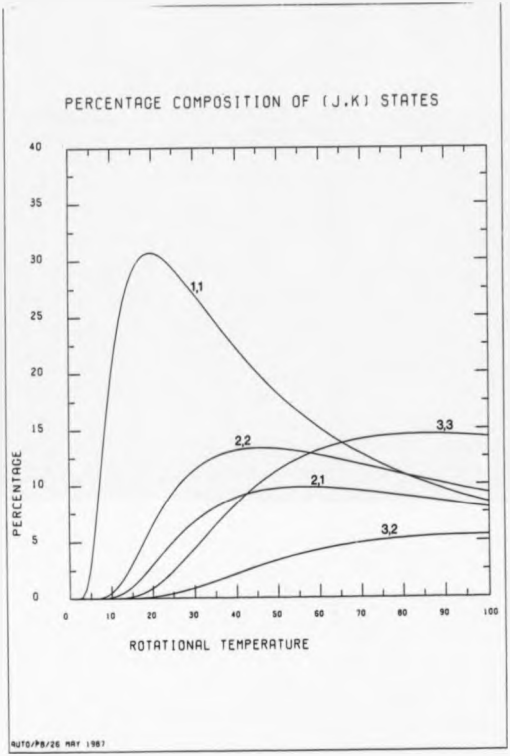
PERCENTAGE COMPOSITION OF (J,K) STATES
PERCENTAGE
ROTATIONAL TEMPERATURE
1,1
2,2
2,1
3,3
3,2
0
5
10
15
20
25
30
35
40
0
10
20
30
40
50
60
70
80
90
100
AUTO/PB/26 MAY 1987

(4.5) $F = ([\mu M_J K/(J+1)J)]^2 E[\partial E/\partial y])/([0.5*h\nu_0]^2+[\mu M_J KE/(J+1)J]^2)^{0.5}$.

As can be seen from this expression, at high field the focusing force is proportional to F where,

(4.6) $F = \mu|M_J|K/(J(J+1))$.

Here M_J is the projection of the rotational angular momentum quantum number in the direction of the applied electric field. To a first approximation it is assumed that the number of molecules state selected within the state selector will be proportional to the focusing force F. The validity of this assumption will be considered later in this section. The quantum number M_J may take integer values from +J to -J, (2J+1 values). The number of molecules in each M_J state will be proportional to 1/(2J+1). The number of molecules state selected in each M_J state will be proportional to NM_J where,

(4.7) $NM_J = \mu|M_J|K/[(2J+1)J(J+1)]$.

The total number of state selected molecules will thus be the sum over all values of NM_J = N,

(4.8) $N = \sum_{MJ=-J}^{MJ=+J} \mu|M_J|K/[(2J+1)J(J+1)]$.

Here the assumption is made that the value of M_J and its spatial orientation are preserved as the molecules in the beam pass from the state selector to the resonator. This may not be realised in practice due to the rotation of molecules in the fringe field of the state selector (Basov et al 1963).

Consider finally the interaction strength between the molecules and the microwave electric field. This is given by the non-zero matrix elements of the dipole moment (Townes and Schawlow 1955), $|\mu_{jk}|^2$ where for J→J K→K transitions,

(4.9) $|\mu_{jk}|^2 = [\mu^2 K^2 |M_J|^2]/[J^2(J+1)^2]$.

It is assumed here that the interaction time of the molecules in the resonator is the same for all M_J states. The total interaction between the microwave field and the molecules, taking into account both

state selection and interaction strength, is given by α where,

(4.10) $\alpha = \sum_{MJ=-J}^{MJ=+J} [|M_J|^3 K^3 \mu^3]/[(2J+1)J^3(J+1)^3]$.

The number of molecules in the molecular beam prior to state selection (neglecting scattering) required to produce oscillation will be proportional to $N_0 = (1/\alpha)F_{JK}$, where F_{JK} is the fractional population in that state. Taking the value for the line J=K=3 at its optimum rotational temperature as a unity value for N_{0_*} the values of N_0 for other transitions have been calculated. Thus an approximate value of the number of times the oscillation factor for the J=K=3 transition has to be overfulfilled to lead to a threshold of oscillation on weaker transitions is obtained. These values are shown in Table 4.1.

In the derivation given above it was assumed that the number of state selected molecules was proportional to the focusing force F. This, however, has to be modified in the system under consideration here, as the state selection process reaches saturation at a state selector voltage of approximately 20kV, ie, all the molecules in the molecular beam have been state selected. State selection on a transition with a stronger or weaker focusing force F will simply saturate the state selectors at a lower or higher voltage respectively, rather than increasing the number of state selected molecules. Assuming total saturation, the total number of state selected molecules in each M_J state will be given by $N_J = 1/(2J+1)$ $M_J<0$ or $M_J>0$. This approximation breaks down for very small values of M_J where the saturation is not complete. However the interaction with the microwave electric field is proportional to $(M_J)^2$ so these terms do not contribute heavily to the final result. The value of α will now be given by,

(4.11) $\alpha = \sum_{MJ=-J}^{MJ=+J} [|M_J|^2 K^2 \mu^3]/[(2J+1)J^2(J+1)^2]$.

Tables for the number of times the oscillation factor for the J=K=3 transition has to be overfulfilled to give oscillation on weaker inversion transitions for both the unsaturated state selector and

saturated state selector approximation are given in Table 4.1. Curves of $1/N_0$ as a function of rotational temperature are given in Fig. 4.3 and Fig. 4.4 for the saturated and unsaturated state selector approximation, this gives the oscillation strength of each of the transitions as a function of rotational temperature. The two strongest inversion transitions of $^{14}NH_3$ on which oscillation has not yet been obtained are the J=K=6 and J=K=4 transitions. Oscillation has however been obtained on the J=K=6 transition of the isotope $^{15}NH_3$ using a closed resonator (Takahshi et al 1960). It is interesting to note at this point that the maximum oscillation overfulfilment factor observed on the J=K=3 transition was estimated at 3.3.

4.4 NOZZLE SOURCES AND ROTATIONAL COOLING

Whenever high pressure nozzles are used as gas sources substantial rotational cooling takes place. If the pressure behind the nozzle is sufficiently high, however, condensation effects start to become dominant, ie, the ammonia molecules start to form dimers and higher clusters. This has two effects: firstly of reducing the fractional population of the monomer, and secondly of again increasing the rotational temperature through the heating effects of condensation. For each transition there will be a source pressure which will produce the optimum rotational temperature for the transition. The problem is to find a source which when operated at that pressure gives optimum gas throughput for the maser.

Initially the maser was operated using single hole 100μm diameter sources. These gave optimum performance with nozzle pressures of 200, 300, and 600 torr on the J=K=1, J=K=2 and J=K=3 transitions respectively (Al-Jumaily 1979).

Since the J=K=1 transition has the maximum of state population at the lowest rotational temperature, it was assumed that the lowest

FIGURE 4.3

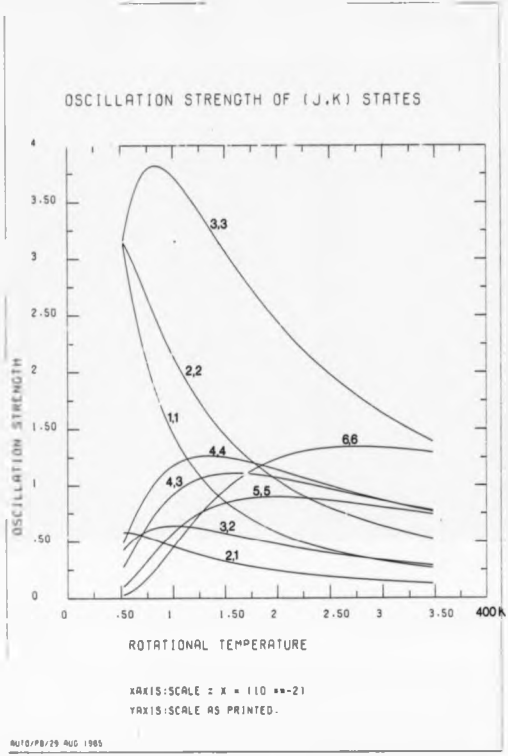

SATURATED STATE SELECTOR

FIGURE 4.4

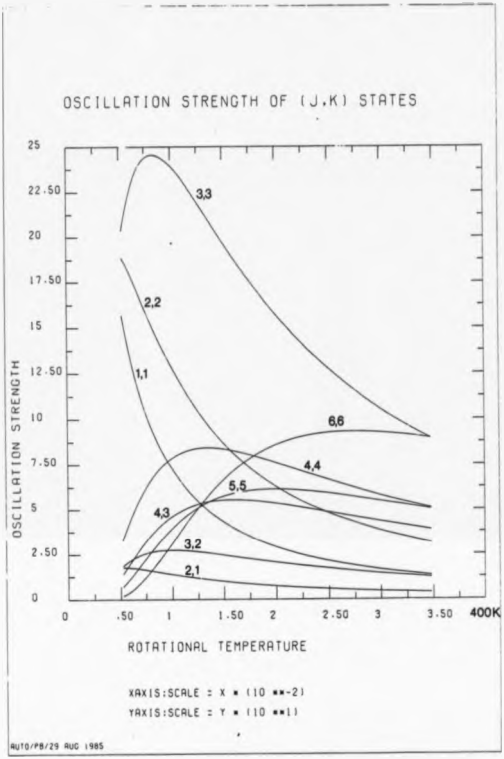

UNSATURATED STATE SELECTOR

TABLE 4.1

THE OSCILLATION STRENGTH REQUIRED ON THE J=K=3 TRANSITION, TO OBTAIN OSCILLATION ON THE FOLLOWING TRANSITIONS

J,K VALUES	SATURATED STATE SELECTOR	UNSATURATED STATE SELECTOR
1,1	1.2*	1.5*
2,2	1.2*	1.3*
3,3	1.0	1.0
4,4	3.1	3.0
5,5	4.2	4.1
6,6	2.8	2.7
2,1	5.7	16
3,2	5.4	9.7
4,3	3.4	4.5

*Calculated at T=50K

rotational temperature obtainable must be reached at, or below, 200 torr, and above this pressure the molecular beam was being warmed by condensation. A series of 2mm long slit sources of width between 12.5μm and 125μm were investigated and a direct comparison was made between these and the 100μm hole sources in continuous mode oscillation operation. With single beam operation using a 12.5μm slit source, oscillation was obtained on the J=K=2 transition with an oscillation threshold of 9kV. For a single circular hole source no oscillation could be obtained. With double beam operation the oscillation threshold for operation with the slit sources was 6kV, whereas 5.3kV threshold could be obtained using two 100μm diameter hole source beams. Replacing the 12.5μm wide slit source by a 25μm wide slit source no single beam oscillation could be obtained.

For the 100μm diameter hole source the pressure behind the nozzle, and hence the gas throughput was limited by condensation effects. On increasing the nozzle pressure above 300mb, any advantage gained by increased flux was lost by depletion of the J=K=2 state by dimer formation and a warmed molecular beam. The result was a beam flux which was below that required to load significantly the gas pumps and cause an increase in background gas pressure and scattering of the beam. For the 12.5μm slit, optimum pressure behind the nozzle was found to be between 60 and 80mb. This represented a significantly higher gas flux than that obtained with the 100μm hole source, the high flux being required to run the sources at a high enough pressure to give a significant degree of rotational cooling. Using one molecular beam only, the slit source operation was advantageous when compared with operation of the hole source. However using two slit sources, the gas loading of the main chamber was much increased, with extensive scattering of the molecular beam. A less extensive scattering effect occurred when two 100μm diameter hole sources were used.

It should be noted that the spatial distribution of molecules leaving the hole and slit nozzles are different, the hole source gives a cone-like distribution of molecules, whereas the slit sources give fan-like distribution of molecules, which is better suited to the geometry of the present system (Sulkes, Jouvet and Rice 1982).

4.5 EXPERIMENTAL METHOD AND SET-UP

Consider now the state population as a function of rotational temperature for the major rotational transitions of $^{14}NH_3$. The J=K=4 transition possesses a maximum of population at 273K. The shape of the curve for the J=K=4 transition follows the same form as for the curve for the strong J=K=3 transition, and so any nozzle source which will allow for oscillation on the J=K=3 transition should give excellent results with the J=K=3 transition. No curve of a strong transition resembles that of the J=K=6 line.

In order to obtain oscillation on the J=K=4 transition, the maser was operated initially on the J=K=3 transition, in order to optimise nozzle sources and alignment, which would then be suitable for operation on the J=K=4 transition. The maser cavity was therefore initially tuned to the J=K=3 transition. Each nozzle pipe was fitted with a pulsed valve, fitted with a small $27mm^3$ cap which housed a nozzle source 2mm long and 125μm wide. These extremely wide slit sources allowed for a high gas throughput and gave the strongest maser overfulfilment yet reached in the present system when operated with the pulsed beam. The maser was carefully aligned to optimise the maser power output. The maser cavity was then tuned to the transition frequency of the J=K=4 transition. On operation, the maser system gave pulsed oscillation on the J=K=4 transition with a threshold of 8.4kV. It was found that the maser alignment was almost optimum for this transition.

The J=K=6 transition is optimized at a much higher rotational temperature 273K and so almost any nozzle gas source which gives rotational cooling will have the effect of depopulating this rotational state. Wider slit sources were not available at the time, and effusive sources which have been tried with this maser system before failed to give a strong enough stimulated emission signal due to the geometry of the system. The maser cavity was tuned to the transition frequency of the J=K=6 transition, with the existing pulsed 125μm wide slit nozzle sources. Strong stimulated emission was observed with both continuous wave and pulsed operation. The results with continuous wave operation suggested that the gas flux was quite small. An increase in the gas pressure produced a depopulation of the J=K=6 state. Direct measurements of nozzle source pressure is impossible as it is the combined pressure across the valve and the slit source which is recorded, but since this is directly proportional to the pressure across the the slit source it is a useful indication. For the J=K=3 transition, the optimum pressure behind the valve was found to be between 50-80mb, for the J=K=4, and J=K=6 transitions optimum pressures were found to be 40-50 and 15mb respectively. An attempt was made to improve the flux passing through the valve by heating the nozzle pipe and valves, in order to compensate for the effect of rotational cooling. This method had the disadvantage of decreasing the interaction time inside the cavity as the beam velocity was increased, but had the advantage of reducing the effects of any dimer formation. On heating the nozzle pipe and valve to 420K, optimum performance was obtained with the maser, giving pulsed oscillation with a threshold of 9.5kV on the J=K=6 transition.

4.6 CHARACTERISTICS OF THE MASER OSCILLATION ON THE J=K=4 AND J=K=6 TRANSITIONS OF $^{14}NH_3$

Despite the relatively low thresholds of 8.4kV and 9.5kV the oscillation obtained on either of the J=K=4, and J=K=6 transitions was weak even when the EHT applied to the state selector was taken up to 20kV. This suggests that the state selection process is saturating at a relatively low voltage on both inversion lines. The weakness of the oscillation is indicated by the fact that it was necessary to leave the maser system standing for several hours with the liquid air traps charged, in order to reduce the background pressure sufficiently to allow enough flux to enter the maser cavity and to reach the threshold for oscillation.

There was no evidence for the existence of oscillation amplitude settling transients on the J=K=6 transition; however a small aperiodic transient was observed on the J=K=4 transition. This suggests that the overfulfilment factor is very low on the J=K=6 transition, and no more than approximately 1.5 on the J=K=4 transition. An example of an oscillation pulse on the J=K=6 transition is shown in Fig. 4.5a.

On both the J=K=4 and J=K=6 transitions, low frequency beats could be obtained upon application of a weak magnetic field in a direction perpendicular to the plane of the plates of the resonator. An example is shown in Fig. 4.5b, the beat frequency being approximately 1kHz with the application of a 1×10^{-4}T magnetic field. The presence of beats suggested that the oscillation had become elliptically polarized. However rotation of the coupling waveguide did not conclusively show oscillation in an orthogonal linear polarization. It appeared that changing the position of the waveguide changed the loading on the cavity and moved the cavity resonance frequency slightly. This was sufficient to quench the oscillation in both linear polarizations. The conditions for maser oscillation for both of these spectral lines is critically

FIGURE 4.5
J, K, 6,6 TRANSITION

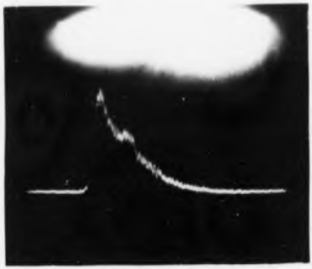

a

b

dependent on cavity tuning. Finally it should be noted that the signal contributed by the beam originating in the right hand side of a system was the somewhat weaker signal relative to that contributed by the left. There may then be a possibility of improving the signal by careful realignment of the maser. For the J=K=6 transition of $^{14}NH_3$ the use of wider slit sources may increase the value of the oscillation overfulfilment factor.

CHAPTER FIVE

TIME EVOLUTION OF THE OSCILLATION POLARIZATION ELLIPSE DURING THE FORMATION OF A GAS PULSE

5.1 INTRODUCTION

The time evolution of the microwave oscillation output power from the maser disc resonator has been studied in two linear orthogonal polarizations (Chapter 2). In this chapter, both oscillation settling transients and biharmonic oscillation during the time evolution of a gas pulse are discussed, using the Lissajous figure method. The idea of displaying the output power originating from the two linear orthogonal polarizations, in the form of a Lissajous figure, was first successfully demonstrated by Yassin and Lainé (1981), using the present maser system. Static polarization ellipses were displayed with maser oscillation on the J=K=2 and J=K=3 transitions. Polarization bistability was observed on both the J=K=2 and J=K=3 transitions (Lainé and Yassin 1981), and the rotation of the major axis of polarization in an applied magnetic field (Yassin and Lainé 1985). It was found that the ellipticity of the oscillation ellipse was dependent upon the strength of the applied state selector electric fields (Yassin 1981). In this chapter, a method is developed to display the time evolution of the oscillation ellipse during the progress of the oscillation pulse, resulting from oscillation build-up following the opening of the pulsed valves.

5.2 THE METHOD OF LISSAJOUS SPIRALS

The build-up process of oscillation from thermal noise in a disc resonator is a complex process, being essentially chaotic in nature. Here near-identical initial maser parameters produce widely different build-up processes. The first indication of the fluctuation in the nature of the oscillation build-up was observed when Q-switched oscillation transients were induced in the present system (Lainé and

Al-Jumaily 1979). The time of silence and amplitude of the transients produced, varied widely from one oscillation pulse to the next. Transients induced by the opening of the pulsed gas valve show the same effect, and have been investigated in detail in two linear orthogonal polarizations (Chapter 2). The effect of this observation is that averaging methods, or methods of successive sampling, cannot be used to determine the form of the time evolution of the oscillation ellipse. All the information on the form of the oscillation build-up must therefore be obtained from a single gas pulse, and hence single oscillation pulse.

Consider now the method of detection of the maser signal. A detailed description of the detection system used to display the static ellipse is given (Yassin 1981), and a diagram showing the modified system used here is given in Fig. 5.1. The key for Fig. 5.1 is as follows, A = phase shifter, B = 30MHz I.F. amplifier, C = Hatfield mixer, D = 45kHz bandpass filter, E = signal generator, F = isolator, G = matching unit, H = resonant cavity, I = molecular beam and J = circulator.

The microwave signal at 24GHz originating from the maser system, was mixed with a portion of a 24GHz signal which originated from an Oki klystron. This signal was offset from the maser oscillation signal by 30MHz, and thus produced a 30MHz difference signal. A second 24GHz maser signal was mixed with the second portion of power from the same Oki klystron, and a second 30MHz difference signal was produced on a separate channel. The relative phase between the two 30MHz signals was kept the same as the relative phase shift between the two 24GHz signals by use of a phase shifter in the microwave bridge. The two 30MHz signals were detected using crystal diodes, Type IN26A, and the resultant signals amplified using two intermediate frequency amplifiers, one for each channel. The two 30MHz signals were mixed with a 30MHz

FIGURE 5.1

EXPERIMENTAL ARRANGEMENT

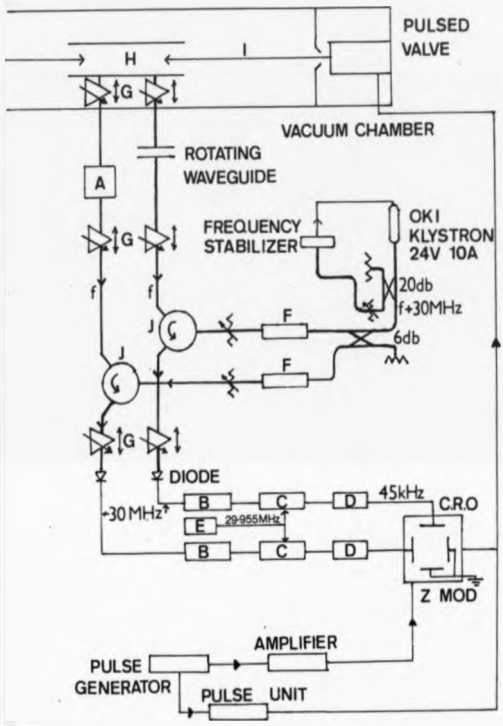

signal from a crystal oscillator, offset initially at 100kHz, in a Hatfield mixer (Modulator type MD4). In the original system (Yassin 1981), the two 100kHz signals were connected to the X and Y plates of the CRO to construct a Lissajous figure. The present system is a modification of that of Yassin, in so far that rather than adjusting the two final downconverted signals to 100kHz a frequency of 45kHz was chosen. The signals at this frequency were bandpass filtered and amplified. For this to be successful however, the klystron oscillator had to be carefully phase locked to a quartz crystal oscillator, in order to reduce frequency jitter. Two new 30MHz I.F. amplifiers were constructed, based on integrated circuit technology, which had improved signal to noise of approximately three times compared with the earlier tuned circuit amplifiers.

Consider now the final 45kHz signals, combined to form a Lissajous figure. In the case of a static continuous maser signal where there are clean filtered signals, producing a fine-trace elliptical Lissajous figure on the CRO, the spot on the CRO screen will complete one orbit of the displayed ellipse every 1/45,000 s. In the ideal case a finely resolved ellipse would be produced. This is represented by Fig. 5.2a. Consider the dynamic case where, for example, rapid oscillation build-up is taking place. During the 1/45,000 s required for the CRO spot to complete one orbit of the ellipse, the amplitude of the maser signal may have changed significantly. If the signal to noise ratios of the final 45kHz signals are sufficiently good, the trace on the oscilloscope will now become an open Lissajous figure in the form of a spiral. This is represented by Fig. 5.2b. If the change in amplitude or phase is not great during the period of the final downconverted signal (1/45,000s), the form of the oscillation ellipse at any one time may be determined from the spiral patterns. The final downconverted signal may be changed from 45kHz in order to "follow" faster or slower

FIGURE 5.2

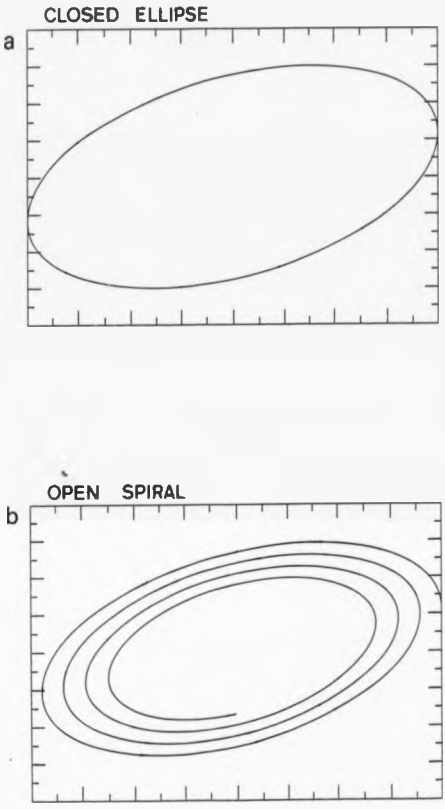

events. Spiral patterns have been produced for both single and biharmonic oscillation on the J=K=2 and J=K=3 transition of NH_3 from which the form of the oscillation build-up in terms of changes of amplitude, eccentricity, and orientation of the oscillation ellipse, has been determined.

5.3 FILTER CIRCUITS

Two filter circuits were constructed here from a design of Bell (1984). The circuit diagrams are shown in Fig. 5.3. Both of the filters are two stage bandpass types, based on 741S operational amplifiers. Each filter has a gain of approximately 200, and a variable bandwidth between the limits of 10 and 25 kHz. The centre frequency of the filters could be adjusted between 35 and 50 kHz. The filter circuits introduce a phase shift between their input and output signals. This phase shift is amplitude independent, but is highly dependent upon the frequency of the input signal. The technique used to correct this is to balance the relative phase shifts between the two filters, so that each filter introduces the same phase shift at a given operating frequency, and at all frequencies within its bandpass. The filter circuits were initially tuned to a reference signal. The outputs from the first stages of the filters were tuned, so that their centre frequencies were offset below the required centre frequency. The reference signal was divided and fed to the inputs of both filters, and the outputs from the first stages of the filters were fed to the X and Y channels of a CRO. The filters were adjusted so that a linear Lissajous figure was obtained, and the figure remained linear as the reference signal was tuned across the bandpass of the filters. The second stage of the filters were now connected to the CRO and the procedure repeated, so that the centre frequencies of the two stage filters were at the desired value. Using this method the phase shifts introduced by both

FIGURE 5.3

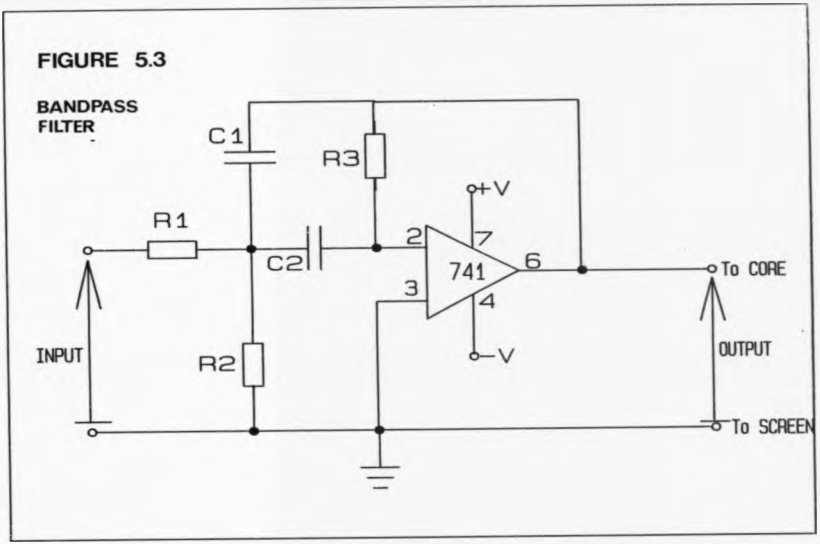
BANDPASS
FILTER
C1
R3
+V
R1
2
7
C2
741
6
To CORE
3
4
INPUT
R2
-V
OUTPUT
To SCREEN

filters were balanced against each other, so that there was no relative phase shift introduced as the reference signal was swept across the bandpass of the filters.

5.4 SETTING-UP PROCEDURE

The following setting up procedure was followed in order to produce spiral build-up patterns from the pulsed maser oscillation.

1) The maser output power detected via the 30MHz intermediate frequency amplifiers was displayed as a function of time, in the same superheterodyne display method with zero sweep as was used for experiments described in Chapter 2. The nozzle pressures and cavity tuning were then optimised, in order to give a strong pulsed maser oscillation signal.

2) The Oki klystron was phase-locked to a stable quartz crystal using a microwave frequency lock box (Microwave Systems, Type MOS3606). It was found far easier to phase-lock the klystron if the microwave lock box was left switched on to stabilize thermally for several days prior to the experiment. The drift in the klystron frequency can be reduced to few 10s of Hz per minute. The klystron was left to frequency stabilize for several hours prior to the experiment.

3) The circulator was now inverted on the second arm of the superheterodyne microwave detection system, and a second channel was set up, showing again the oscillation output power against time. Both channels now displayed the horizontal component of the oscillation as a function of time. The klystron frequency was monitored via a microwave frequency counter.

4) The output from one of the 30MHz amplifiers was placed in one outer port of a Hatfield Mixer (Modulator type MD4). The 30MHz fixed frequency source was then fed into the second outer port of the mixer. The difference frequency was received from the centre port of the mixer.

Initially the difference frequency was fed directly to the CRO. Since a portion of the oscilloscope trace (output power against time), showed the signal level before and after the onset of oscillation, the trace could be used to display the signal to noise level of the final signal. The fine tuning of the klystron frequency lock-box was adjusted until a position of zero beats was obtained on the final downconverted signal.

5) The filter circuits were then placed between the final downconverted signals and the CRO. The klystron frequency was offset by approximately 45kHz. The filtered signal was then optimised again by adjusting the fine tuning on the microwave frequency lock-box. After the second 45kHz signal was obtained, the two signals were then connected to the X and Y plates of the CRO to display Lissajous figures. By adjusting the phase shifter placed in one of the microwave arms, a linear Lissajous figure was obtained. If this was not the case, it was usually due to one of the filters approaching saturation, this could be corrected either by reducing the klystron power supplied to the stronger channel, via an attenuator, or by attenuating the 30MHz fixed frequency supply to that channel. Once a linear Lissajous figure was obtained, the input signals were adjusted to give identical power levels on the CRO display (adjusting the two gains of the X and Y channels), so that the linear figure lies at 45 degrees to the X and Y axes. One of the waveguides was then rotated by 90 degrees, and the Lissajous spiral patterns were then obtained.

6) A suitably delayed voltage pulse from the drive unit to the gas valve was amplified and fed to the Z modulation of the CRO. With careful adjustment, the brightness of the oscilloscope trace could be completely suppressed in the period between each gas pulse. Each pulse could then be individually brightened just before the onset of oscillation. The brightness of the oscilloscope trace would then decrease approximately exponentially, with a "half brightness" of

approximately 0.5ms. The oscillation trace was then photographed, with a time exposure of the camera just less than the time between successive gas pulses, so the whole of the spiral pattern was recorded on a single trace, without a double exposure.

5.5 SOURCES OF MEASUREMENT ERROR

There are several sources of error which must be considered when examining the spiral patterns produced. The main sources of error are introduced by the use of the filter circuits. The filters have a rise time which is comparable with the faster dynamic effects produced in the maser system, and so will modify the traces obtained. The rise time of the filters is dependent upon their bandwidth. By increasing the bandwidth of the filters from 10kHz, to a value in excess of 20kHz, the situation was improved so that oscillation settling transients and low frequency beats could be clearly observed, unmodified by the presence of the filters. However, high frequency beating effects, and transients obtained at high levels of overfulfilment condition, were noticeably modified by the presence of the filters.

A second source of error is due to the saturation of the filters. This effect often occurs when the maser signal obtained from one channel is rather weak. Increasing the fixed frequency signal at 30MHz to enhance the signal to noise ratio of the weaker signal causes the stronger signal, (whose amplitude has also been increased), to saturate the filter circuit. A sketch of a faulty trace is given in Fig. 5.4. Here the same signal is being fed to both of the X and Y traces of the CRO, except that the Y signal is saturating the filter circuits. As the gas pulse progresses the oscillation level changes and the relative X to Y amplitudes change (due to saturation), an apparent rotation of the linear trace is caused. The solution is either to attenuate the 30MHz fixed frequency signal applied to the strong

FIGURE 5.4
SATURATION EFFECT

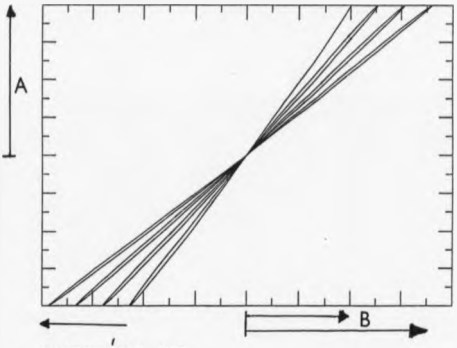

DIRECTION OF
APPARENT ROTATION

A = Y SIGNAL, SATURATED

B = X SIGNAL, UNSATURATED

channel, or to attenuate the maser signal produced by the strong channel.

Another source of error may occur when one of the microwave waveguides is rotated, the distance between the crystal detector and the maser cavity may be slightly changed. Any large change in this distance will alter the pressure applied to one of the cavity plates, spoiling the cavity Q value and preventing maser oscillation. This results in the production of an arbitrary phase shift between the two maser signals and possibly a change in amplitude of the signal out of the rotated waveguide. A check on the magnitude of this effect may be made by rotating the waveguide back to the vertical position at the end of the experiment. Any phase shift between the two channels will now be due to the above effect. In practice a small phase shift of few degrees was observed.

The bandpass nature of the filter circuits may lead to errors due to differential amplification of signals at various frequencies. This may cause a slight error when biharmonic oscillation is being studied, as the ratios of amplitudes of the two components may not be preserved after filtering. Any frequency jitter of either the maser signal or the klystron may be converted into amplitude jitter by the filters. In practice however the klystron frequency may be held stable enough to reduce this effect to a negligible amount. Finally the relative phase shifts of the two filters across their bandpass may not be completely balanced.

5.6 EXPERIMENTAL RESULTS

The phenomena observed in the experiment may be considered under the following headings;- Low frequency biharmonic oscillation on the J=K=2 transition under an applied magnetic field; single frequency oscillation build-up on the J=K=2 transition, including the observation

of oscillation amplitude settling transients; oscillation on the J=K=2 transition with modified cavity anisotropy, brought about by placing a thin wire within the cavity. Oscillation on the J=K=3 transition, and low frequency biharmonic oscillation in zero applied field have been observed with this technique.

5.7 LOW FREQUENCY BIHARMONIC OSCILLATION WITH AN APPLIED MAGNETIC FIELD

5.7.1 GENERAL COMMENTS

When a magnetic field is applied in a direction perpendicular to the plane of the resonator discs, the degeneracy of the two $\Delta M = \pm 1$ transitions is lifted and biharmonic oscillation is possible through Zeeman splitting of the spectral line. For static maser operation, biharmonic oscillation below a beat frequency of 4.8kHz (Al-Jumaily 1979) does not occur, due to phase-locking of the two oscillation components. Under pulsed operation of the maser (Chapter 2), low frequency beats are obtained at frequencies as low as 800Hz. The beat effect dies away after few cycles, as one oscillation gains strength at the expense of the other.

The spiral pattern obtained via the Lissajous figure display resembled a rosette pattern. Three examples of the pattern are shown in Fig. 5.5a,b,c. To a first approximation the two oscillations may be considered as two counter-rotating elliptically polarized oscillations which beat together to give a nearly linearly polarized resultant oscillation. This linear oscillation rotates at the beat frequency to give the resultant rosette pattern. It must be remembered however, that the observed signal is the beat pattern from the two downconverted signals both at 45kHz with a frequency difference of one or two kHz. The CRO Z-modulation bright-up pulse will highlight the initial one or two cycles of the beat pattern. However in many cases the orientation of the final single frequency stable elliptical oscillation may be

FIGURE 5.5

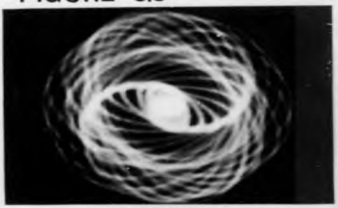

a

b

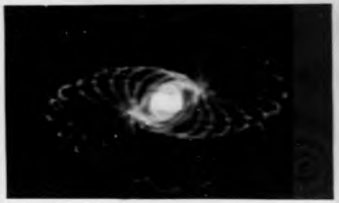

c

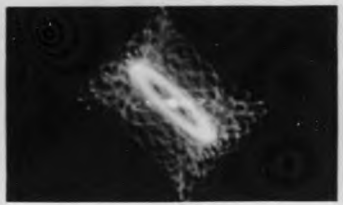

d

observed.

5.7.2 EXPERIMENTAL OBSERVATIONS

The following general trends were noted.

The direction of rotation of the final composite ellipse, (formed from the sum of the two oscillation ellipses), was dependent on the direction of the applied magnetic field. When the direction of the applied magnetic field was inverted, this reversed the direction of rotation of the composite ellipse.

The rate of rotation of the composite ellipse and hence the beat frequency was dependent upon the applied magnetic field, an increase in the applied magnetic field produced an increase in the rate of rotation of the composite ellipse.

The form of the envelope of the observed beat pattern was dependent upon the applied magnetic field and cavity tuning. At relatively high applied magnetic fields and under some operating conditions with relatively low applied fields, the beat envelope shape approached a circle, as shown in Fig. 5.5a,b. The beat envelope may also become elliptical (Fig. 5.6a). At relatively low applied magnetic fields under different operating conditions, the shape of the envelope approached a parallelogram whose sides were inclined at approximately 45 degrees to the horizontal and vertical axes, as shown in Fig. 5.5d. These angles vary from pulse to pulse. At approximately the same applied magnetic field, and hence beat frequency, the variety of the beat envelopes was extremely varied. Several examples are shown (Fig. 5.5 to Fig. 5.7), displaying the variety in the beat envelope produced. The envelope shape was also highly dependent on the tuning of the cavity resonance across the maser oscillation frequency, and secondly the initial alignment of the cavity and hence the orientation of the cavity plates relative to each other, and therefore the

FIGURE 5.6

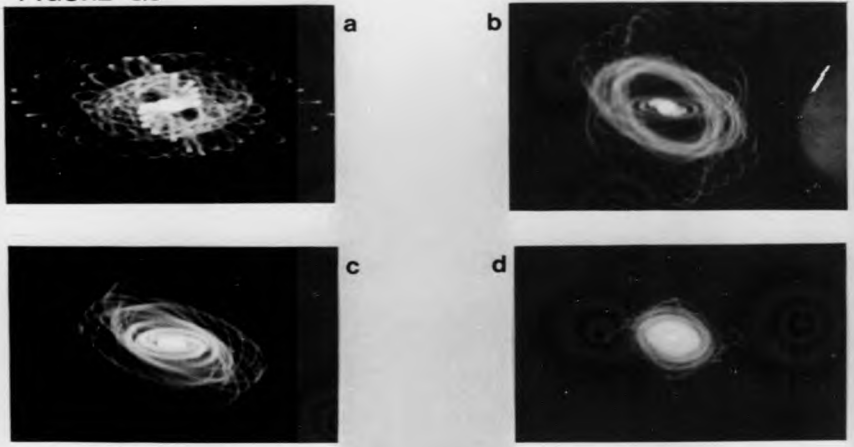

FIGURE 5.7

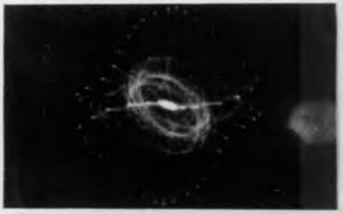

a

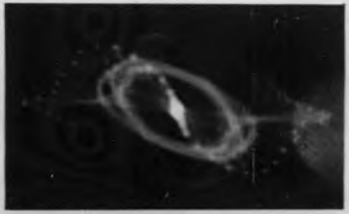

b

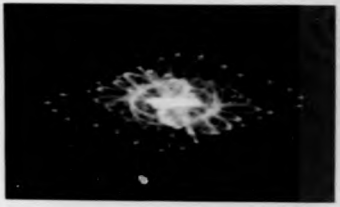

c

d

anisotropy of the cavity.

In the case of the parallelogram beat envelope, the final oscillation ellipse was orientated such that its major axis was aligned in the same direction as the largest side of the parallelogram (Fig. 5.5d). There is an occasional exception, however, when the major axis of the ellipse is aligned in the same direction as the smallest side of the parallelogram, as shown in Fig. 5.8a.

The ellipticity of the rotating composite ellipse changes periodically as the ellipse rotates. The ellipse has its greatest eccentricity as its major axis passes the corners of the parallelogram, and least eccentric as the ellipse major axis of the ellipse perpendicularly bisects one side of the parallelogram. As the oscillation ellipse developed in time it became less eccentric, and one of the oscillations died away, and finally the ellipse settled down to a stable shape and orientation.

The rate of rotation of the composite ellipse varies in time. It is most non uniform as the envelope of the beat pattern approaches a parallelogram. The rate of rotation of the ellipse is fastest at the positions where it is least eccentric; these correspond to the positions where the major axis of the rotating ellipse perpendicularly bisects one of the sides of the parallelogram. The rate of rotation is slowest when the major axis of the ellipse is in line with one of the corners of the parallelogram as shown in Fig. 5.8a,c. The beat frequency remained constant as the oscillation pulse evolved. Where two or more complete half cycles were observed the time taken to complete these was identical.

The initial build-up of biharmonic oscillation was quite varied, this depended to a large extent on the maser parameters and anisotropies. Operating conditions which produced a near-circular beat pattern produced a build-up pattern where the initial development of the

FIGURE 5.8

a

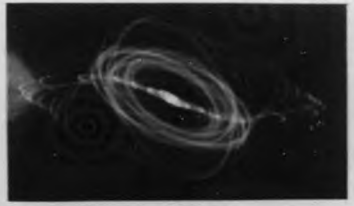

b

c

d

composite oscillation ellipse increased in amplitude and rotated at the same time (Fig. 5.5a,b,c). Where there are near-parallelogram beat envelopes, some traces show a similar rotating composite ellipse build-up (Fig. 5.9c). Under the same operating conditions it is possible to produce a strong linear initial build-up (Fig. 5.7a, Fig. 5.9d and Fig. 5.14b) of the composite ellipse along the horizontal axis. This composite ellipse only starts to rotate when its maximum amplitude has been reached. Composite ellipses which started their build-up in the near vertical direction continued to increase in amplitude and rotate at the same time (Fig. 5.7d and Fig. 5.9c), hence an apparent discrepancy between initial build-up in the horizontal and vertical directions has been observed. A final set of operating conditions may be obtained where it was possible for the composite ellipse to build-up linearly either vertically or horizontally to its full amplitude and then start to rotate (Fig. 5.8a and Fig. 5.13a). However linear build-up in any other linear position was not obtained. Under these conditions, it was still possible to obtain traces in which the composite ellipse built up and rotated at the same time (Fig. 5.13b).

Consider the final oscillation ellipse observed at the end of the majority of the oscillation pulses. The final ellipse appears to have two possible stable orientations, whose major axes lie parallel to a pair of sides of the parallelogram beat envelope. The interesting point here is that under certain fairly critical operating conditions the build-up process differs on successive gas pulses, so that the orientation of the final oscillation ellipse orientation changes from one final stable position to the other. The pair of longer sides of the parallelogram beat envelope change orientation in a similar way on successive gas pulses (Fig. 5.13c,d). The choice of final polarization orientation for the oscillation ellipse, and the orientation of the

FIGURE 5.9

a

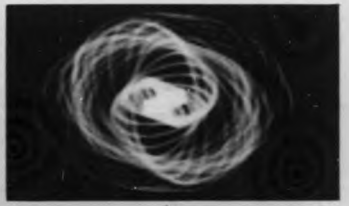

b

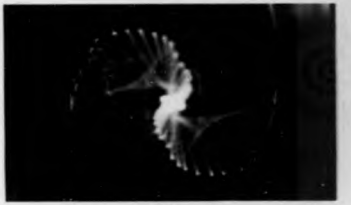

c

d

longer side of the parallelogram appears to be an almost random process, with nearly identical initial conditions giving a possibility of one of two final orientations. Under other operating conditions, it is possible to obtain parallelogram beat envelopes where there is only one stable position for the final stable oscillation ellipse (Fig. 5.14a,b).

The major axes of the two final stable elliptical orientations differ from each other by approximately 90 degrees for the J=K=2 transition. It is interesting to note however, that when considering the two stable orientations of the oscillation ellipse with previous static work on the system (Yassin 1981), the difference in orientation of the two polarizations was only 2 degrees. This was measured under conditions of zero applied field. As the final oscillation ellipse dies away due to gas scattering, the ellipticity of the ellipse increases and the major axis rotates from a position at 45 degrees to the horizontal axis, towards the horizontal axis itself (Fig. 5.14c,d).

5.7.3 COMPUTER SIMULATION OF ANTIPHASE BEATS

A simple computer model of the beat patterns may easily be obtained. To a first approximation, it is assumed that the output power level remains constant and that the orientation and eccentricity of the component oscillation ellipses are also constant. The trace observed on the oscilloscope is the beat pattern between the two down-converted oscillations, centered at approximately 45kHz with a frequency difference of one or two kHz. The coordinates of a point in a anticlockwise elliptical orbit may be represent by the following coordinate system (Fig. 5.10), $x_1 = a\cos(\omega t)$, $y_1 = b\sin(\omega t)$, where x_1 and y_1 are the coordinate axes with respect to the major and minor axes of the ellipse, a and b represent respectively the amplitude of the major and minor axes, b/a gives the eccentricity and ω the angular frequency of the oscillation (= 2×π×45kHz). Consider a second

FIGURE 5.10

COORDINATE SYSTEM USED FOR BEAT SIMULATION

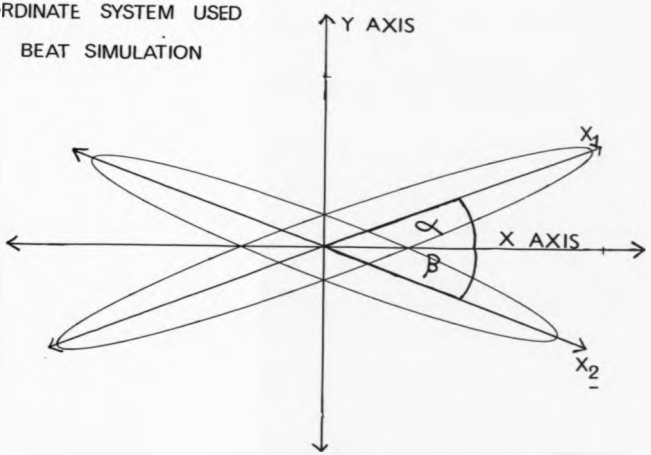

clockwise elliptical orbit orientated to different coordinate axes, x_2, y_2. This ellipse may be represented by the following coordinate system $x_2 = c\cos(\omega t)$ $y_2 = -d\sin(\omega t)$. Now the system must be considered in normal cartesian coordinates x,y, where x corresponds to the horizontal axis of both the oscilloscope and the maser cavity (Fig. 5.10). Let the first ellipse axis be orientated by an angle α, and the second ellipse by an angle β, in the opposite direction to the x axis in the normal x,y coordinate system. The rotation matrices for coordinate system x_1,y_1 and x_2,y_2 are given by,

$$\begin{pmatrix} \cos(\alpha), & -\sin(\alpha) \\ \sin(\alpha), & \cos(\alpha) \end{pmatrix} \qquad \begin{pmatrix} \cos(\beta), & \sin(\beta) \\ -\sin(\beta), & \cos(\beta) \end{pmatrix}$$

In the normal coordinate system the first oscillation is represented by,

$$\begin{pmatrix} x \\ y \end{pmatrix} = \begin{pmatrix} \cos(\alpha), & -\sin(\alpha) \\ \sin(\alpha), & \cos(\alpha) \end{pmatrix} \begin{pmatrix} a\cos(\omega_1 t) \\ b\sin(\omega_1 t) \end{pmatrix}$$

and the second oscillation is represented by:

$$\begin{pmatrix} x \\ y \end{pmatrix} = \begin{pmatrix} \cos(\beta), & \sin(\beta) \\ -\sin(\beta), & \cos(\beta) \end{pmatrix} \begin{pmatrix} c\cos(\omega_2 t) \\ -d\sin(\omega_2 t) \end{pmatrix}$$

adding both of these to give a beat pattern and rearranging gives:

$$x = a\cos(\alpha)\cos(\omega_1 t) - b\sin(\alpha)\sin(\omega_1 t)$$
$$+ c\cos(\beta)\cos(\omega_2 t) \simeq d\sin(\beta)\sin(\omega_2 t)$$
$$y \simeq a\sin(\alpha)\cos(\omega_1 t) + b\cos(\alpha)\sin(\omega_1 t)$$
$$- c\sin(\beta)\cos(\omega_2 t) - d\cos(\beta)\sin(\omega_2 t)$$

By plotting y against x for a time t of one half beat cycle a theoretical beat pattern may be obtained. By making α and β functions of time any rotation of the composite ellipses may be simulated, by making a,b,c, and d functions of time, the changes in amplitude and eccentricity of both component ellipses may be simulated. In the traces presented here all the parameters a,b,c,d remain constant.

5.7.4 THEORETICAL BEAT PATTERNS

The beat pattern obtained from two counter-rotating circularly polarized ellipses is shown in Fig. 5.11. The beat envelope is circular, and the pattern is that of a linear resultant, rotating in time. The beat pattern from two orthogonal linear oscillations of the same amplitude produces a square beat pattern, for the oscillations placed vertically and horizontally, the sides of the square lie along the horizontal and vertical axes, for the oscillations being polarized at 45 degrees to the horizontal and vertical axes the sides of the square also lie at 45 degrees to the horizontal and vertical axes (Fig. 5.12a,b). By adjusting the orientations of the two linear polarizations from 45 degrees and varying the relative amplitude of the two linear polarizations, the parallelogram beat patterns could be simulated (Fig. 5.12c,d). On increasing the eccentricity of the two ellipses other beat patterns obtained experimentally could be simulated. It was concluded that the parallelogram beat envelopes were produced by the beating of two linear polarization (ellipses) orientated each at near 45 degrees to the horizontal and vertical axes, in opposite directions. The conclusion was also drawn, that the near-circular beat envelopes were produced by the beating of two near-circular oscillations. This is in agreement with previous experimental work (Yassin 1981), where it was shown that the stronger the applied magnetic field, the nearer to circularity the oscillation ellipse became. In the present case, increasing the applied magnetic field increases the circularity of the two component ellipses, with the result that the beat envelope changes from a parallelogram towards a circle.

The parallelogram and near-parallelogram beat envelope computer traces are in good agreement with the experimental results obtained (Fig. 5.5d, Fig. 5.8a,c, Fig. 5.13a, Fig. 5.14c). Here the rate of rotation of the simulated composite ellipse is non uniform, being at its

FIGURE 5.11

BEAT SIMULATION

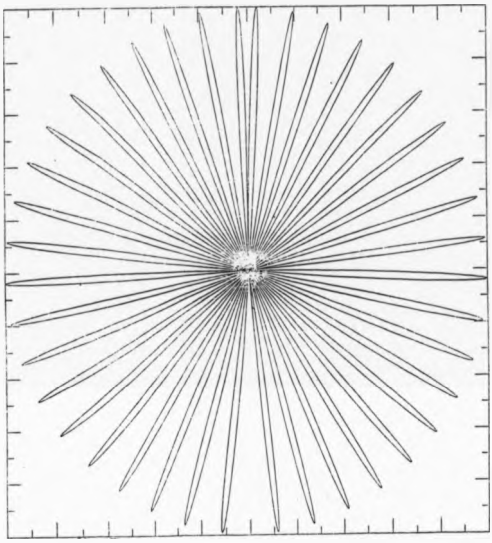

FIGURE 5.12a

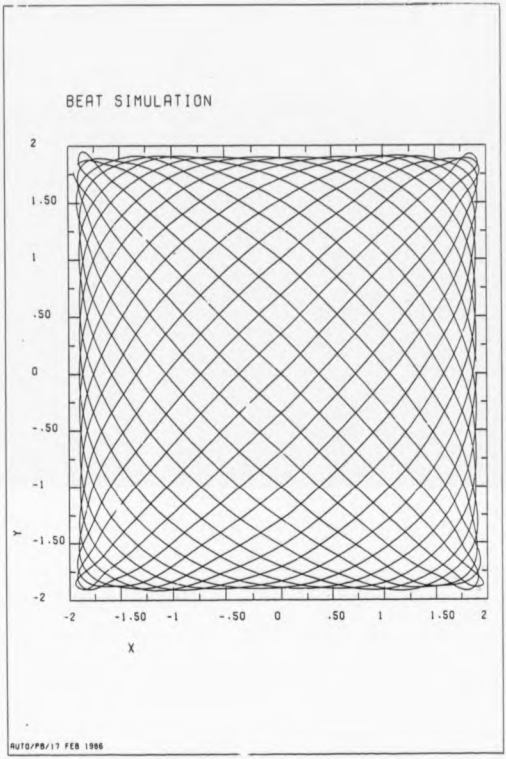
BEAT SIMULATION
2
1.50
1
.50
0
-.50
-1
-1.50
-2
Y
-2
-1.50
-1
-.50
0
.50
1
1.50
2
X
AUTO/PB/17 FEB 1986

FIGURE 5.12b

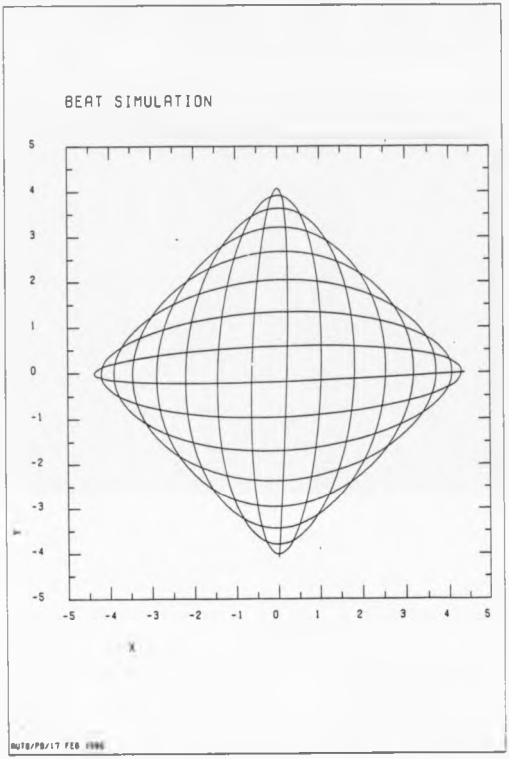
BEAT SIMULATION
5
4
3
2
1
0
-1
-2
-3
-4
-5
Y
-5 -4 -3 -2 -1 0 1 2 3 4 5
X
AUTO/PB/17 FEB 1986

FIGURE 5.12c

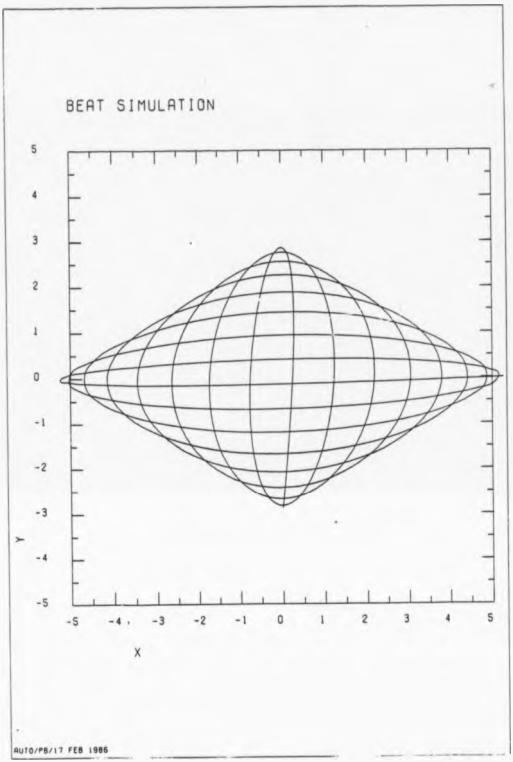
BEAT SIMULATION
5
4
3
2
1
0
-1
-2
-3
-4
-5
Y
-5
-4
-3
-2
-1
0
1
2
3
4
5
X
AUTO/PS/17 FEB 1986

FIGURE 5.12d

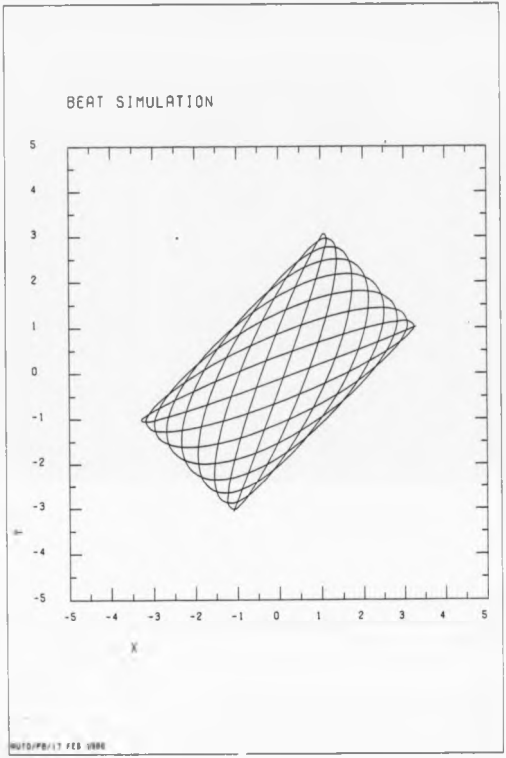

slowest as the major axis of the simulated composite ellipse is in line with a corner of the parallelogram, and fastest when the major axis of the simulated composite ellipse bisects the parallelogram. Further-more, the ellipticity of the simulated composite ellipse is almost linear when the major axis of the simulated composite ellipse lies in a corner of the parallelogram, and least eccentric when the major axis of the simulated composite ellipse is perpendicular to one of the sides of the parallelogram.

5.7.5 PRELIMINARY INTERPRETATION OF RESULTS

The changes that take place in the component oscillation ellipses during the evolution of the gas pulse may be determined by a study of the beat patterns. Firstly, consider the traces showing a parallelogram beat envelope. The final single frequency oscillation ellipse may be observed on many of the traces. Here the major axis of this oscillation ellipse is orientated in the same direction as one of the sides of the parallelogram, and hence orientated in the same direction as one of the linear component oscillations producing the beat envelope. The conclusion is drawn that this oscillation component develops into the final oscillation ellipse, changing its polarization from linear to elliptical as the beat envelope dies away, due to the suppression of the second oscillation. These two processes, although occuring at the same time, appear to be independent. On most traces (Fig. 5.8a), the beat pattern decays while the envelope still remains near-parallelogram shaped, while on other traces obained under different operating conditions (Fig. 5.35a,b), the beat pattern becomes near-circular due to the change in the two oscillation components from linear to elliptical polarizations before there has been any substantial decay in the beat envelope.

The parallelogram beat envelope traces which show either

horizontal or vertical initial linear oscillation build-ups are now examined (Fig. 5.8a and Fig. 5.13a). The composite ellipse here is not rotating in time, nor is its eccentricity changing. The rest of the parallelogram beat pattern is produced from two near linearly polarized oscillations inclined at near 45 degrees to the x and y axes. It is impossible, however, for the two near-linearly polarized oscillations inclined at nearly 90 degrees to each other to produce a beat pattern where the composite ellipse does not rotate in time and remains linearly polarized. The linear polarization build-up observed here can only have been produced by either a single or a biharmonic linearly polarized oscillation, where the oscillations remain linearly polarized in the direction of the linear build-up. These oscillations presumably rotate by approximately 45 degrees during the course of the build-up.

It is interesting to consider why the linearly polarized oscillation build-up occurs under some operating conditions in the horizontal direction only, under other operating conditions in the horizontal and vertical directions only, and has never been observed at any intermediate angle near 45 degrees. It is proposed here that the initial linear build-ups are due to one or both component oscillations displaying oscillation amplitude settling transients (Chapter 2), which, in many examples of single frequency oscillation build-up occurs linearly along the horizontal axis. Due to the anisotropies in the system, the threshold for initial linear transient build-up in the horizontal direction is lower than the threshold for initial linear transient build-up in the vertical direction. Under some operating conditions the threshold for transients in the horizontal direction is fulfilled, but the threshold for transients in the vertical direction is not, hence only horizontal linear initial build-ups are observed. Under other operating conditions the thresholds for both horizontal and vertical linearly polarized transients are reached, and both vertical

FIGURE 5.13

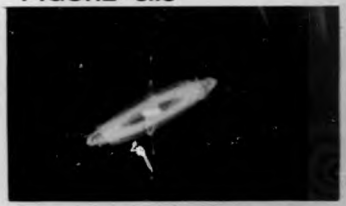

a

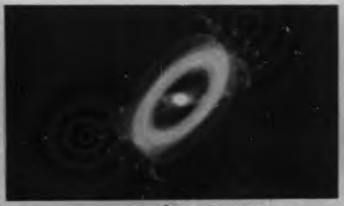

b

c

d

FIGURE 5.14

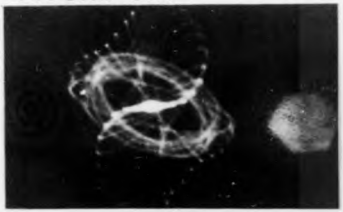

a

b

c

d

FIGURE 5.15

a

b

c

d

FIGURE 5.16

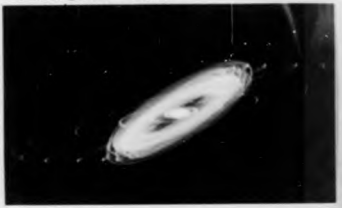

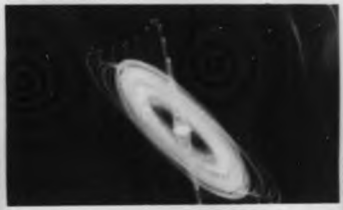

and horizontal linearly polarized initial build-ups are observed. In single frequency oscillation, linearly polarized transients inclined at approximately 45 degrees to the horizontal and vertical axes have been observed, although they are not common. Consider now a transient build-up at 45 degrees to the horizontal and vertical axes. This oscillation build-up is very close in orientation to one of the stable oscillation orientations. It is proposed here that initial build-up in this direction favours the oscillation component with its major ellipse axis aligned in the same direction as the initial build-up, rather than the oscillation component aligned with its major axis at 90 degrees to the direction of initial build-up. The advantage may be so great as to prevent the second component from reaching oscillation threshold, and so single frequency oscillation is observed. Evidence for this idea is shown in (Fig. 5.15b), where under the same operating conditions required to produce parallelogram beat envelopes, only single frequency oscillation build-up is observed. The initial direction of build-up is between 35 and 45 degrees to the horizontal axis, close to the final stable position inclined at between 40 and 45 degrees to the horizontal axis.

No linear initial build-up has been observed on traces displaying near-circular beat patterns. The near-circular beat patterns (Fig. 5.5a,b) are produced when two-component oscillation ellipses are nearly circular. Any linear transient would have to become elliptical extremely rapidly in order to produce circularly polarized oscillation ellipses early in the build-up. This would cause any linear initial build-up observed to become an elliptical composite ellipse rather rapidly, with the composite ellipse both building up and rotating at the same time. Further-more, the greater applied magnetic field usually required to produce circular beat envelopes would increase the threshold for the transients, and reduce the amplitude of any transients produced.

Finally a specific trace is shown and the evolution of component ellipses discussed. Fig. 5.13a shows an initial linear vertical oscillation build-up, where one or both of the oscillation ellipses build-up nearly linearly and vertically. Any transient effect here will modify the beat envelope pattern slightly. One or both of the linear oscillations rotate approximately 45 degrees to give two linear polarizations at 90 degrees to each other, producing a near square beat envelope. After a quarter of a cycle the beat pattern rapidly decays as one of the linear oscillations is lost. The second oscillation now changes from being linearly polarized to being elliptically polarized; as the oscillation decays its orientation remains constant. This type of analysis may be repeated for most of the observed traces.

A few traces show unexplained features, examples are Fig. 5.15c,d, there appears to be an oscillation prepulse present on these traces.

5.8 SINGLE FREQUENCY OSCILLATION ON THE J=K=2 TRANSITION OF $^{14}NH_3$

5.8.1 GENERAL COMMENTS

Single frequency oscillation build-ups on the J=K=2 transition of $^{14}NH_3$ show a variety of Lissajous spiral patterns, depending upon the initial conditions of the maser system. Examples are shown in Fig. 5.17 to Fig. 5.24. The build-up patterns are highly dependent upon the anisotropies within the system, both the anisotropies of state selection which are EHT dependent, and the anisotropies of the maser cavity, which are dependent on the flatness and alignment of the cavity plates. The build-up patterns are also dependent on the cavity tuning and any applied fields, either electric or magnetic.

The build-up process may be divided into three parts, the initial build-up of a settling transient, an intermediate region where the oscillation ellipse rearranges itself, with its orientation and

eccentricity changing in time due to the dynamic processes involved, and a final "stable" oscillation ellipse position, (governed by the static maser parameters), which slowly decays in time due to the time dependence of some of these parameters. On some traces either the transient build-up or the intermediate period may be absent, and on some traces the Z-bright-up time of the CRO was too short to observe the position of the final ellipse. Each of these stages of the build-up process will be commented upon in turn and any emerging trends discussed. Two examples of traces are shown (Fig. 5.17a,b).

5.8.2 EXPERIMENTAL OBSERVATIONS

The following general trends were noted.

The direction of the build-up of the initial settling transient is highly dependent on initial conditions, in the majority of cases however the initial build-up is along or near to the horizontal axis and to a close approximation linearly polarized (Fig. 5.17c,d and Fig. 5.18a,b,c,d). A few traces show build-up in the vertical polarization and intermediate positions (Fig. 5.17b, Fig. 5.19a,b,c,d and Fig. 5.20a,b). In all cases of linear polarized build-up the oscillation passes from a linear polarization to an elliptical or circular polarization, which is observed later in the oscillation pulse. Only in a few examples (Fig. 5.20c,d) did the very early stages of the build-up process produce an elliptical or circularly polarized build-up.

At low levels of EHT (6-12kV) only linearly polarized build-ups along or near to the horizontal axis were observed. Here the build-up patterns are similar on successive gas pulses. At higher levels of EHT (15-20kV) an initial linear build-up is observed in all directions. Here the build-up patterns may be very different on successive gas pulses, transient build-ups occur in different directions, and with different amplitudes.

FIGURE 5.17

a

b

c

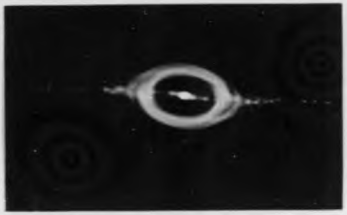

d

FIGURE 5.18

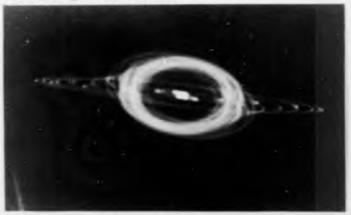

a

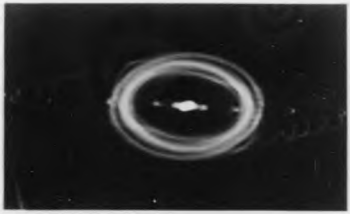

b

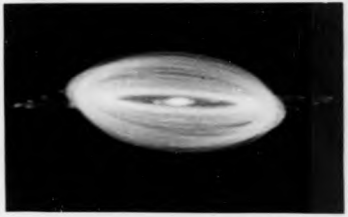

c

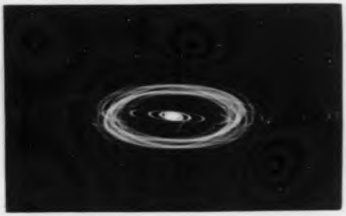

d

FIGURE 5.19

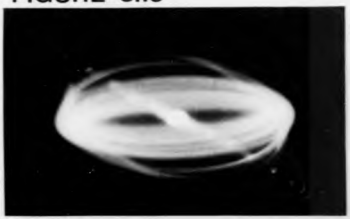

a

b

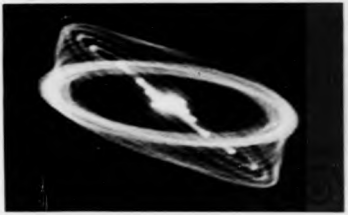

c

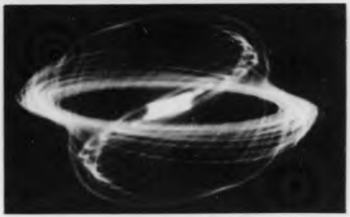

d

FIGURE 5.20

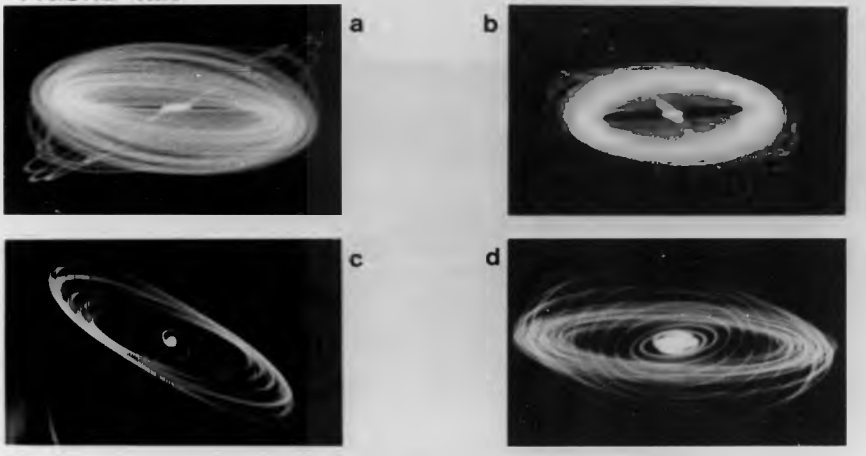

For an oscillation build-up close to the horizontal, the oscillation transient remained nearly linearly polarized until it reached its maximum amplitude (or even later), and as the transients decayed into the intermediate region the oscillation becomes elliptical (Fig. 5.17c,d and Fig. 5.18.a,b,c,d). With oscillation build-up in the vertical direction, the oscillation became elliptical as it was developing, so that as the transient reached maximum amplitude it is already elliptical (Fig. 5.19b and Fig. 5.21a,b). Here the major axis of the experimental polarized oscillation transient often did not remain constant but rotated in time as the transient developed and died away (Fig. 5.17b and Fig. 5.21b). In some cases the transient ellipse finally rotated to the horizontal position. This is very common with linear transient build-up at orientations intermediate between horizontal and vertical (Fig. 5.20a,b). The rate of rotation was non-uniform and its direction may have reversed during, or after the transient build-up (Fig. 5.17b).

The rate at which transient build-up changes from linear to elliptical polarization varies also on successive gas pulses (Fig. 5.17d and Fig. 5.18d). Here two linear horizontal build-ups are shown. In Fig. 5.17d the oscillation remains linearly polarized until the total decay of the transient, where as in Fig. 5.18d the oscillation has become elliptical at the maximum excursion of the transient.

On many traces the intermediate region is simply the movement of the oscillation ellipse from its initial near-linearly x-polarized transient build-up, to one which is an elliptically polarized final stable orientation in a different direction. In several examples, under high values of EHT state selection and critical cavity tuning, the intermediate region is far more complicated (Fig. 5.21c,d and Fig. 5.22a,b,c). Fig. 5.21d and Fig. 5.22b show near-vertically polarized settling transients rotating as described previously. There

FIGURE 5.21

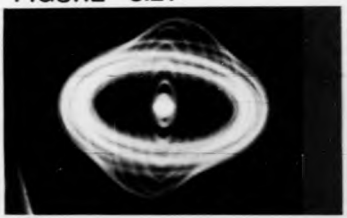

a

b

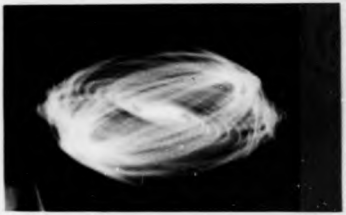

c

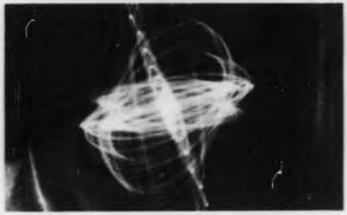

d

FIGURE 5.22

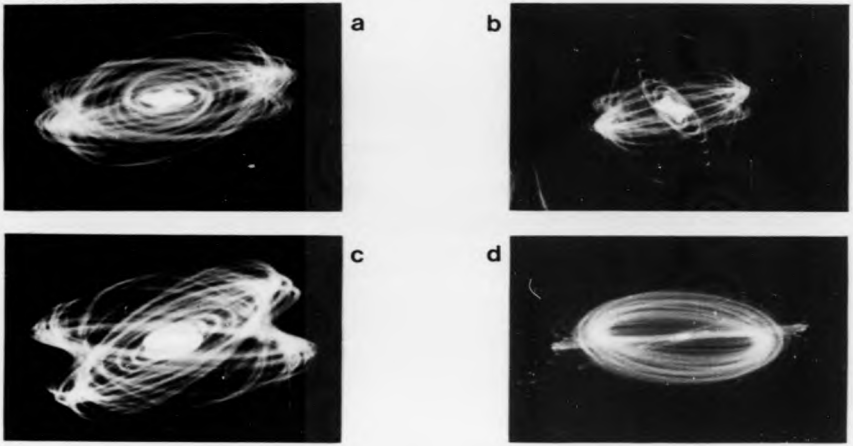

appears to be two stable or near-stable oscillation orientations where the major axis of the oscillation ellipse is inclined at 20 degrees and 5 degrees respectively, on opposite sides of horizontal axis. It appears that the major axis of the oscillation ellipse rotates to one or other of these positions on the decay of the oscillation transient. The oscillation ellipse then appears to become elliptical with its major axis orientated along the horizontal axis, as the oscillation ellipse passes from the first near-stable position to the second, the major axis of the oscillation ellipse having crossed the horizontal axis in the process. Fig. 5.21c and Fig. 5.22a,b show the effect in the absence of the initial vertical transient. It is interesting to note that this effect has not yet been observed following an initial horizontal linear build-up.

A few traces show unexplained features, an example being Fig. 5.22d, where a linearly polarized transient build-up begins at approximately 30 degrees to the horizontal axis. This transient rotates towards the horizontal axis and then remains stationary, linearly polarized in the horizontal direction, for 0.10 milli seconds, before rotating further.

The final stable oscillation ellipse orientations show a variety of elliptical polarizations and near-circular polarizations. In many examples the major axis of the ellipse is positioned along the horizontal axis (Fig. 5.17 to Fig. 5.19). In other examples the major axis of the ellipse may be inclined to the horizontal axis by an angle of approximately 30 degrees. The angle of inclination of 45 degrees which was obtained for the angle of inclination of the oscillation ellipse under an applied magnetic field was not reached.

Under conditions of high EHT (15-20kV) and critical cavity tuning and alignment there were two possible stable final orientations of the oscillation ellipse, each with the major axis of the ellipse

FIGURE 5.23

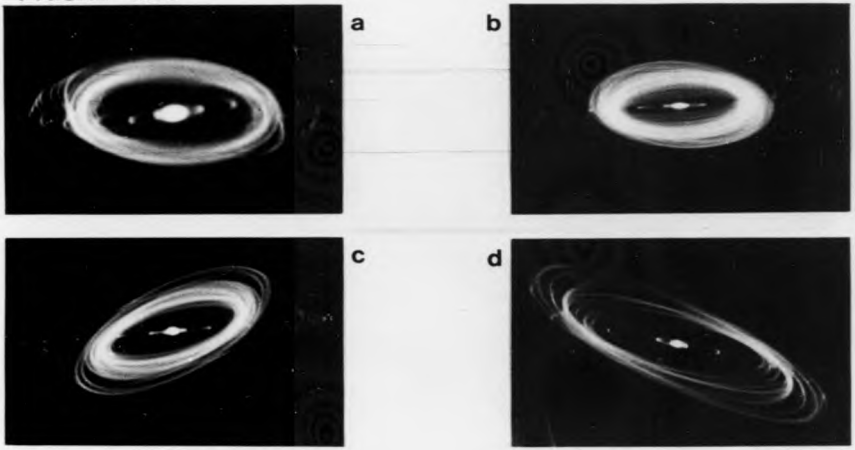

inclined to the horizontal axis by an angle of up to 30 degrees, the two ellipse major axes being inclined in opposite directions (Fig. 5.24a,b). It is possible, on successive gas pulses for an initial linearly polarized oscillation build-up in the near horizontal direction to arise, and to be followed by one of two possible rotations of the oscillation ellipse. On the first oscillation pulse the oscillation ellipse may rotate clockwise to one stable final elliptical orientation, and on the following oscillation pulse the oscillation ellipse may rotate anticlockwise to a second stable final elliptical orientation (or vise versa) (Fig. 5.24a,b). This effect is similar to the two stable final elliptical orientations obtained under conditions of an applied magnetic field (Chapter 5.7). However, in the latter case, rotation of the major axis of polarization under an applied magnetic field (Yassin and Lainé 1985) increased the angle between the two major axes of the stable ellipses, from approximately 60 degrees to approximately 90 degrees.

As the the final stable oscillation ellipse decays, both the eccentricity and the orientation of the ellipse change in time. In many examples the major axis of the ellipse rotates towards the horizontal axis and the eccentricity decreases so that the oscillation becomes more linear. The same effect was observed under an applied magnetic field (Fig. 5.17b, Fig. 5.18c, Fig. 5.19a, Fig. 5.23c, Fig. 5.24a,b).

5.8.3 PRELIMINARY INTERPRETATION

At low levels of EHT, the anisotropies in the system are dominated by a large state selector gain anisotropy, which favours gain and hence oscillation build-up in the horizontal direction. As the EHT is increased the anisotropy is reduced. However it does not appear to be eliminated.

The direction of initial oscillation build-up depends not only

FIGURE 5.24

a

b

on static values of the various anisotropies, but also on fluctuations of various types within the maser system, including thermal noise. Such fluctuations may possess an anisotropy time dependence, for example, via vibrations of the cavity plates, This would change the relative gains between the horizontal and vertical directions, and hence the most favourable orientation for oscillation build-up. However the time-averaged gain anisotropies over a few milliseconds evidently still favours oscillation build-up in the horizontal direction for the following argument to hold.

The rate of build-up of the maser oscillation is dependent on the maser oscillation overfulfilment factor (Oraevskii 1964), at low EHT values, the gain in the vertical direction is insufficient to produce either Rabi oscillation settling transients or rapid oscillation build-up, whereas the gain in the horizontal direction is sufficient to produce both. The result is strong horizontal linear build-up irrespective of the initial direction of the oscillation polarization at the moment oscillation began, due to thermal noise or other rapid fluctuations. The polarization of the oscillation at the moment it begins determines only the point in the build-up process where the oscillation ceases to be horizontally linearly polarized. At higher levels of EHT the gain in the vertical direction is now sufficient for the production of rapid settling transients. However the gain and rate of the build-up process in the horizontal direction is greater. Oscillation build-up which begins along, or near, the horizontal direction continues to build-up in this direction, since this is the direction of greatest gain. The much later and slower build-up of oscillation in the vertical direction causes the linear oscillation to become elliptical, although this is noticeable only after the peak value of the oscillation transient has been obtained. Oscillation build-up which begins along or near the vertical direction is more complicated,

as a high level of oscillation output power cannot be sustained in that direction. The build-up of oscillation in the horizontal direction will occur much faster than oscillation build-up in the vertical direction although it may begin later. The result is that when the oscillation transient has reached its maximum value in the vertical direction there is already a substantial build-up of oscillation in the horizontal direction. There are two possible effects. Either the oscillation becomes elliptical in its early stages of build-up or the linear oscillation polarization rotates from a vertical to a near horizontal direction. Both of these effects are observed experimentally.

In the static case, the combination of state selector linear gain anisotropy, and both gain and phase anisotropies introduced by the cavity resonator lead to the observation of polarization bistability (Lainé and Yassin 1981). It appears that the two possible polarization orientations observed in the final "stable" portion of the gas pulse (Fig. 5.24a,b) correspond to the two possible bistable positions. As noted previously, under an applied magnetic field the angle between the two possible polarization orientations is approximately 90 degrees under the earth's field, whereas in the present case the angle between the two polarization orientations is approximately 50-60 degrees. Note however, that the angle between the two polarization orientations reported by (Yassin 1981) for the J=K=2 line of $^{14}NH_3$ the angle was only 2 degrees. This suggests that the angle between the two stable orientations is a function of the anisotropy and magnetic field present in the system at the time of observation. It is unlikely that a difference of orientation of 2 degrees would have been observed by the present method of operation.

The intermediate portion of the oscillation build-up process is highly variable. Under certain operating conditions two stable or near-stable oscillation ellipse orientation positions are observed on

the same oscillation build-up trace, the angle between the major axis of these orientations is approximately 15 degrees (Fig. 5.21c,d and Fig. 5.22a,b,c). It is not clear whether or not these two stable or near-stable polarization orientations correspond to the bistable positions of the static case (Lainé and Yassin 1981). If so, the passage of the oscillation ellipse from one elliptical polarization orientation to another may give some indication of the form of the time evolution of elliptical polarization orientation flips.

The change in the eccentricity and orientation of the oscillation polarization ellipse as the oscillation pulse slowly decays in time is interesting to discuss. These parameters of the polarization ellipse depend on the gain and phase anisotropy of the maser cavity and the gain anisotropy of state selection (Yassin 1981). There are several possible explanations for the changes that occur with the polarization ellipse. These are discussed below.

1) The anisotropies of the system may remain constant throughout the gas pulse, but the dynamic settling processes may not have been completed, so that the the changes in orientation and eccentricity may be a dynamic effect.

2) The anisotropies may remain constant, but the ellipse parameters may be a function of the oscillation overfulfilment condition. The number of state selected molecules R required to reach maser oscillation will be different for the vertical and horizontal polarizations due to cavity gain anisotropy. However, this is small compared with state selector anisotropy and will be neglected here. The ratio of the number of state selected molecules in the horizontal polarization N_X to the number of state selected molecules in the vertical polarization N_Y is assumed constant (constant gain anisotropy)($N_X > N_Y$). The amplitude of oscillation is dependent on the function (N-R) where N is the number of state selected molecules in the

relevant polarization. N_X and N_Y are functions of time, therefore the function $(N_X-R)/(N_Y-R)$, the ratio of the horizontal component of oscillation to the vertical component is also time dependent. As N_X is greater than N_Y, the result of the total oscillation amplitude falling, is that the vertical component of oscillation will decay fastest. This has the result that either the oscillation becomes more linear, or its major axis rotates towards its horizontal axis, which agrees with experimental results (Fig. 5.24a,b).

3) The state selector gain anisotropy may be time dependent. Electric field state selection selects molecules in the $M_J = \pm 2$ and $M_J = \pm 1$ states. The focusing force of the state selection is proportional to $(M_J)^2$. Molecules in the $M_J = \pm 2$ state are normally completely state selected and contribute mainly to the horizontal polarization of oscillation. Molecules in the $M_J = \pm 1$ state are less well state selected, the number of state selected molecules entering the maser cavity being dependent on the intensity of the molecular beam and its scattering (Al-Jumaily 1979). These molecules contribute to the oscillation output power in both polarizations. As the gas pulse progresses the scattering of the molecular beam increases, the molecules in the $M_J = \pm 1$ state are more easily scattered. The fraction of molecules in the $M_J = \pm 1$ state reaching the maser cavity is reduced, and so the anisotropy of state selection increases. The effect is as in (2) above.

5.9 OSCILLATION ON THE J=K=2 TRANSITION OF $^{14}NH_3$ WITH MODIFIED CAVITY ANISOTROPY

5.9.1 GENERAL COMMENTS

In order to examine further the effect of the cavity anisotropy on the oscillation build-up process, the cavity anisotropies were deliberately modified by stretching a thin metal wire along the fringe

field of the maser cavity, such that it was positioned symmetrically between the two cavity plates, with the wire at its midpoint extending up to approximately 1 cm inside the cavity. The wire was placed both horizontally and vertically on different occasions. The effect of the wire was firstly to lift the degeneracy of the cavity modes in the vertical and horizontal directions, and secondly to introduce a slight phase and loss anisotropy due to the differential dielectric constants of free space and the wire, and the modified geometry of the system. The centre frequency for oscillation in a polarization perpendicular to the wire was modified depending on the depth that the wire was placed within the cavity. The centre frequency for oscillation in a polarization parallel to the wire remained unaltered. The effect of the presence of the wire was to change dramatically the gain anisotropy as the maser cavity was tuned across its resonance. During the setting up procedure the cavity mode had only been observed through its horizontal component and consequently the quality factor of this component had been maximised, possibly at the expense of the vertical component.

5.9.2 EFFECT OF PLACING A THIN HORIZONTAL WIRE DEEPLY INTO THE FRINGE FIELD OF THE RESONATOR

Consider firstly the effect of placing a horizontal wire in the fringe field. Initially the thin wire was placed approximately 1 cm inside the cavity. The centre frequency of the cavity resonance of the horizontal component of the cavity mode was changed noticeably by placing the wire inside the fringe field. The cavity resonance was now retuned to its original frequency and the quality factor of the horizontal component of the cavity mode was maximised. On operating the maser in conventional and Lissajous figure modes of display the following trends were observed.

1) The total oscillation power level observed here was large

with clear second peaks of the self-induced Rabi oscillations observed in zero applied field. The introduction of the wire into the fringe field of the maser cavity did not significantly degrade the cavity Q-value. On application of a magnetic field in a direction normal to the plane of the cavity plates a large enhancement of the self induced Rabi oscillation effect was observed (Chapter 2)(Fig. 2.7d).

2) The low frequency beating effect in an applied magnetic field discussed earlier in this chapter was absent here, due to the removal of the degeneracy between the vertical and horizontal components of the cavity mode.

3) In zero applied magnetic field the oscillation observed was linearly polarized along the horizontal axis (Fig. 5.25a), with any component of oscillation in the vertical direction being too small to monitor above the noise level of the detecting system. On application of a magnetic field the plane of polarization rotated slightly and the oscillation became slightly elliptical. The ratio of horizontal to vertical component oscillation levels was here approximately 10:1. The signal to noise ratio of the vertical component was at best only 3:1, and so the results were not precise.

4) On adjusting the cavity tuning so that the cavity Q curve passed through the oscillation frequency, no position could be found which enhanced the vertical component of oscillation. In the absence of any applied magnetic field the oscillation remained linearly polarized.

The centre frequency of the vertical Q_Y component of cavity Q will be offset from the oscillation frequency due to the retuning to the horizontal Q_X component of quality factor undertaken in the setting up procedure. The gain in the vertical polarization will therefore be heavily reduced. The state selector anisotropy already favours oscillation in the horizontal direction, therefore the system as a whole has an extremely high gain anisotropy in favour of the horizontal

FIGURE 5.25

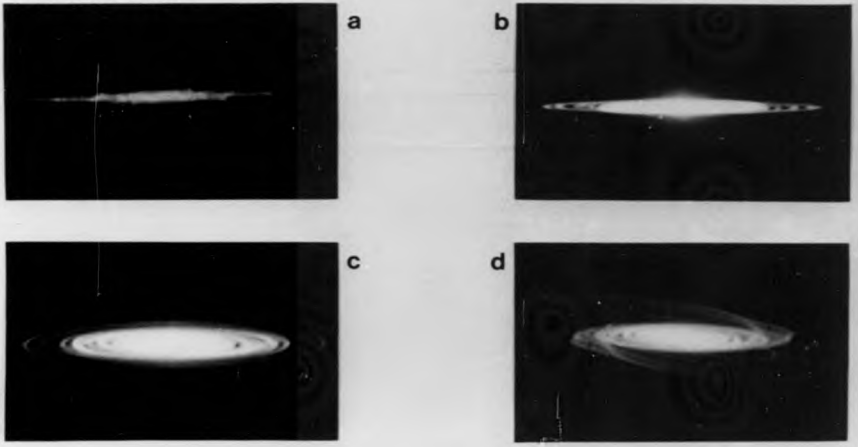

polarization to give the experimental results shown.

5.9.3 THE EFFECT OF PLACING A THIN HORIZONTAL WIRE MODERATELY DEEPLY INTO THE FRINGE FIELD OF THE MASER CAVITY

The experiment was repeated with the horizontal wire less deeply immersed into the fringe field of the cavity. The trends are discussed below.

1) In the absence of an applied magnetic field the oscillation remained almost completely linearly polarized along the horizontal axis. This linear polarization remained constant in direction as the cavity mode was tuned across the oscillation frequency. In the conventional detection mode strong first and second self-induced Rabi oscillations were observed which were used to monitor the strength of the maser oscillation.

2) On application of a magnetic field the oscillation became elliptical with oscillation settling transients present on some of the traces (Fig. 5.25b,c). There was no dramatic slowing of the self induced Rabi oscillation decay constant as seen previously. This effect appeared only when the oscillation was completely linearly polarized. With this system, the anisotropy favours horizontal linear polarization, however it is possible to obtain initial oscillation build-up in directions away from the horizontal axis. This is again attributed to the balancing effect of the applied magnetic field. (Fig. 5.26a,b).

3) When the applied magnetic field was increased further, low frequency beats were again observed, similar to those observed earlier. The beat envelope was again that of a parallelogram; however the sides here were inclined at an angle of approximately 15 degrees to the horizontal, compared with the approximately 45 degrees angle observed in the absence of a wire (Fig. 5.26c,d and Fig. 5.28a). This suggests the two oscillations which combined to give the beat pattern, were both

FIGURE 5.26

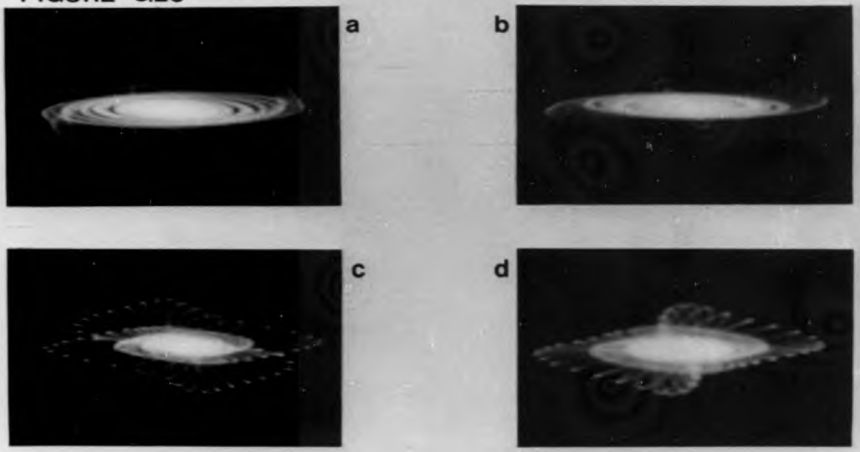

linearly polarized oscillations, inclined at 15 degrees to the horizontal axis, each on opposite sides of this axis. The beat pattern changes rapidly to an elliptical beat envelope (Fig. 5.26c,d). The final "stable" oscillation ellipse was inclined with its major axis at approximately 10 degrees to the horizontal axis (Fig. 5.28a). In several examples (Fig. 5.27a,b), the final oscillation ellipse appears to have almost completely rotated back to align its major axis to the horizontal axis.

4) On application of pressure to one of the waveguides, which applied differential pressure to one of the cavity plates and so changing the cavity anisotropy, low frequency beats were observed in the absence of any applied magnetic field (Fig. 5.27c,d). Similar beats have been observed previously (Smart 1974).

5.9.4 THE EFFECT OF PLACING A HORIZONTAL WIRE SLIGHTLY INTO THE FRINGE FIELD OF THE RESONATOR

A final experiment was conducted using a horizontal wire, this time only slightly immersed into the fringe field. Trends are commented upon as before.

1) Under an applied magnetic field orthogonal to the plane of the cavity plates, low frequency beats were again observed. The beat pattern produced initially was again that of a parallelogram beat envelope, with sides inclined at approximately 20 degrees to the horizontal axis. The final oscillation ellipse was produced with its major axis in the same direction as one of the sides of the parallelogram, this was similar to the situation in the absence of a wire.

2) In the absence of an applied magnetic field, the oscillation polarization build-up was dependent on the value of the applied EHT to the state selectors. At low values of EHT less than 12kV, the

FIGURE 5.27

a

b

c

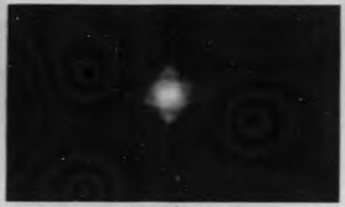

d

FIGURE 5.28

a

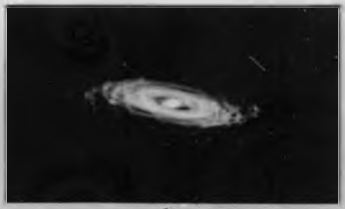

b

c

d

oscillation build-up was completely linearly polarized along the horizontal axis. For EHT values above 12kV a linearly polarized self-induced Rabi oscillation settling transient built up along the horizontal axis, then evolved to an ellipse as before.

3) With an applied magnetic field insufficent to produce low frequency biharmonic oscillation, there was initial build-up of the single frequency oscillation in both the vertical and horizontal directions (Fig. 5.29a,b). This suggests that the magnetic field has the effect of balancing the cavity anisotropy introduced by the thin wire.

4) At a EHT value of approximately 18kV, critical cavity tuning, and zero applied field, two possible highly eccentric possible final oscillation ellipses were observed, the first observed with its major axis rotated at approximately 5 degrees clockwise from the horizontal axis, the second observed with its major axis rotated at approximately 5 degrees anticlockwise from the horizontal axis. On examination of two successive oscillation pulses the following was observed. On the first oscillation pulse the oscillation ellipse built up as a linearly polarized oscillation transient along the horizontal axis, and then the ellipse major axis rotated clockwise to the first stable highly eccentric elliptical orientation (Fig. 5.29c). On the second oscillation pulse the oscillation ellipse again built up as a linearly polarized oscillation transient along the horizontal axis, and this time the oscillation ellipse rotated anticlockwise to second stable eccentric elliptical orientation (Fig. 5.29d). This is similar to the effect observed in the absence of a wire.

FIGURE 5.29

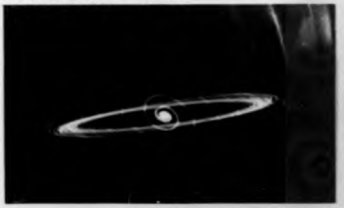

a

b

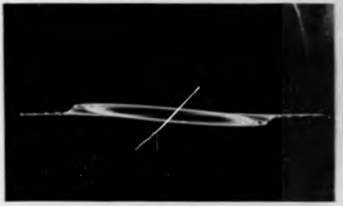

c

d

5.9.5 THE EFFECT OF PLACING A VERTICAL WIRE INTO THE FRINGE FIELD OF THE MASER CAVITY

The motivation for repeating the previous experiment with a vertical wire placed in the fringe field of the maser originated from the work of the previous sections. Placing a horizontal wire in the fringe field of the cavity has had the effect of apparently enhancing the total anisotropy of the system by inducing a cavity gain anisotropy in favour of the horizontal direction. It was assumed that placing a vertical wire in the cavity fringe field would produce a cavity gain anisotropy which would then be used to balance the state selector gain anisotropy. The objective of this experiment was to produce a system where only phase anisotropy, and negligible gain anisotropy, is present, and so study the evolution of the oscillation ellipse under these near-isotropic conditions.

5.9.6 MASER OPERATION WITH A THIN VERTICAL WIRE SLIGHTLY IMMERSED IN THE RESONATOR

Single frequency oscillation and low frequency biharmonic oscillation were both observed here. The major trends in the observed traces are discussed and preliminary interpretations are made.

In many examples oscillation amplitude settling transients are observed. Here most of the transients remain almost completely linearly polarized until their maximum amplitude has been reached. Such transients appear to build-up in all the possible linear polarizations (Fig. 5.30). Unlike the settling transient build-up in the absence of the wire, the form of the transient build-up was independent of its initial direction. Several traces show build-up patterns with no obvious transients (Fig. 5.31c). It is also possible to observe transients which build-up and become elliptical at the same time (Fig. 5.31d). The most favourable direction for initial transient

FIGURE 5.30

a

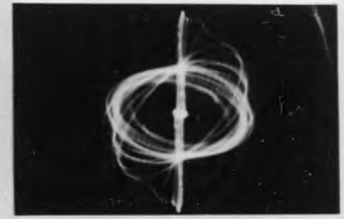

b

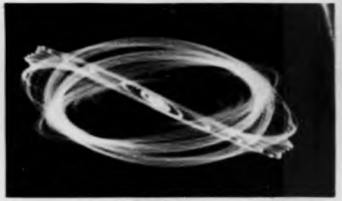

c

d

FIGURE 5.31

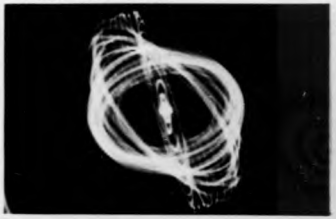

a

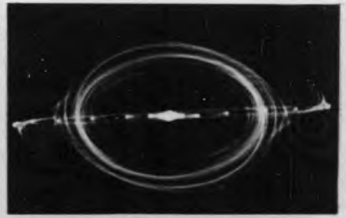

b

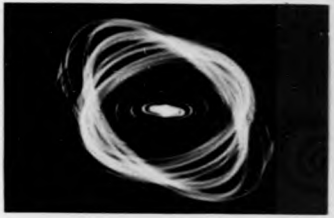

c

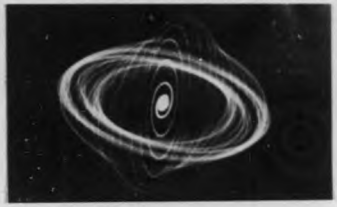

d

build-up was highly dependent on cavity tuning.

The intermediate portion and final stable position of the oscillation build-up are best considered together. In many examples the oscillation ellipse simply rotates from its position of initial linear build-up to a final elliptical orientation (Fig. 5.30b and Fig. 5.31a). Transient build-up in the vertical direction may rotate either clockwise, or anticlockwise, to a final elliptical orientation (Fig. 5.30a,c). Transient build-up in the near horizontal direction may similarly rotate either clockwise or anticlockwise. Transients which build-up at intermediate positions tend to rotate towards the horizontal axis (Fig. 5.30a,c).

The intermediate portions of the oscillation ellipse evolution may be quite complex. There appear to be two stable or near stable oscillation polarization orientations, each inclined with its major axis inclined at approximately 30 degrees to the horizontal axis, on on either side of this axis. In many examples the oscillation ellipse builds up with a linear horizontal transient which then rotated clockwise to the first near stable position, the oscillation becoming elliptical in the process. The oscillation ellipse then moved from the first near stable oscillation ellipse orientation to the second stable orientation, with its major axis inclined on the other side of the horizontal axis (Fig. 5.32a,b). In the intermediate positions the oscillation ellipse appeared to be elliptically polarized with its major axis lying close to the horizontal axis (Fig. 5.32c,d). It is interesting to note that the evolution of the oscillation ellipse varies on successive gas pulses, yet for quite a variety of oscillation ellipse evolutions the general description given above is followed. Several traces show elliptical oscillation build-up with orientation close to that of the near stable oscillation ellipse positions, with no observed linear transients (Fig. 5.33a,b). The major axis of the elliptical

oscillation build-up then rotates, passing through the horizontal axis, to finally settle down to elliptical oscillation at the stable position. Several examples of the above effects are shown, in (Fig. 5.33d) the order in which the oscillation ellipse pass through the two stable or near stable positions reverses. It is possible to observe traces which show intermediate behaviour between Fig. 5.33b and Fig. 5.32c,d. Two examples are shown, Fig. 5.34a,b. A few traces show almost circularly symmetric oscillation build-up and evolution, an example is shown in Fig. 5.34d. A few traces again show unexplained behaviour, an example is Fig. 5.34c where the oscillation ellipse is observed passing from elliptical to a linear polarization.

With initial transient build-up in any direction, the final oscillation ellipse is elliptically polarized with its major axis inclined at angles up to 30 degrees from the horizontal axis. This posed an interesting puzzle question. The orientation of the final oscillation ellipse suggests that the anisotropy in these examples favours oscillation in the horizontal direction, whereas the strong linear transient build-up observed over a large number of orientations suggests that the gain anisotropies of the system are almost completely balanced. There is an apparent contradiction here.

In order to resolve the above problem, the equations governing oscillation amplitude settling transients should be reexamined. A very simple model is to consider the transient build-up in the horizontal and vertical polarizations as independent, and to apply the equations used for oscillation transients in a closed cavity to each. It was assumed that the effect of the vertical wire placed in the fringe field was to move the cavity resonator mode centre frequency for the vertical and horizontal components to different frequencies. It was also assumed that the cavity resonator was tuned such that the vertical component of the cavity mode is on tune with the oscillation. The horizontal

FIGURE 5.32

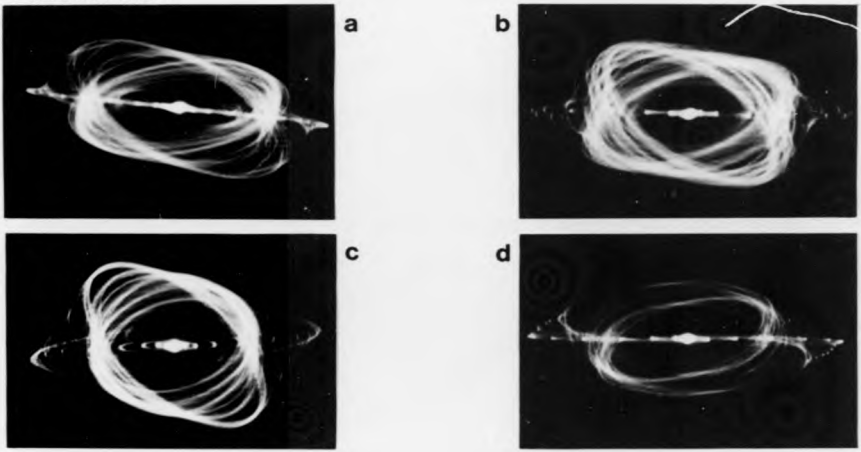

FIGURE 5.33

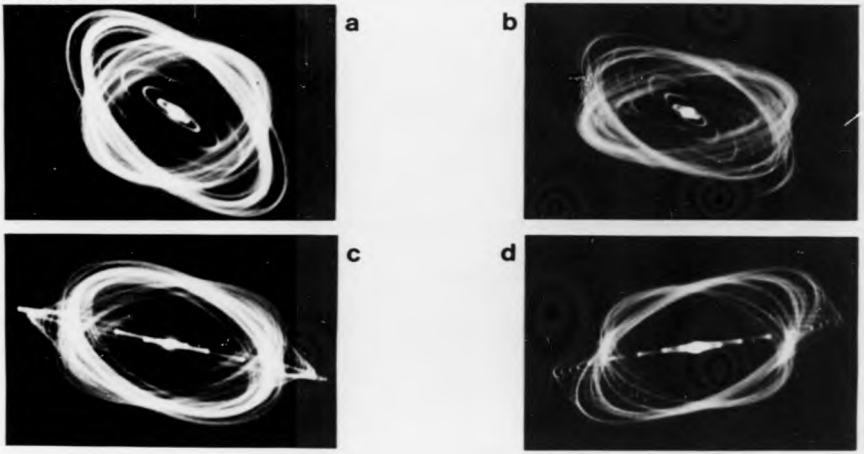

FIGURE 5.34

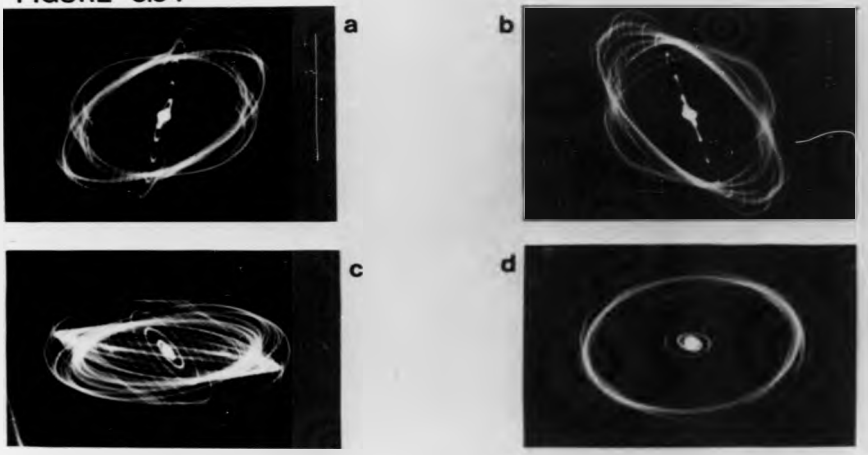

component of the mode must therefore be off tune with respect to the oscillation frequency. The equations governing the build-up of transient oscillation in a detuned resonator are given (Oraevskii 1964). On solving these equations it was observed (Fig 5.34A) that the effect of a detuned resonator mode was to dramatically slow the build-up and period of the transients. This effect is of importance in deciding the direction of the initial transient build-up.

It is proposed here that the total anisotropy of the system still favours oscillation in the horizontal direction, due to the large state selector anisotropy present. The wire-induced cavity anisotropy favours oscillation in the vertical direction, although this is still insufficent to balance the state selector anisotropy. The oscillation frequency matches the centre frequency of the vertical component of the cavity mode, with the horizontal component of the cavity mode detuned. The favourable anisotropy which should give an advantage to the initial transient build-up in the horizontal direction, is offset by the slow nature of the build-up in this direction, due to this component of the cavity mode being off tune. This is sufficient to give equal priority to oscillation transient build-up in any linear polarization. The initial direction of linear transient build-up is then possibly dependent on the thermal noise within the cavity, which leads to a rich variety of directions of initial linear build-up. The initial direction of linear transient build-up is also dependent on the cavity tuning, which changes the cavity anisotropy, and amount of slowing of transient build-up, and so changes the most favourable direction initial oscillation transient build-up.

The effect of the oscillation ellipse passing from one stable orientation to another, was far easier to observe then with previous use of the maser. This was attributed to the reduced total gain anisotropy of the maser system.

FIGURE 5.34A

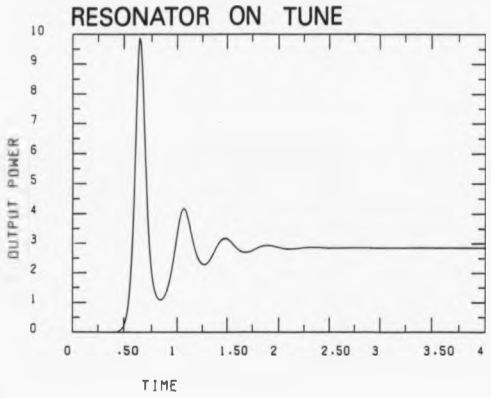
RESONATOR ON TUNE
OUTPUT POWER
10
9
8
7
6
5
4
3
2
1
0
0
.50
1
1.50
2
2.50
3
3.50
4
TIME

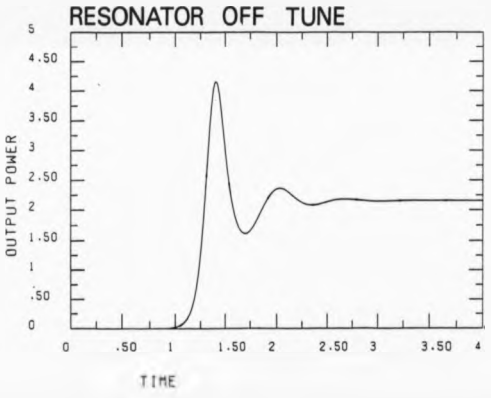
RESONATOR OFF TUNE
OUTPUT POWER
5
4.50
4
3.50
3
2.50
2
1.50
1
.50
0
0
.50
1
1.50
2
2.50
3
3.50
4
TIME

Low frequency biharmonic oscillation under an applied magnetic field was studied in the presence of a vertical wire (Fig. 5.35 and Fig. 5.36). The following trends were noted and discussed.

In many examples the observed beat envelope was almost square shaped and the bottom side of the square was rotated at an angle of 30 degrees anticlockwise from the horizontal (Fig. 5.35a,b). The beat envelope changed from being nearly square to being nearly circular as the beat envelope evolved (Fig 5.35a,b). In some cases the beat envelope became rectangular or parallelogram shaped. Only in a few cases was a final oscillation ellipse observed, after one oscillation had decayed, and in these cases the ellipse was nearly circular, although it was difficult to observe. In these examples the initial oscillation build-up was linearly polarized, this took place in a variety of different directions (Fig. 5.35a,b,c,d), although there was a bias towards linear horizontal build-up. The linear build-up had reached its maximum amplitude before it began to rotate. The beat frequency then remained constant as the oscillation pulse developed. These build-ups were similar to those observed before and may be interpreted as follows. One or two linearly polarized oscillations build-up in the same direction, this being the direction observed on the traces. These two oscillations, (the second oscillation having developed) which are of similar amplitude, then rotate, one becomes parallel with each of the two sides of the square, these then beat together to produce a square beat pattern. Both oscillations then become elliptical and one oscillation dies away as the beat envelope changes from square to circular and the final remaining oscillation eventually becomes circular.

In several examples the initial oscillation builds up linearly and a nearer circular beat envelope is produced. This then decays to a near circular oscillation ellipse (Fig. 5.36a,b).

FIGURE 5.35

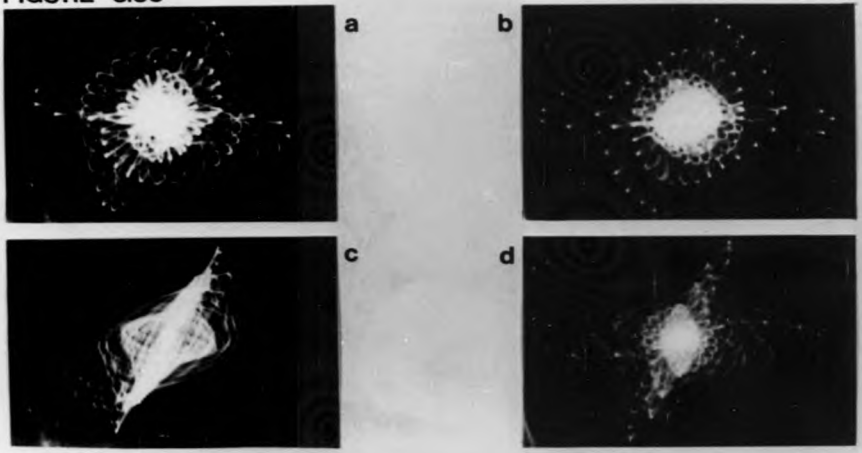

FIGURE 5.36

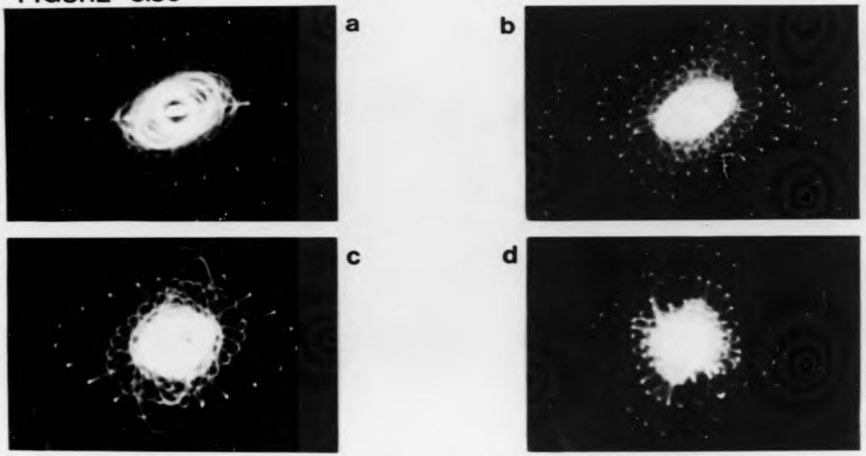

5.9.7 MASER OPERATION WITH A THIN VERTICAL WIRE IMMERSED SLIGHTLY DEEPER INTO THE FRINGE FIELD OF THE RESONATOR

The experiment was repeated with the thin wire placed further inside the fringe field of the maser. The trends observed are again noted and discussed. Examples are shown in Fig. 5.37 to Fig. 5.42.

Oscillation amplitude settling transients are observed on most of the traces. The transients are however almost exclusively observed in the vertical direction. Only in rare exceptions do linear transient build-ups occur in other directions, and there was no observed transient build-up in the horizontal direction. On some of the traces the oscillation transient builds up linearly to its full amplitude before becoming elliptical (Fig. 5.37a), whereas some traces become elliptical as the oscillation transient builds up (Fig. 5.37b). The governing factor for when the transient build-up becomes elliptical, depends on the initial direction of thermal noise or other fluctuations. The following intermediate region appears to be connected with the form of the initial transient build-up.

On some of the simpler examples, the intermediate region is simply the rotation of the oscillation transient, either clockwise or anticlockwise, which then becomes elliptical as it rotates to a stable oscillation ellipse position (Fig. 5.38a,b). However with many examples the intermediate regime is extremely complicated, a series of such traces are shown (Fig. 5.38c to Fig. 5.40). On most of these traces there appears to be a stable oscillation ellipse with its major axis rotated approximately 10 degrees anticlockwise from the horizontal. On most of these traces the oscillation ellipse appears to pass through several intermediate near-stable ellipses, on its evolution to its final stable position. One of these intermediate positions lies with the its major axis rotated at an angle of approximately 35 degrees clockwise from the horizontal, another has its major axis inclined vertically.

FIGURE 5.37

a

b

c

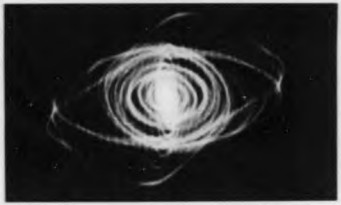

d

FIGURE 5.38

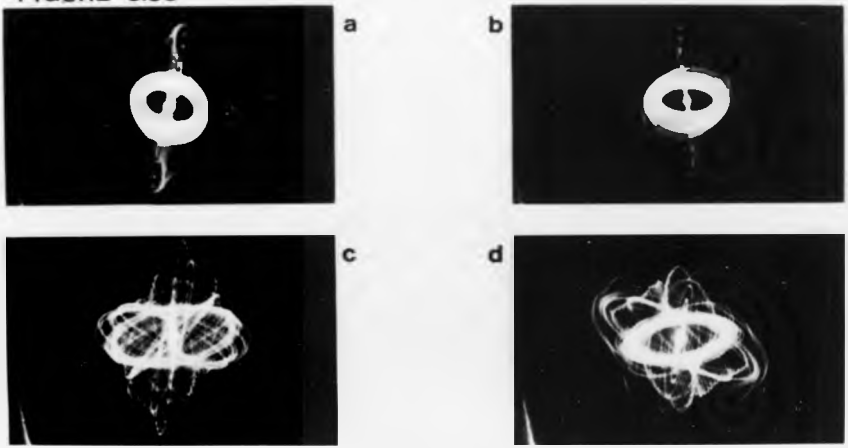

FIGURE 5.39

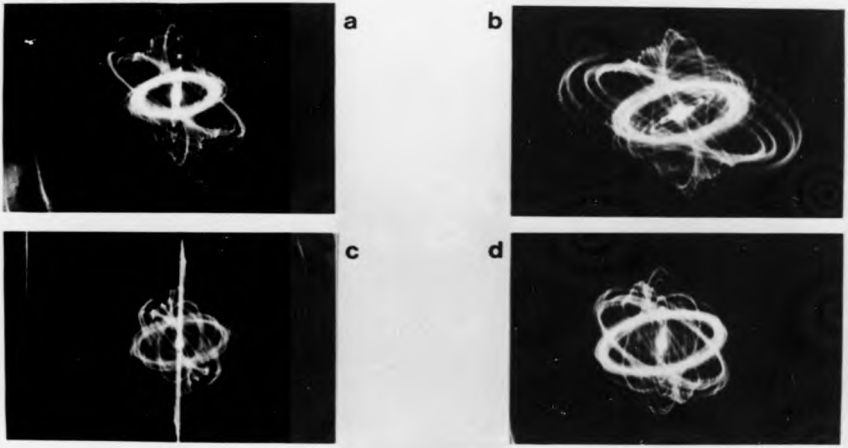

FIGURE 5.40

a

b

c

d

Under the operating conditions which give the most varied intermediate oscillation evolutions, the initial oscillation build-up is highly varied, where-as under other operating conditions the oscillation transients always build up in the vertical direction. A few traces show complicated unexplained intermediate build-up patterns, two examples are shown in Fig. 5.40c,d.

The final oscillation orientation position observed on most of the traces, show a variety of elliptical or circular orientations, with the major axis of the oscillation ellipse inclined at angles up to 60 degrees from the horizontal axis (Fig. 5.41a,b). This suggests that the gain anisotropy in the vertical and horizontal components of oscillation are nearly completely balanced. The detuning of the horizontal component of the cavity mode and the resultant slowing of transient build-up in that direction has resulted in transient build-up being highly favoured in the vertical direction. It would be tempting to conclude that the extremely complicated intermediate ellipse evolution patterns correspond to the condition where the cavity gain anisotropies are complete balanced. However the final oscillation ellipse on these traces has its major axis inclined near to the horizontal axis. It is proposed here that the condition to obtain these complicated intermediate ellipse evolutions depends on both closely balancing the gain anisotropies and also on balancing the rate at which the transient processes take place, through the relative tuning of the two cavity mode components.

With careful cavity tuning it is possible for the oscillation ellipse to become strongly near linearly polarized along the vertical axis (Fig. 5.42a). A few traces show nearly circularly symmetric build-up processes, an example is shown in Fig. 5.42b.

Under an applied magnetic field, low frequency biharmonic oscillation was again observed. Here the beat envelope produced was

FIGURE 5.41

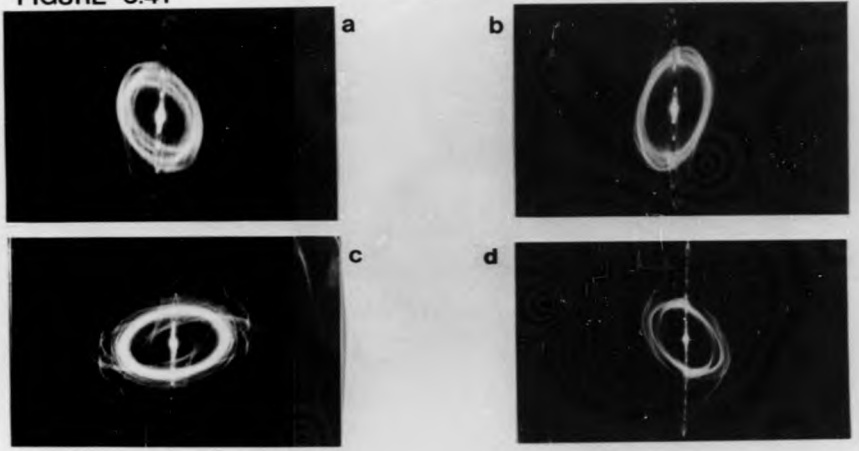

FIGURE 5.42

a

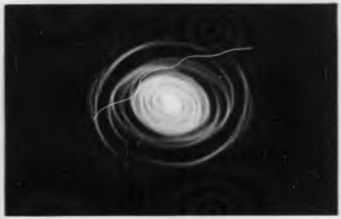

b

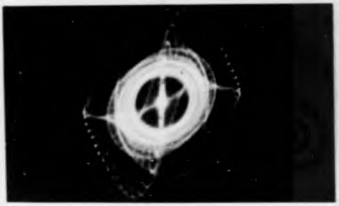

c

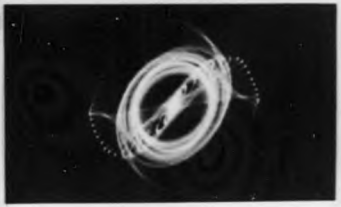

d

nearly circular. As the opposite ellipse built up, it enlarged its amplitude while rotating. As one oscillation died away a circular final oscillation ellipse was observed (Fig. 5.42c,d). The striking feature here is the highly circular nature of the beat envelope which was obtained at avery low beat frequency and hence very low applied magnetic field. This is attributed to the near-isotropic system, giving two near circular oscillation ellipses under the applied magnetic field which then beat together.

5.10 GENERAL COMMENTS ON RESULTS

In the preceding sections, detailed description has been given on the oscillation build-up processes on the J=K=2 transition of $^{14}NH_3$. The experiments have been repeated on the J=K=3 transition of $^{14}NH_3$ and preliminary results show similar trends. Linearly polarized horizontal oscillation amplitude settling transients have been observed in zero applied field, and under an applied magnetic field low frequency beats were observed. This suggests that the build-up patterns are more dependent on the conditions present in the maser cavity, rather than the spectral line on which the oscillation takes place.

Qualitative explanations have been made in terms of relatively simple ideas. Examine further the idea of considering the cavity mode in terms of a component Q_x in the horizontal direction and a component Q_y in the vertical direction. The problem here is that the cavity is circularly symmetric with the exception of two cavity ports, so it would appear that the choice of directions for splitting the cavity into Q_x and Q_y components would appear completely arbitrary. however the direction of the strong state selector anisotropy which may be considered along with the cavity anisotropy (Yassin 1981) may define the direction of one of the components. Considering the cavity Q in terms of a Q_x and a Q_y component has been developed on work with laser systems

(D'Yakonov 1966).

The most striking theme throughout this chapter has been that of the reproducibility of the results. Under many operating conditions successive oscillation pulses give build-up patterns which are very different to each other. Many examples have been discussed in this chapter. Possible explanations are discussed below.

The maser parameters may be changing with time. It has already been proposed that vibrations of the cavity plates, induced from the motion of the backing pumps, may change the cavity anisotropy in the time between each gas pulse. However, as explained in the text this does not give an adequate explanation of the Rabi oscillation transient fluctuations. The gas pulse profile may change on successive gas pulses, due to perhaps mechanical imperfections in the valves. There is also a very slight residual thermal drift on the cavity tuning, however, before any of these experiments were performed the maser had been left with charged liquid nitrogen traps for several hours, the cavity taking at the time of the experiment approximately 1-2 hours to drift to a position where oscillation is extinguished. This slow drift would not appear to have an appreciable effect over a time period of one second.

A second possible explanation is that the oscillation build-up is chaotic in nature. A closed cavity maser system can theoretically give chaotic operation. Such a system has far fewer degrees of freedom for its operation than the system under consideration here. A closed maser system operated under an applied magnetic field, with the maser on tune, may be described in terms of four variables (Oraevskii 1981). For the open resonator system each of these variables may be considered in two orthogonal (not necessary linear) polarizations. These being the microwave electric field, (producing the amplitudes of the components of the oscillation ellipse), the real and imaginary parts of the macroscopic polarization, and the number of state selected molecules

entering the cavity resonator. At the relatively low maser oscillation overfulfilment factors observed here, the imaginary part of the macroscopic polarization will remain proportional to the microwave electric field. This may reduce the number of variables to six. However with the cavity resonator off-tune the system becomes far more complicated, with phase dependent parameters required. A variable dependent on relative phase would be required to describe the eccentricity of the oscillation ellipse. At its very simplest the maser oscillation build-up may be described as the build-up of a three dimensional object (describing the oscillation ellipse parameter) in a minimum of a seven dimensional phase space.

Consider the path of two trajectories through a phase space. A chaotic system is one where regions exist in this phase space where two infinitely close trajectories through the space take highly divergent paths, so that in a relatively short time, the two trajectories have seperated to different regions of the phase space. In such a physical system a slight perturbation of the initial conditions may lead to a completely different evolution. It is proposed here that such a chaotic regime exists in the phase space describing the present maser system, and that this is around the region where the microwave electric field is zero. The thermal noise in the system acts both as the perturbation from which the oscillation develops, and secondly as the perturbation which places successive oscillation build-up trajectories onto slightly different positions in the chaotic region of the phase space. This results in the rich variety of build-up patterns observed in this chapter. The existence of two stable elliptical orientations further complicates the process; there are probably more chaotic regions in the phase space, for example at the position where the trajectories divide for the oscillation ellipse to move to one of two stable orientations.

CHAPTER SIX

SUGGESTIONS FOR FUTURE WORK

6.1 INTRODUCTION

In this chapter the possible extentions of the work undertaken, both theoretical and experimental, are discussed. Continuations of the work of Chapters 2, 3, 4, and 5 are considered here.

6.2 POSSIBLE CONTINUATIONS OF THE EXPERIMENTAL WORK

6.2.1 LISSAJOUS FIGURE WORK WITH THE EXISTING SYSTEM

Consider the Lissajous figure work of Chapter 5. Detailed spiral build-up patterns may be obtained for oscillation on the J=K=1, J=K=3, J=K=4 and J=K=6 transitions of $^{14}NH_3$. The form of the spiral build-up on the J=K=1 transition is interesting because linear oscillation polarization only, has been reported for this transition, in contrast to the results obtained on the J=K=2 transition. Here the state selector anisotropy should also be at its greatest.

An advantage would be gained by redesigning the present filter circuits, moving their centre frequency from 45kHz to either 100kHz or 200kHz, and increasing their bandwidth. It should then be possible to design filters with a quicker rise time capable of observing faster dynamic effects. The high frequency beating effects due to maser oscillation on the second order mode TEM_{101}, and transient build-up under very strong oscillation conditions may then be examined. The relatively high frequency of the final downconverted signal would give a large number of spiral orbits per unit time on the CRO trace, sufficient for "mapping" these fast effects. Any congestion of spirals on the CRO trace may be compensated by using a shorter oscillation "bright up" pulse.

6.2.2 POSSIBLE MODIFICATIONS TO THE PRESENT SYSTEM

Several modifications would be required to increase the strength of the maser oscillation.

The maser cavity may be redesigned. The copper resonator discs should be reground in order to improve their surface flatness and hence the quality factor of the resonator. The mechanical cavity tuning mechanism should be replaced or supplemented by tuning using lengths of piezo-electric material, whose size changes on application of an electric field across their volume. Three pieces of piezo-electric material would be used, one in each position that is now occupied by the present glass rods. This will enable fine positioning of the cavity plates to be undertaken, during the operation of the maser, and so the value of the cavity quality factor may be maximised at all times. By applying a relatively large electric field to one of these piezo-electrics, the orientation of the cavity plates and hence the gain anisotropies of the cavity system may be adjusted in a controlled way, during the course of the experiment. A fourth piezo-electric unit may be used to complement the present mechanical gear tuning system, so that the cavity resonance may be smoothly tuned across the maser oscillation transition frequency. The electric fields required for operating the piezo-electric ceramics must be designed not to interfere with the fringe field of the maser cavity and so weaken the oscillation by inhomogeneous broadening of the spectral line.

Two new sets of ladder state selectors may be designed and constructed out of stainless steel. The length of the state selectors, the spacing between the metal rods, and the distance between the two rows of rods may all be increased. This will increase the angle of capture of the state selectors, and allow for a greater proportion of the molecular beam to be state selected, and so overcome the saturation effects discussed in Chapter 4. The greater separation of the state

selector rods should reduce the attenuation of the molecular beam by scattering, and enable the state selectors to operate at a higher potential before electrical breakdown occurs.

The two skimmer slits may be redesigned, based on the use of very sharp stainless steel skimmer edges. The increased entrance width of the state selectors should allow for the skimmer slits to be placed further apart and so reduce further the "skimmer interference" (Deckers and Fenn 1963) of the pulsed molecular beam further by placing the slits in a less intense portion of the molecular beam.

6.2.3 POSSIBLE EXPERIMENTAL WORK WITH THE MODIFIED SYSTEM

The static Lissajous figures obtained previously (Yassin and Lainé 1981) may be re-examined with the filter circuits included in the experiment. The variation of the oscillation ellipse parameters may then be carefully mapped out as a function of the operating parameters. The static Lissajous figures may be studied on the J=K=1, J=K=2, J=K=3, transitions of $^{14}NH_3$ and possibly the J=K=4, and J=K=6 transitions also.

It may be possible to study the mechanism of the polarization flips observed with continuous wave operation. In the process of a polarization flip the oscillation changes from one elliptical polarization orientation to another, there is a change in amplitude, orientation, and eccentricity of the oscillation ellipse (Lainé and Yassin 1981). It is unlikely however, that these changes will be faster than the fastest dynamic processes which may be observed using the Lissajous spiral method. The oscillation power output from the maser may be "sampled" by triggering the z modulation of the CRO (Chapter 5). Here, for example a 1ms "pulse" "bright-up" applied to the CRO would make it possible to observe any changes in the static ellipse which took place during this time. A controlled method is needed to induce polarization flips in the maser system. Tuning the cavity resonance

across the maser oscillation frequency will cause the oscillation polarization to flip during the course of the tuning (Lainé and Yassin 1981). If this could be repeated, frequent polarization flips may be induced. The simplest way to achieve this is to place a repeating triangular waveform across the proposed tuning piezo-electric of the maser cavity. The cavity tuning is effected during the period of the triangular wave, so that the centre frequency of the cavity mode moves right across the oscillation frequency, and then back again across the oscillation frequency in the opposite direction, during one cycle of the applied waveform. This should induce two polarization flips during each cycle of the triangular wave. A frequency should be chosen for the triangular wave so that the movement of the plates is too slow to change the oscillation level rapidly (due to detuning) and so induce any dynamic effects (other than polarization flips), and slow enough for the piezo-electric to respond to the applied voltage, but fast enough to obtain a good repetition rate, so that the time during which a flip may be induced may be reduced to a minimum. A suggestion is 7 Hz. The same triangular wave is used to trigger the brighten-up pulse to the CRO, with a variable delay built into the electronics. The brighten-up pulse will only last for a few milliseconds. Using a z-modulation pulse of, for example 1ms, the delay electronics should enable the brighten-up pulse to be triggered at any point on this waveform. The brighten-up pulse should then be triggered at a point where there is high probability of a polarization flip occuring. By taking a large number of exposures of successive light pulses at 0.125s exposure, a trace should eventually be obtained showing both static oscillation ellipses with a series of Lissajous spirals inbetween. This trace should show the movement of the polarization ellipse from one polarization orientation to another, during the course of its flip.

The possibility with this modified system of gaining oscillation

on other spectral lines of $^{14}NH_3$ is realistic. The two spectral lines which have a high probability of giving pulsed maser oscillation are the J=K=5 and J=4, K=3 transitions at 24.533 GHz and 22.688 GHz respectively. An improved system may allow for pulsed oscillation on one or more of the hyperfine satellite lines of the J=K=1 transition, and also allow for their Lissajous spiral build-up patterns to be monitored. It would then be possible to compare the build-up patterns on two different components of the same transition, under otherwise similar operating conditions.

With suitable filters, and very strong oscillation, the form of the oscillation ellipse may be traced out, not only through the first, but through the second and third self-induced Rabi oscillation transients as well. Under an applied electric field, the form of the oscillation ellipse may be determined through the chain of slowly decaying transients observed under such operating conditions (Chapter 2).

Experiments may be performed to determine the dependence of the variation of the oscillation build-up on successive oscillation pulses, on fluctuations of the maser parameters (Chapter 5). The system may be operated with the backing pumps switched off for several minutes in order to minimise the effect of pump vibrations reaching the maser cavity. Here the volume of the vacuum chamber between the backing and the diffusion pumps may have to be increased to sustain the pumping speed of the diffusion pumps for a sufficiently long period. Vibrations may be induced into the cavity plates, by applying an alternating voltage to the one of the piezo-electric of the cavity tuning system. This would give a cavity disc tilt in a known direction. Applying two alternating voltages in antiphase to the other two piezo-electrics would produce a disc tilt in a perpendicular direction.

Transient build-up in a maser system employing a closed cavity

resonator remains fully reproducible on successive oscillation pulses (Lefrere 1974). These experiments may be repeated using a pulsed molecular beam to induce the transients. Any variation in the oscillation build-up on successive gas pulses may then be attributed to possible fluctuations in the gas pulses. Lissajous spiral build-up patterns may be studied also while injecting a microwave signal into the maser cavity. Both the coupling ports to the maser cavity are employed in the detection scheme. It may therefore be required to add a third coupling port to the maser cavity. The fluctuations in the oscillation build-up may then be examined when the oscillation build-up originates from a controlled microwave signal rather than from thermal noise. The implementation of the above proposals should give an insight into possible causes of the varied oscillation ellipse build-up patterns on successive gas pulses.

The work on oscillation amplitude settling transients may be extended. The above modified system operated with an inhomogeneously Stark-broadened spectral line or Zeeman split spectral line (Chapter 2), may give continuous modulation of the oscillation power output and even chaotic operation, when operated under a pulsed regime with very strong pulsed oscillation. A thin wire placed horizontally across the fringe field, approximately 2cm inside the cavity at greatest depth, will give strongly linearly polarized oscillation (Chapter 5). This may give continuous modulation of the output power, leading to period doubling and chaotic operation.

6.2.4 CONSTRUCTION OF POSSIBLE NEW MASER SYSTEMS

The possibility of constructing a new maser system in order to obtain very high maser oscillation overfulfilment conditions is now considered. Two possible machines are considered. A large double pulsed beam maser operating with a closed resonator may be constructed

in order to obtain sufficient maser oscillation overfulfilment condition to reach the chaotic regime of operation. Such a machine may have three very large diffusion pumps (30cm diameter or greater), to give fast pumping and low dynamic vacuum between gas pulses, and large area cold traps. The maser may have very large volume vacuum chambers, so that there is only a slow rise in the background pressure as the pulsed valves are opened. The system would have two large diameter circular skimmers, and two long, relatively large diameter ring-type state selectors, held at as high a potential as possible. Improving on the best designed closed cavity maser system of Maroof at Keele, it should be possible to build a maser system where each beam gives an overfulfilment condition well in excess of 30 times for each beam when operated continuously. On pulsing both the molecular beams, the maximum overfulfilment factor should be well in excess of that required to produce chaotic operation on a Zeeman split spectral line. The onset of period doubling may also be studied in detail with this machine.

The alternative is to build a large multibeam maser with a horizontally placed resonator, in an extremely large vacuum chamber, pumped by large diffusion pumps. The use of approximately 20 pulsed molecular beams, each with its own state selector, skimmer, and vacuum chamber, would give a device of extreme versatility. An overfulfilment factor of at least 5 times may be obtainable during pulsed operation using only one beam. With 20 such beams an overfulfilment factor which is well in excess of that needed for chaotic operation on a Zeeman split spectral line. Simply placing an electric field across the cavity plates may induce chaotic operation, or placing a thin wire in the maser fringe field and applying a magnetic field as before should give chaotic operation on pulsing the maser. Such a system will display very little state selector anisotropy, due to the axially symmetric positioning of the state selectors. By changing the number of molecular beams in

operation, the state selection anisotropies may be changed. Such a system would give an excellent illustration of the Lissajous spirals oscillation ellipse build-up patterns under very large overfulfilment conditions. The number of possible transitions on which oscillation may be obtained of $^{14}NH_3$ would be extremely large, including several hyperfine satellites of the J=K=1 transition. Maser oscillation on maser transitions of other molecules may be undertaken, for example the J=2 J=1 transition of OCS, and so investigate how the Lissajous spiral build-up patterns change for a different type of molecule.

6.3 POSSIBLE EXTENSIONS TO THE THEORETICAL WORK

The equations which govern the dynamic properties of a closed cavity maser system (Oraevskii 1967) may be extended to consider the cases where the two components of the spectral line are no longer placed symmetrically with respect to the centre frequency of the cavity resonator. The model may be extended to consider the cases where there are more than two components of the spectral line each of different intensity. This would help interpret the onset of chaos with oscillation on an inhomogeneously broadened spectral line, and help to study the effect of cavity detuning on both the onset of chaos and continuous oscillation modulation. This would help further to interpret the results of Maroof (1975).

A theory is required to explain the build-up of the oscillation polarization ellipse as described in Chapter 5. There appears to be two possible approaches. Firstly the dynamic equations for oscillation build-up in a closed cavity maser may be adapted for use in the case of an open resonator. This has been discussed in Chapter 5. Here each of the maser parameters described in the dynamic equations must be described in two orthogonal coordinates. In a disc resonator, the oscillation frequency does not correspond always to the centre frequency

of the maser cavity mode even when the cavity is on tune. Detuning effects must also be considered which lead to frequency pulling and phase shift in the two orthogonal components of the oscillation. These must then be interpreted to give the ellipticity of the oscillation ellipse. Such an approach would be require substantial time deriving equations for the system and then solving them numerically. A second approach would be to start with the static theory of the oscillation polarization and then to attempt to place a time dependence on some of the parameters involved.

APPENDIX ONE

AN EXAMPLE OF A COMPUTER PROGRAM USED IN CHAPTER 3

This program is typical of the simple BASIC programs used to obtain the traces displayed in chapter 3. This specific program will produce step up and step down transients similar to those displayed in Fig. 3.5a.

```
10 REM "STEP DOWN TRANSIENTS"
20 FILES 4,' .AAAA'
30 PRINT "K2="
40 INPUT K2
50 LET Q3=3E8
60 LET K1=1E-4:H0=6E-5:H1=1.3E-7
70 LET H0=2*H0
80 LET R=K1*K2/(H1*H0)
90 LET S=H0/H1
100 LET W0=0
110 LET W2=75
120 LET T1=10000
130 LET A=SQR(((K2*K1)/(H1*H0))-1)
140 LET B=-H0*A/K1
150 LET C=H0/K1
160 LET D=-K2/H1
170 LET X0=A
180 LET Y0=-(H0/K1)*X0
190 LET Z0=-C
200 LET T2=6E8
210 LET V2=0.9*Q3
```

```
220 LET W=0
230 PRINT "XO=";XO
240 PRINT "YO=";YO,"ZO=";ZO
250 FOR T=0 TO T2 STEP T1
260 LET V2=V2+T1
270 IF V2>Q3 THEN LET V2=-Q3
280 IF V2>=0 THEN LET E=0
290 IF V2<0 THEN LET E=0.85
300 LET XO=XO+T1*(-(HO*XO)-(K1*YO))
310 LET YO=YO+T1*H1*(-YO+(B*E*WO)+(XO*ZO))
320 LET ZO=ZO+T1*H1*((-ZO-(C*R))-(XO*YO))
330 LET WO=WO+T1*H1*(-WO-(E*YO/B))
340 LET W=W+1
350 IF W>W2 THEN PRINT "T=";T,"XO=";XO,"P=";XO*XO
360 IF W>W2 THEN PRINT 4,6.71E-12*TXO*XO
370 IF W>W2 THEN LET W=W-W2
380 NEXT T
390 STOP
```

REFERENCES

AL-JUMAILY, A. M., (1979). PhD Thesis, University of Keele.

AL-JUMAILY, A. M. and LAINÉ, D. C., (1979). Acts du Colloque Optique Hertzienne et Dielectriques, Lille, France pp. 161-164

BASSI, D., IANNOTTA, S. and NICCOLINI, S., (1981). Rev. Sci. Instrum. 52, 8.

BARCHUKOV, A. I., PROKHOROV, A. M. and SARVANSKII, V. V., (1963). Radio Eng. Electron Phys (USSR), 8 385.

BARDO, W. S. and LAINÉ, D. C., (1969). Electronics Lett. 5 26.

BARDO, W. S. and LAINÉ, D. C., (1971). J. Phys. D, Appl. Phys. 4 L42.

BASOV, N. G., (1964). Soviet Phys. JETP, 18 1211

BECKER, G., Z. Argew Phys, 15 13.

BELL, K., (1984). Private Communication.

CVITANOVIC, P., (1984) Universiality in Chaos (Introduction). Adam Hilger Ltd.

DECKERS, J. and FERN, J. B., (1963). Rev. Sci. Instrum. 34, 96.

DELUCIA, F. C., (1969) PHD Thesis, Duke University.

D'YAKONOV, M. I., (1966). J. Exptl. Theoret. Phys. (USSR), 49 1169

FAIRBAIRN W., (1986) Phys Bull 37

GIGLIO, M., MUSAZZI, S. and PERINIV, V., (1981). Phys. Rev. Lett. 47 243

GOOD, W. E., (1946). Phys. Rev. 70 213.

GORDON, J. P., ZEIGER, H. J. and TOWNES, C. H., (1955). Phys. Rev. 99 4.

GRAZYUK, A. Z. and ORAEVSKII, A. N. (1964). Radio Eng. Electron. Phys. 9 424 and 443.

INGRAM, D. J. E., (1955). Spectroscopy at Radio and Microwave Frequencies; Butterworth Scientific Publications.

JAIN, M. K., (1981). Numerical Solutions to Differential Equations, Wiley Eastern Ltd, New Dehli.

JONES, D., (1984). Private Communication.

KADANOFF, L. P., (1983). Phys. Today, December 1983.

KRUPNOV, A. F. and SKVORTOV, V. A., (1964). Sov. Phys. JETP, 18 1426.

LAINÉ, D. C., (1975). Advances in Electronics and Electron Phys. 39. ed. L, Martin, Academic Press, New York.

LAINÉ, D. C. and AL-JUMAILY, A. M., (1979). Electronics Lett. 15 21.

LAINÉ, D. C. and BARDO, W. S., (1969). Electronics Lett. 15, 14.

LAINÉ, D. C., and MAROOF, A. K. H., (1974). 18th Ampere Conf, Nottingham, 1 , 199.

LAINÉ, D. C. and MAROOF, A. K. H., (1975). Proc V International Symposium on Molecular Beams. Nice, France, F1, 1.

LAINÉ, D. C., SMART, G. D. S. and CORB, A. I., (1976). Ann. Scient. Univ Clermont (France) 59. Phys, 16e.

LAINÉ, D. C. and TRUMAN, M. J., (1977). Phys. Lett. 62A, 5.

LAINÉ, D. C., TRUMAN, M. J. and HOPE, S., (1980). Am J. Phys 48 11.

LAINÉ, D. C. and YASSIN, G., (1981). Phys. Lett. 62A, 5.

LEFRERE, P. R., (1974). PhD Thesis, University of Keele.

LEFRERE, P. R. and LAINÉ, D. C., (1975). Chem. Phys. Lett. 35 4.

LEFRERE, P. R. and LAINÉ, D. C., (1977). Proc VI International Symposium on Molecular Beams. Noordwijkerhort, Holland.

LIBCHABERA, A., LAROCHE.C, and FAUVES, (1982). J. Phys. Lett. 43 L211

MAROOF, A. K. H., (1975). PhD Thesis, University of Keele.

MAROOF, A. K. H, and LAINÉ, D. C., (1974). J. Phys. E, Sci. Instrum. 7

MAROOF, A. K, H, and LAINÉ, D. C. (1976). J. Phys D. Appl. Phys, 9.

ORAEVSKII, A. N., (1964). Molecular Generators, Nauka, Moscow, USSR.

ORAEVSKII, A. N. (1964a). In "Soviet Maser Research", D. V. Sobel'tsyn ed p192, Consultants Bureau, New York.

ORAEVSKII, A. N., (1981). Sov. J. Quan. Electronics, 11 71.

RUELLE, D., (1980). Math. Intelligencer 2 126.

SCHAWLOW, A. L. and TOWNES, C. H., (1958). Phys. Rev. 112 1940.

SHAKHOV, V. O., (1969). Translated from Izvestiya Radiofizika 12 10.

SHENG, H., BAKER, E. F., and DENNISON, D. M., (1941). Phys. Rev. 60 786.

SHIMODA, K., WANG, T. C. and TOWNES, C. H., (1956). Phys. Rev. 60 786.

SMART, G. D. S. (1973). PhD Thesis, University of Keele.

SULKES, M., JOUVET, C. and RICE, A., (1982). Chem. Phys. Lett. 87 6.

TAKAHASHI, I., HASHI, T., YAMANO, M., YAMAMOTO, M., SUZUKI, S. and MAKITA, T., (1960). J. Phys Soc. Japan 15, 513.

TOWNES, C. H. and SCHAWLOW, A. L., (1955). Microwave Spectroscopy (McGraw-Hill) New York.

WHITE, J. D. W., (1984). Private Communication.

YASSIN, G., (1981). PhD Thesis, University of Keele.

YASSIN, G., DAVIS, J. A., CORB, A. I. and LAINÉ, D. C., (1985). Coll. Optique Hertzienne et Dielectrics, Grenoble, France, Sept 1985, p. A6.1

YASSIN, G. and LAINÉ, D. C., (1981). Electronics Lett. 54 156.

YASSIN, G. and LAINÉ, D. C., (1985). Phys. Lett. 113A 5.